Towards ecological and efficient electrochemical energy storage in supercapacitors and sodium ion batteries using onion-like carbon

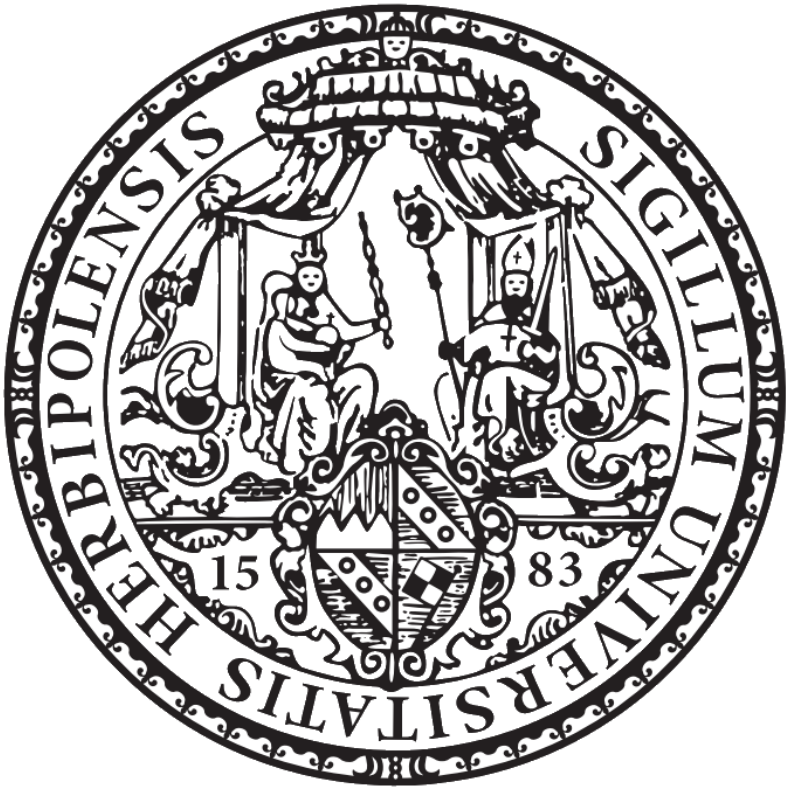

Dissertation zur Erlangung des naturwissenschaftlichen Doktorgrades der Julius-Maximilians-Universität Würzburg

vorgelegt von

Christian Bauer

aus Helmstadt

Würzburg 2022

Eingereicht bei der Fakultät für Chemie und Pharmazie am

_____

Gutachter der schriftlichen Arbeit

1. Gutachter: _____

2. Gutachter: _____

Prüfer des öffentlichen Promotionskolloquiums

1.Prüfer: _____

2. Prüfer: _____

3.Prüfer: _____

Datum des öffentlichen Promotionskolloquiums

_____

Doktorurkunde ausgehändigt am

_____

The more knowledge you have, the more you are free to rely on your instincts.

Arnold Schwarzenegger

Danksagung

Zuerst möchte ich mich bei Frau Prof. Dr. Anke Krüger bedanken, die mich als ersten Funktionswerkstoffler des Arbeitskreises ins Chemielabor gelassen hat. Thematisch gesehen boten Sie mir mit der Etablierung der Energiespeicherforschung in der Arbeitsgruppe diverse fette Herausforderungen und damit auch viele Gelegenheiten in diverse Richtungen zu wachsen. Dies wurde vor allem aufgrund der vielen gestalterischen Freiräume hinsichtlich der Versuchsplanung möglich, wofür ich sehr dankbar bin.

Auch bei Prof. Dr. Gerhard Sextl und seiner Truppe rund um das Fraunhofer ISC möchte ich mich bedanken, da mir dadurch die Benutzung des Potentiostaten ermöglicht wurde. Hier sind Andreas Bittner, Mara Göttlinger, Lukas Gold, Benedikt Schug, Dr. Dietmar Jansen und Dr. Michael Hofmann, Vilija Anfimovaite und Dr. Sarah Hartmann zu nennen, welche mir geduldig die ein oder andere Frage beantwortet haben. Auch für den Zugang zum Zentrum für Angewandte Energieforschung und die vielen BET Messungen möchte ich mich bei Dr. Gudrun Reichenauer und Stephan Braxmaier bedanken. Bei Dr. Stephan Kirchmeyer möchte ich mich bedanken, dass er mir aus so manchen dunkeln Tal während meiner Arbeit mit PEDOT geholfen hat. Außerdem gilt mein Dank diverser Firmen die mich telefonisch aber auch mit der Bereitstellung kostenloser Materialien unterstützt haben, hier sind Cellgard, Göttle GmbH & Co. KG, HOLDERS TECHNOLOGY GmbH, Schlenk Metallfolien GmbH & Co. KG, Zeon Corporation, Transcontinental Advanced Coatings und Brother zu nennen. Besonders gilt mein Dank Jutta Fiford die mir den letzten Lagerbestand Alufolie überlassen hat sowie Andreas Riedel, der mir einen Druckkopf geschickt hat. Danke auch an meine ehemaligen Lehrer Daniela Weber und Norbert Edelmann sowie meiner Oma Maria, die mein Interesse an Experimenten schon in frühen Jahren gefördert haben.

Danke auch an alle, die hinter den Kulissen und aus Maschinenraum heraus das Schiff des Instituts für Organische Chemie am Laufen halten. Hier gilt mein Dank Bernd Brunner, Markus Braun, Christiana Toussaint, Anette Krug und Dr. Christian Stadler und Dr. Alfons Ledermann, der mich stets für Karteikarten lernen, während der Klausuraufsicht gefoppt hat. Michael Ramold und Manfred Reinhart ihr habt so manch tolles Werk für mich gebaut, auch Frank Förtsch hat mich als innovativer Quell stets unterstützt. Bei Team Lambert möchte ich mich besonders für die Nutzung der Gerätschaften, quasi als würden sie mir gehören, bedanken. Danke an Michael Moos für die entspannte Arbeitsweise.

Bedanken möchte ich mich auch bei meinen Praktikanten, von denen ich mindestens genauso viel gelernt habe wie sie von mir. Besonders die dynamische Phase mit Max, Abdu, Tizian und Tobi hat mir gezeigt, was es heißt Entscheidungen unter knappen Ressourcen zu treffen. Hier wurde es nie langweilig. Mein Dank geht auch an das alte Inventar: Dr. Stefan Wachtler, Andreas Muzha, Dr. Rachel Buschmann, Dr. Sarah Schweeberg, Dr. Benjamin Kiendl und Dr. Stefan Wachtler, für die vielen Dinge die ihr mir im Labor gezeigt habt. Danke auch den neuen Leuten, Dr. Sinem Toksabay, Elisabeth Mayerhöfer, Dr. Adam Day, Lena Roos, Julia Puck, Dr. Johannes Ackermann, Dr. Viktor Merz, Tobias Neff und Sebastian Vettermann. Sebastian du warst nie müde mein Chemiewissen aufzufrischen und hast immer gewusst, wo welches Glasrohr hingesteckt werden musste, damit die Apparatur hinreichend dicht ist. Lena konnte mir immer zeigen wie man die Destille ausmacht. Was piept hier denn nun schon wieder? Kaffee als ein integraler Bestandteil wäre nicht ohne Tobi und Julia realisierbar. Bei meinem Bankbuddy Jo möchte ich mich für die entspannte Arbeitsatmosphäre bedanken, die ganze Bench schwarz, passiert halt mal, ich brauch ab dem Monat alle Steckdosen, nur zu! Mal schauen wie viel Phosphorsäure die Roststangen da vertragen, wie viel Ampere das Netzteil aus China wohl bringt? Wissenschaft zum Mitfiebern los geht’s! Danke auch an Viktor, wegen dir wurde der FunFriday stets ein Erlebnis, man konnte erleben wie ein Wechsel des Aggregatszustands im Detail abläuft. Auch meinen Bürokollegen Dr. Adam Day danke ich für die tolle Zeit, für das gemeinsame lernen, wachsen und Bier trinken.

Besonders die Zeit vor Corona in diesem Stockwerk bleibt mir in guter Erinnerung. Hier liefen die Uhren noch etwas anders. In Würzburg werden die Zelte geräumt, der ganze Zirkus zieht um, doch die Show geht weiter, hierbei viel Erfolg!

Zudem möchte ich mich bei meiner lieben Freundin Svetlana bedanken, die mich nicht nur fachlich unterstützt, sondern gezeigt auch hat, worauf es im Leben wirklich ankommt. Danke auch an Charlie und Elsa, ihr habt den Lockdown belebt. Danke auch an meine komplette Familie und an meine Freunde für die bedingungslose Unterstützung.

Liste der Publikationen

Ein Teil dieser Dissertation wurde bereits in einem Fachjournal publiziert und wird in der teilkumulativen Arbeit wiedergeben.

Bauer, C., Bilican, A., Braxmeier, S., Reichenauer, G., & Krueger, A. (2022). Sustainable supercapacitor electrodes based on preagglomerated carbon onions and a green binder. *Carbon*, *197*, 555-562.

doi.org/10.1016/j.carbon.2022.06.041

Außerdem basieren Teile auf den Manuskripten:

Bauer, C., Kirncher, M., Krueger, A: In situ polymerization of EDOT onto sulfonated onion-like carbon for pseudocapacitor electrodes

Bauer, C., Neff, T., Day, A., Krueger, A: Functional ink with onion-like carbon for energy storage

Contents

1 Motivation

The biggest challenge for our and future generations is to preserve the integrity of the planet in contemplation of an accelerating global warming. A progressive shift away from fossil fuels, in favor of regenerative energy sources is an important step towards carbon neutrality. However, the availability of electricity produced by regenerative energy is reliant on external factors, as 50% of their production in the European Union (2020) is provided by sun (14%) and wind (36%).[1] Both technologies can not increase their output by demand, which becomes problematic, especially in periods of anticyclonic gloom, where energy output by solar and wind systems is insufficient. This missing redundancy makes it impossible for one technology to countervail an unforeseen demand gap. The solution for this problem is the installation of an energy storage capacity within the grid, capable to buffer energy demand and supply shocks. These storage systems provide necessary flexibility and stability for a functional and stable power grid which is the backbone for a successful energy transition. Holistic sustainability aspires to be maintained throughout the supply chain starting from renewable supply to green storage. There is no one-fits-all storage technology as energy consumption is allocated to different sectors and applications. A combination of different storage systems (Fig. 1) provides a resilient solution.

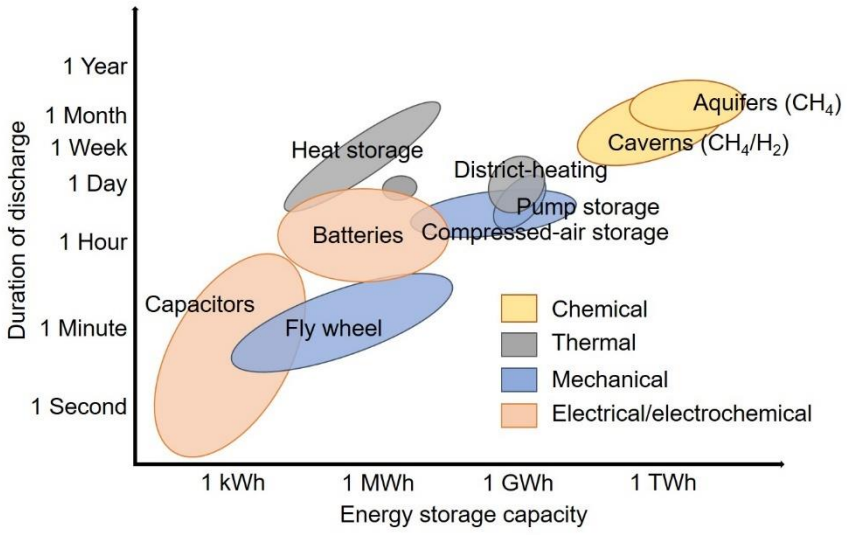

Fig. 1: *Discharge time of different energy storage technologies plotted against their storage capacity. Figure modified with the permission from the author from ref.[2] and under using the CC BY 2.0 license from ref.[3]*

These storage systems differ regarding their energy storage capacity and power output, which is expressed by discharge time and therefore requires assignment towards a specific use case. Demand for stationary energy for a city of 150.000 inhabitants consuming around 200 GW per annum can be buffered by power-to-gas technology in pore or cavern storage (Fig. 1, yellow region). Energy storage used for heating of model households (2MW per annum) can be covered by heat reservoirs or district heating supply (Fig. 1 grey region). Additionally, physical storage sites such as pump or compressed air storages can be used to store energy in the range of 1 GWh.[2]

Transportation requires mobile and therefore lightweight sources of energy storage, widely realized by fossil fuels. If those carbon intensive fuels are replaced with electrochemical energy storage solutions like batteries and capacitors, a huge contribution towards carbon neutrality can be accomplished. (Fig. 1, orange region).[4]

This work aims to create knowledge in the field of these lightweight electrochemical energy storage applications. The focus is on the technology of sodium-ion batteries and supercapacitors utilizing onion-like carbon as active material. Key aspects addressed concern the effects of active material treatment prior to electrode production via structural, physical and chemical modification to enhance the capability to store energy but also to facilitate the production of sustainable electrodes.

2 Characteristics and analytics of electrochemical energy storage

2.1 Electrochemical energy storage

For mobile electrochemical energy storage solutions, the weight of the devices expressed in their energy density is crucial, as they have to be carried alongside the electric consumer. Beside the energy density, also the time needed to charge and discharge is of importance. These two parameters distinguish supercapacitors and batteries (Fig. 2).[5] Among electrochemical energy storage applications, batteries offer a high energy density but lack specific power density, as they require long charging and discharging times in range of hours (Fig. 1). Prominent examples in battery technology are sodium-ion (SIB), lithium-ion (LIB) or lead acid (LA) batteries. Supercapacitors can be charged and discharged within minutes but store less energy compared to batteries (Fig. 2). Supercapacitors can be further dived into Electric double layer capacitors (EDLC) which solely rely on an electric field to store energy and pseudocapacitors which are an intermediate technology and therefore, can not be separated conclusively from batteries.[5]

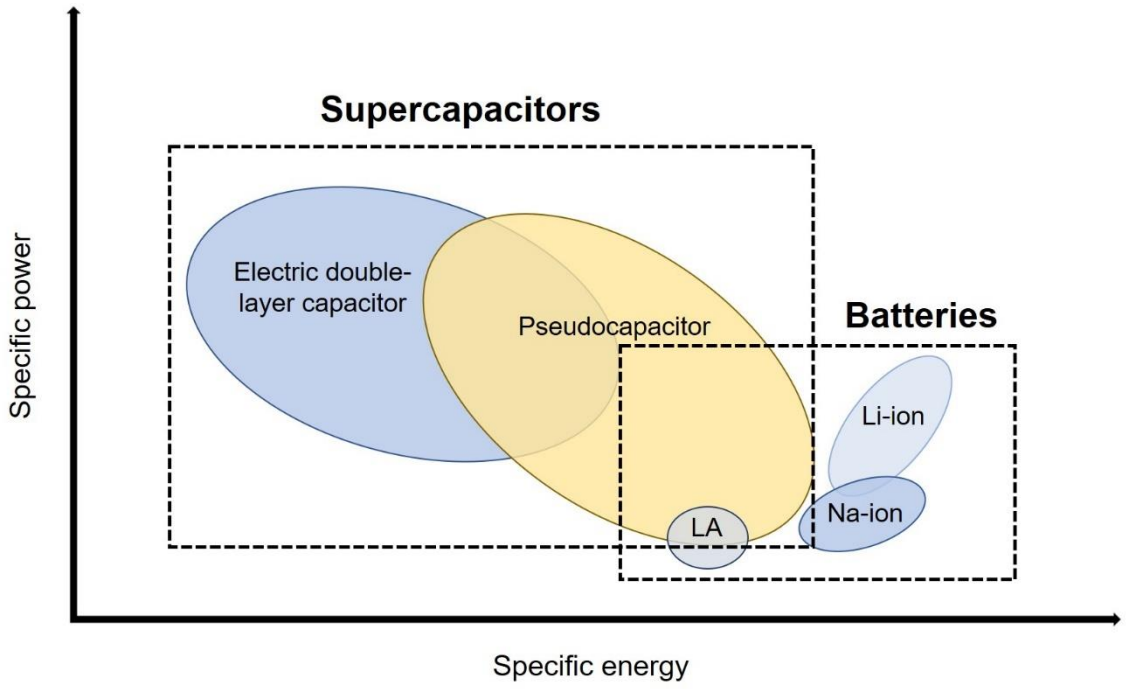

Fig. 2: *Ragone plot for energy storage technologies featuring their specific power plotted against their specific energy. Figure modified using the CC BY 2.0 license from ref. [6] and permission from ref. [7]*

2.1.1 Batteries

Batteries or electrochemical cells consist out of two half-cells featuring different active materials (Fig. 3). In each half-cell, energy is stored by electrochemical redox reactions promoted by their active material (1). The electrical current required for the reaction from the oxidized state *Ox* towards the reduced state *Red* is externally introduced by an electric field acting as a driving force and source of energy.[8]

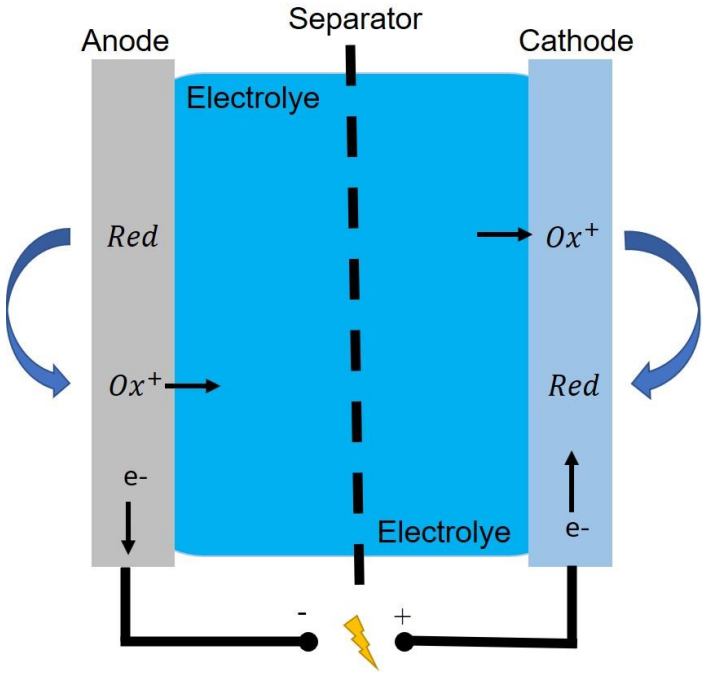

Fig. 3: *Schematic representation of an electrochemical cell with a redox reaction at the anode and cathode. Both electrodes are connected ionically with the electrolyte and mechanically isolated by the separator.*

$$ox^+ + ne^- \rightleftarrows red \quad (1)$$

The energy is then transferred and stored in the bulk of active material by the redox reactions (Fig. 3). This electrochemical reaction is reflected energetically by the potential difference *E* between the reduced (red) and oxidized state (ox) of the active material of the respective half-cell. This relation is explained by the Nernst equation[9]:

$$E = E_0 + \frac{kT}{v_e e}\, ln\left(\frac{a_{ox}}{a_{red}}\right) \quad (2)$$

Where a_{red} or a_{ox} is the activity of the respective redox species, *k* the Boltzmann constant accounting for the probability of the oxidized (reduced) state with regard to the temperature *T*,

the electron transfer number v_e and the elementary charge e. The potential E_0 is the standard reduction potential of the redox pair in one electrode versus the reduction potential of a standard hydrogen electrode. The resulting electrochemical potential E reflects the driving force to release the energy by reversing the reaction and reversing the phase transition of the active material. By reducing (oxidizing) the active material the flow of electric current is also reverted, resulting in discharging of the half-cell back into equilibrium.[9] The energy, which was stored in the device by overcoming the reaction barrier of the charge transfer process, is now available to perform work. The transport processes are enabled by an electrolyte, which acts as an insulator for electrons but as a conductor for ions, necessary to maintain charge neutrality in the system.[2]

The active material undergoing redox reactions is a substantial element for the electrochemical cell and therefore, of key interest. The first rechargeable cells, using lead as active material were developed by Faston Plante (1859).[10] Although known for over 150 years, the lead acid (LA) technology is still widely used today with 29% of battery market share in 2019.[11] The wide usage can be explained by the resilience and therefore, reliability of the system.[12] Beside lead acid technology, lithium-ion batteries are ubiquitously used and also account for roughly one third of the battery market.[12] The outstanding electrochemical potential of alkali metals in combination with their light weight, especially for sodium and lithium, makes those elements promising candidates for a system with high power and energy density.[13] The first rechargeable cell using lithium metal was described in 1913, however it took another 75 years until a system was established by Akira Yoshino which combined satisfying operating conditions regarding size, safety, cyclability, capacity and temperature.[14] As the earlier versions with solid lithium metal electrodes tended to explode after experiencing mechanical stress, the secondary battery of Yoshino used soft carbon to host lithium ions in the anode.[15] This charge storage principle, known as intercalation is fundamental for the lithium-ion battery technology.[16] With soft- and hard carbon, two different kinds of carbon material can be used for this ion intercalation. Soft carbon consists of turbostratically stacked carbon layers, which can be graphitized at high temperatures (3000 °C) (Fig. 4). [17]

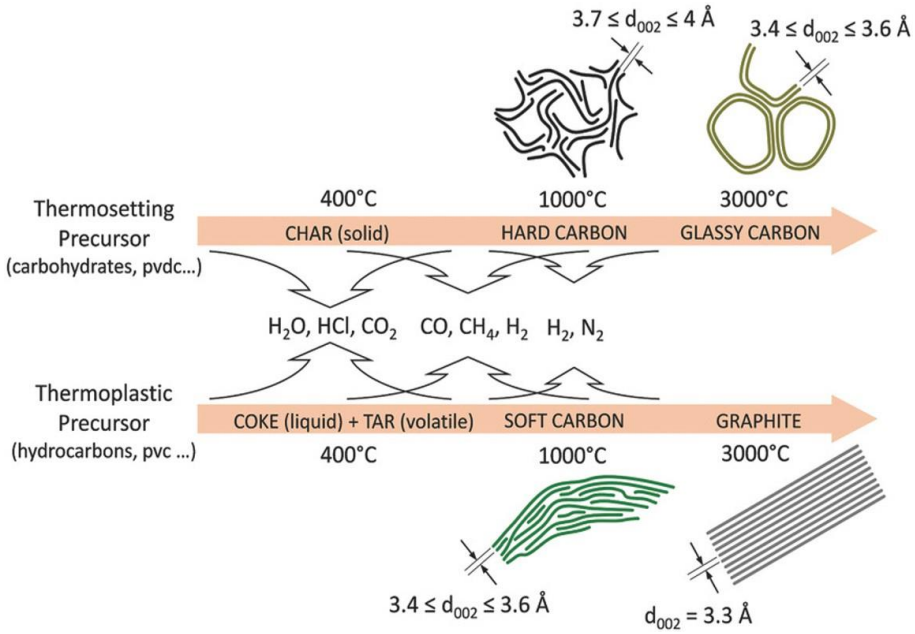

Fig. 4: *Schematic high temperature reaction of different carbon precursors and their high temperature modifications. Figure adapted under license with CC BY-NC-ND 4.0 from ref. [17]*

Hard carbon is non-graphitizable as its precursors are carbon sources like biomaterials or phenolic resins with highly crosslinked structures, whose pyrolysis products do not decompose to a liquid stage. Hard carbon offers various defects which interconnect individual carbon layers leading to a structure comparable to partial crystallinity observable in many polymers. This disorder, originating from the crosslinked precursors creates pores and increases the distance between the carbon layers.[18] For lithium ions, the layer distance of graphite is perfectly suited to accommodate them in between the individual graphene layers forming a graphite intercalation compound LiC_6 (Fig. 5a). This LiC_6 intercalation compound offers a theoretical specific capacity of 372 mAh/g. Sodium ions with their ionic binding character with carbon[19] lead to an energetically unfavorable intercalation compound of NaC_{64} (Fig. 5b) featuring a theoretical capacity of only 35 mAh/g.[20] For sodium ion storage, hard carbon is a more attractive active material, which was shown by Dahn[21] leading to an increase in research activity in the field of SIB (Fig. 5c and d). In contrast to soft carbon or graphite, hard carbon offers a higher interlayer distance between the carbon sheets and also provides more active sites for charge transfer reactions due to various voids and pores originating from its discorded structure (Fig. 5d). SIB featuring biomass derived hard carbon anodes reaching specific capacities around 370 mAh/g [22] can compete with LIB technology.

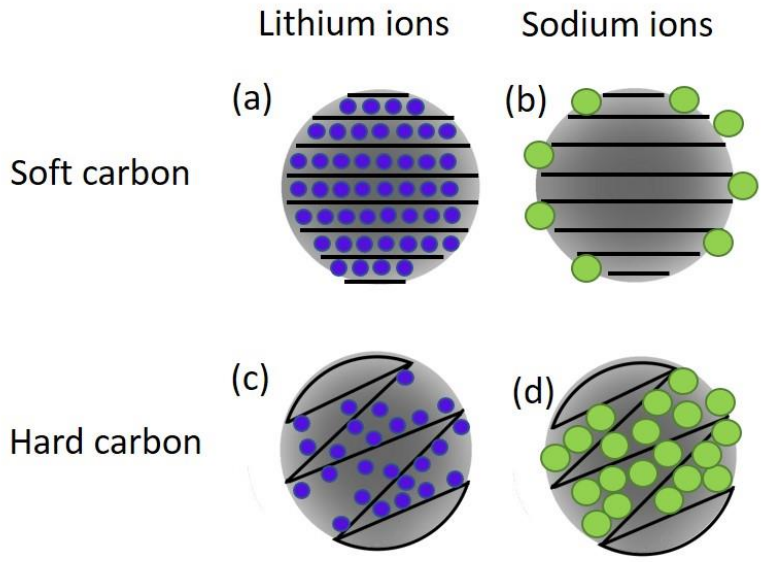

Fig. 5: *Schematic overview over storage of lithium ions (a, c in blue) and sodium ions (b, d in green) in hard and soft carbon active material. Figure modified with permission from ref. [23]*

How storage sites in an active material get successively occupied during charging is still part of research with models like the "House of Cards" theory in discussion.[24] The capacity of an entire cell is limited by the amount of transferred charge, while the power is dictated by the potential, at which the reactions take place. These reactions rely on mass transport in the bulk, entailing an expansion and contraction of the active material due to the phase transition. By nature, those volumetric changes are structurally demanding processes as they are accompanied by mechanical stress, which deteriorates the electrode and their capacity. Besides the mechanical stress also, a high potential, favorable for a high power density, is a driving force for irreversible side reactions. Those side reactions can consume the electrolyte or the active material, which decreases the concentration of mobile charge carriers and ultimately the capacity of the system.[25]

2.1.2 Supercapacitors

Like batteries, supercapacitors consist out of two electrodes, physically disconnected by a separator. The electrodes are immersed in electrolyte, which connects them ionically but is insulating for electric current. In contrast to batteries, charge storage in supercapacitors does not require phase transition or reaction in the bulk material of the electrodes, as no charge transfer occurs between electrolyte and electrode.[26] As energy is only stored on the surface

of the electrode, supercapacitors possess lower energy density compared to batteries (Fig. 2). However, they show also certain advantages of the system regarding its reactivity. With pseudocapacitors and electrochemical double layer capacitors (EDLC) there are two different types of supercapacitors [5] whose characteristics are explained in detail in this chapter.

2.1.2.1 Electrostatic double layer capacitors

When storing electrochemical energy in an electrode of a supercapacitor, the charge carriers are transferred into the electrode consisting of a conductive active material. This current is initiated by an external electric field and with the density of charge carriers, the potential of the electrode is increased. Inside of the supercapacitor, the charge of the electrons or holes in the electrode attracts oppositely charged ions from the electrolyte. As a result, pairs of charge carriers and counterions form an electrostatic double layer at the solid to liquid interface of the electrode as described in the Helmholtz model (Fig. 6a).[27]

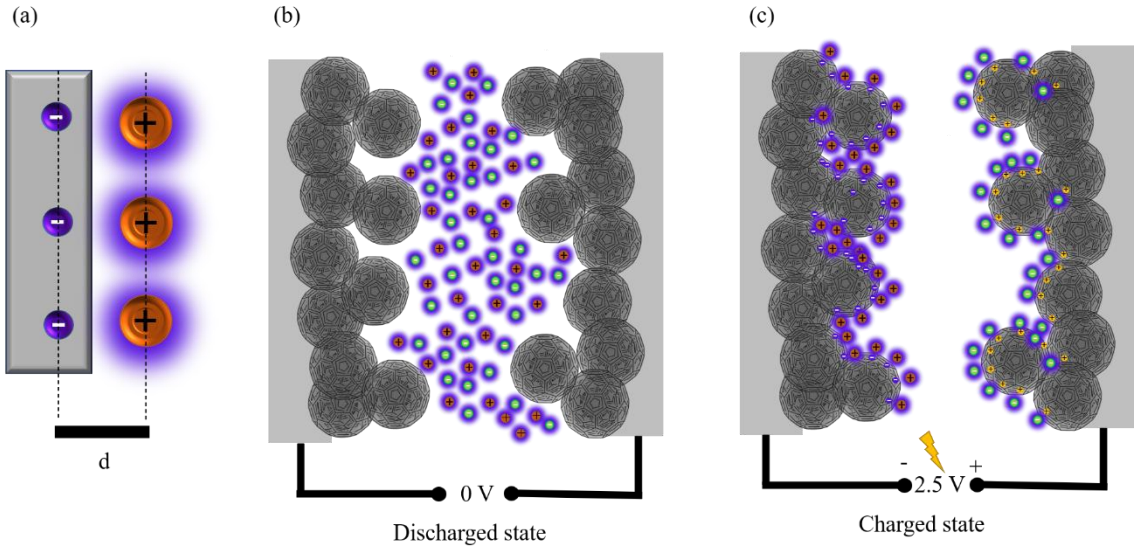

Fig. 6: *Schematic overview of the charge storage in supercapacitors with the Helmholtz layer (a); and schematic representations of a discharged (b) and charged (c) symmetrical electrochemical double layer capacitors. The black spheres represent the active material where the charges (for electrons in purple and for holes in yellow) are located and the ions are absorbed (for positive orange and for negative cyan), the blurry purple area surrounding the ions represents the solvent shell surrounding them.*

By assembling pairs of charge carriers and counterions, the energy can be stored without the need to increase the externally applied voltage (Fig. 6b and c). Therefore, the capacitance *C* is limited to the number of active charge storage sites available at the given potential. Beside the number of charge storage sites which increases with the surface of the electrode *A* also to the

distance *d* between those charge carrier pairs (Fig. 6a) is a factor for the capacitance of the electrode (3).

$$C \sim \frac{A}{d} \tag{3}$$

For liquid electrolyte supercapacitors, the physical distance between the electrode and the ion *d* is restricted by the thickness of the solvent shell of the ions in the electrolyte solution. Following this equation, the capacitance of the electrode can be greatly enhanced by an increase in surface of the electrode material. This boost of capacitance can be implemented by utilizing porous active materials. Those materials exhibit/possess a sponge-like structure with pores of different sizes and tortuous channels leading to specific surfaces reaching up to 3000 m^2/g. With the specific surface, the number of active sites increases and therefore charge storage capacitance as well. If the surface exceeds 1500 m^2/g, compensate the electric field of adsorbed ions in proximity can not be compensated due to a lack of active material. Thus, further increase in surface does not lead to additional capacitance.[28] Beside a high specific surface a performant active material must feature adequate supply and accessibility for the solvated counter ions of the electrolyte. During the limited timeframe of charging or discharging of the electrode these counter ions with their solvate shell, must move from reservoirs into and also out of the structures of the active material (Fig. 6b and c). This tradeoff between surface and accessibility is addressed by the choice of active materials and electrolyte. While state of the art commercial supercapacitors are based on activated carbon[29], research is ongoing to use other materials from the large family of carbon modifications like graphene,[30, 31] carbon nanotubes,[32-34]carbon nanofibers,[35, 36] xerogels,[37] biomaterials,[38] quantum dots[39] and onion-like carbon[40-42] in order to maximize the double layer capacitance, which currently achieves values around 300 F/g at charging rates of 1 A/g.[43] Unlike batteries, EDLC charge storage reactions do not involve a structurally demanding phase change of the active material, which results in superior kinetics, power density and a lifetime of over one million cycles for supercapacitors.[5]

2.1.2.2 Pseudocapacitors

Similar to batteries, pseudocapacitors store energy using redox reactions. The difference to the battery is that charge transfer reactions of a pseudocapacitors occur on the surface rather than in the bulk of the active material.[44] The faradaic reactions also do not proceed at a specific potential like in a battery, but in a wide window at infinitely variable potentials, caused by the

difference in accessibility for ions and electrons for each functional site. By a continuous overlap of these at infinitely variable potentials over a wide potential window, the characteristic capacitive behavior can be observed for pseudocapacitors.[45] Like in EDLC, the current increases linearly with the potential of the pseudocapacitors, which distinguishes the technology from a battery type energy storage.[44] With redox pseudocapacitance, underpotential deposition pseudocapacitance, doping pseudocapacitance and intercalation pseudocapacitance, there are several types of pseudocapacitors relying on different faradaic surface reactions (Fig. 7).[46]

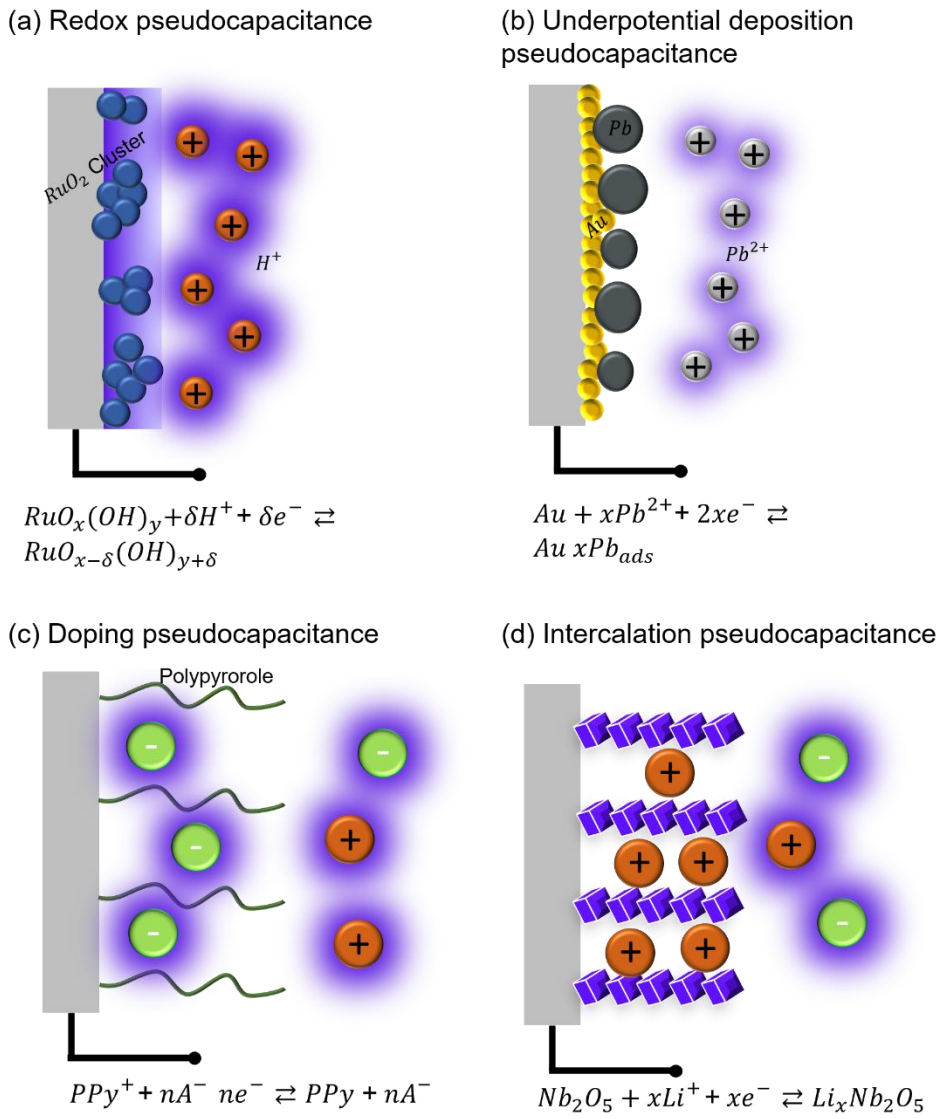

Fig. 7: *Schematical overview over the different type of pseudocapacitors: (a) Redox capacitance, (b) underpotential deposition pseudocapacitance (c) doping pseudocapacitance (d) intercalation pseudocapacitance. Figure modified with permission from ref. [5]*

These surface redox reactions bring several benefits: as there is no phase transition of the bulk material involved during charging and discharging, reducing the stress and its negative structural impact. Redox pseudocapacitance stores energy by forming clusters of transition metal oxides like ruthenium oxide (theoretical capacitance ca. 2000 F/g), [47] manganese (theoretical capacitance ca. 1370 F/g)[48] and cobalt oxide (theoretical capacitance ca. 4000 F/g)[48] at the electrode surface (Fig. 7a). Underpotential deposition pseudocapacitance features metal ions like lead[49] or copper[50] which are dissolved as electrolyte and can be reduced for energy storage, forming a monolayer on the electrode (Fig. 7b).[51] Beside those reactions, there is also doping pseudocapacitance which utilizes conductive polymers as active material (Fig. 7c). For energy storage, the polymer is oxidized and the charge is counterbalanced by ion insertion, which is called doping.[52-55] This is possible due to the π-electron system extension alongside the backbone of the polymer, as well as its oxidative stability. Conductive polymers currently used for doping pseudocapacitors are polyaniline (PANI, theoretical capacitance ca. 750 F/g)[56] poly(3,4-ethylenedioxythiophene) (PEDOT, theoretical capacitance ca. 210 F/g)[57] or polypyrrole (PPY, theoretical capacitance ca. 620 F/g).[56] Pseudocapacitive intercalation (Fig. 7d) combines the capacitive as well as the diffusion limited ion insertion mechanisms described in section 2.1.1. Therefore, this process is considered fast intercalation, however a sharp distinction between battery and pseudocapacitive intercalation can not be made. Therefore devices based on this charging mechanism are considered as hybrid technology.[58]

As the redox active sites are adsorbed on the surface without their solvent layer, more active sites are available for energy storage compared to EDLC. This explains a higher specific capacitance of pseudocapacitors. With those features, pseudocapacitors fill a gap between EDLC and batteries. This edge in specific capacitance comes at the price of sluggish kinetics for electrodes, due to slow ion diffusion and a lack of conductivity in the case of metal oxides. For electrodes using conductive polymers, swelling and shrinking due to repeated ion insertion and extraction from the active material, results in stress leading to cracks and ultimately deteriorates the capacitance. To offset those drawbacks, composites using carbon as stabilizing and conductive backbone are subject of ongoing research. [5]

2.2 Carbon nanomaterials for energy storage

The active material, as the location where the charge is stored, is the key element for each of the presented electrochemical energy storage applications. Different storage mechanisms

require tailor-made active materials to fulfil the unique requirements. Carbon with its various modifications, high abundance and cheap price excels in this challenging operational area.[59] Especially sp^2-hybridized and carbonized solid modifications are of particular interest. Those carbon materials provide sufficient conductivity for the electrons to reach the active sites of the material where energy is stored.[28]

The carbon surface and its structure is the key area for charge transfer reactions in batteries and for the formation of the electrostatic double layer in EDLC. Consequentially, the porous character is of special interest. Each technology requires an active material with specific dimensions and pore sizes offering efficient active sites for energy storage.

According to the use of different electrolytes, a suitable structure of the carbon surface and its pores must be ensured.[60] Following those considerations, knowledge about the surface of the carbon material, porosity including size of the pores, their shape and distribution is of central interest in order to design performant active materials. Key challenge is to balance the tradeoff between surface area and accessibility of the pores mentioned in section 2.1.2.[43] To unify the comparison of materials, whose porosity is usually determined by physisorption, three classes of pore sizes are defined:[61]

- Micropores < 2 nm
- Mesopores 2-50 nm
- Macropores > 50 nm

Beside the porosity, carbon materials can be categorized by their dimensionality. There are 0D, 1D, 2D and 3D carbon materials like fullerenes (Fig. 8a) carbon nanotubes (CNT, Fig. 8b) or graphene (Fig. 8c) and graphite (Fig. 8d).[62]

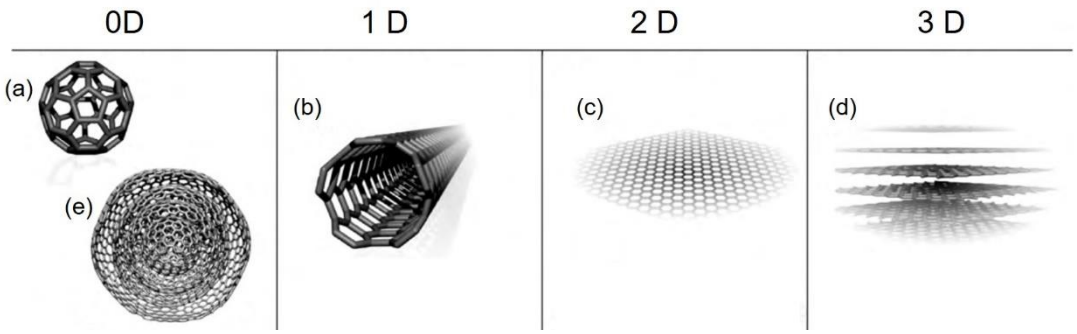

Fig. 8: *Examples for 0D, 1D, 2D and 3D carbon materials. Figure modified with permission from ref. [63]*

If fullerenes are stacked concentrically the spherical structures can extend to size of around 10 nm and above. Those structures are known as onion-like carbon (Fig. 8e) due to their multi-layer assembly, reminiscent of onions. Described by Ugarte in 1992,[64] these multiwall structures can be synthesized from sp^3 carbon precursors like nanodiamonds by annealing[65-68] at high temperatures but also by other methods like beam irradiation,[64, 69] arc discharge,[70] chemical vapor deposition[71, 72] or pyrolysis.[73] OLC is a promising active material as they are synthetically produced and do not entail geopolitical risks like other carbon electrode materials like graphite, which was recently labeled as critical raw material by the European Union.[74] OLC is also considered as a material of low toxicity[40] and features a high degree of external porosity[75] desirable for EDLC applications.

Like many carbon materials, OLC show a distribution of micro-, meso and macropores. For OLC, this distribution is determined by the size of the primary particles and the packing of those spherical particles. The packing is influenced by the method of manufacture[67] as well as the post-production treatment and agglomeration. Residual amorphous carbon can clog micropores by forming sinter necks at the contact points of primary particles.[75] This amorphous interparticle connection promotes the formation of macroporous voids within the secondary particles. The mesoporosity in OLC agglomerates is a result of octahedral and tetrahedral pores in the dense packing of equal spheres,[75] as shown for a cubic close packing (Fig. 9a and b).

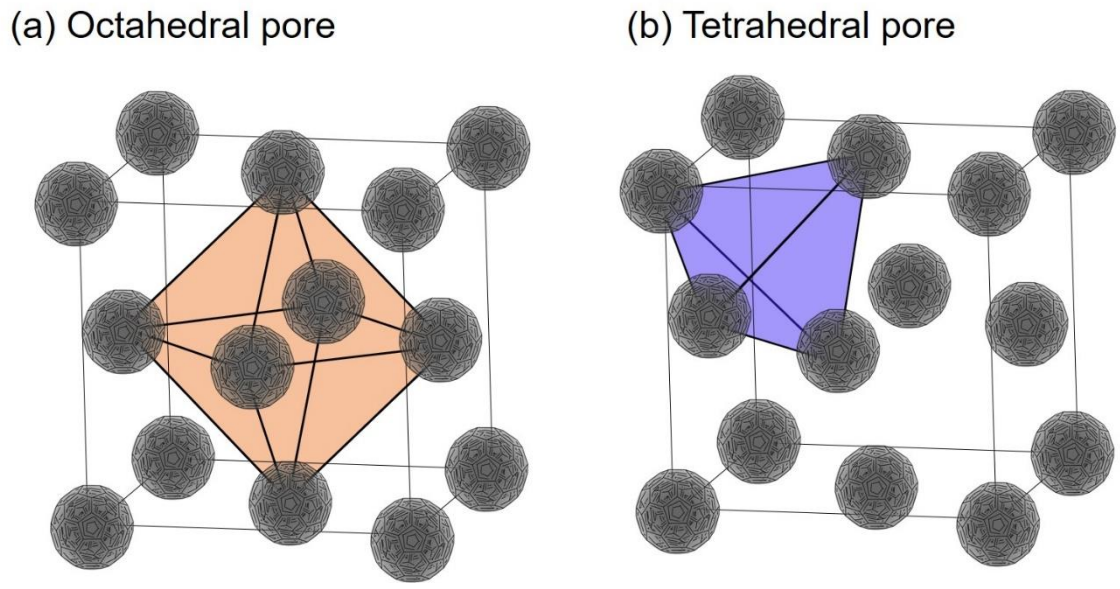

Fig. 9: *Pores schematically displayed in a cubic close packing of onion-like carbon.*

With the diversity of pores and a moderate but highly accessible specific surface, OLC represent a platform for energy storage, which can be widely used in energy storage devices. In batteries, OLC are utilized as active material[76] but also as conductive additive.[77, 78] OLC are also applied as active material in EDLC[42, 79-82] as well as in pseudocapacitive applications,[82-86] where the external surface is a suitable template for redox active functionalization e.g. with conductive polymers,[85, 87, 88] quinones[89, 90] or transition metal oxides.[83, 91]

2.3 Electrochemical characterization

For electrochemical measurements, the potentiostat is the instrument of choice as it is capable of applying different input potentials, currents and frequencies and is able to report the system's electrical response This response can be assigned to various processes responsible for energy storage but can also expose side reactions within the system. With cyclic voltammetry, galvanostatic charging and electrochemical impedance measurements three key techniques are explained in the following subsections

2.3.1 Cyclic voltammetry (CV)

Cyclic voltammetry (CV) is a standard technique to detect and evaluate electrochemical processes within a specific potential window. The potentiostat varies the voltage between the electrodes with a constant linear rate, called sweep or scan rate, until the desired potential is reached. During this voltage change, the system responds by a flow of the electric current.[92] A rise or peak current is indicating the occurrence of a reaction or charge storage process, which can be attributed to a certain potential. After the desired potential limit is reached, the current is reversed until the starting potential is reached, again with a predefined scan rate. By reversal of this process, back reactions of the system can be observed with the potential information as well as the corresponding current.[5, 93] This delivers information on the type and reversibility of reactions observed in the system but also reveals if undesired side reactions are occurring.[92] By repeating this experiment, the irreversibility of the reaction can be monitored over a wider time window. Additional information regarding the charge storage capacitance of the device can be extracted by integration of the current as a function of time (4).

$$C_{CV} = \frac{\int_{t_0}^{t_1} I\,(t) * dt}{2 * \Delta V} \tag{4}$$

The shape of the CV curve is characteristic for the type of charge storage mechanism of the material and originates from the current response of the material. As explained earlier, this allows a classification between electrochemical double layer, pseudocapacitance and battery-like behavior (Fig. 10).[94]

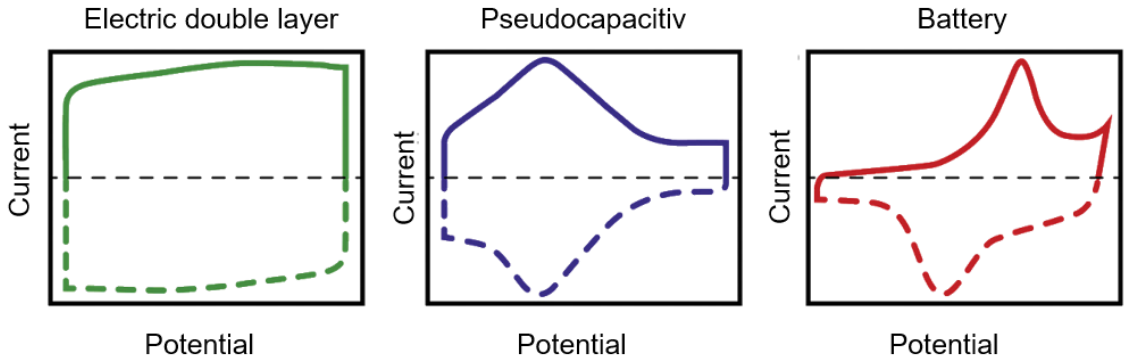

Fig. 10: *Comparison of different charge storage mechanism and their characteristic shape in CV measurements. Figure modified with permission from ref. [94]*

By adjusting the scan rate, the kinetics of the processes, like fast charging and discharging of the device, can be investigated. Also, the life cycle of a device can be analyzed by long term measurements with thousands of cycles. CV can be performed using a two- or three-electrode setup (Fig. 11).

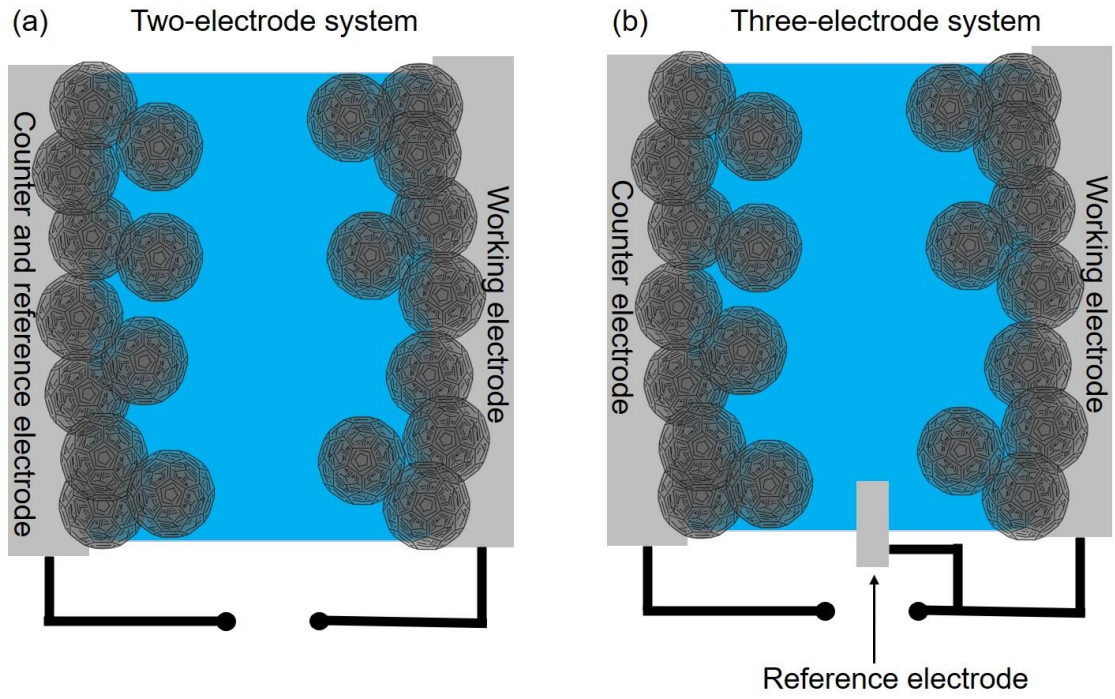

Fig. 11: *Schematic cell setup with: (a) symmetrical two-electrode system and a (b) three-electrode system.*

The two-electrode system consists of working and counter electrodes, the latter simultaneously acting as reference electrode (Fig. 11a). In contrast, the three-electrode setup consist of three individual electrodes (Fig. 11b). The reference electrode in an ideal three-electrode setup is not taking part in any reactions and no current is flowing. The main advantage over the two-electrode system is that the potential of the reference electrode should remain constant, allowing an accurate determination of the potential of the working electrode.[95] Therefore, three-electrode systems are used for research of individual specific cell components and to analyze processes in asymmetrical electrodes.[92] The two-electrode configuration, as a more simple and therefore cost efficient system, is used to characterize final devices or prototypes.[96]

2.3.2 Galvanostatic cycling (GC)

Galvanostatic cycling maintains a constant current flow *I* into the cell while the potential response of the system is tracked. Again, the direction of the current flow is reversed, if a predefined cutoff voltage is reached.[92] Where CV can be used to determine at which potential processes occur, GC is used to estimate how long those processes at a certain potential proceed. The constant current fed into an electrode is directly linked to an electrochemical process

during the experiment. When the current is plotted versus the applied voltage, discreet reactions form a plateau at certain potentials. By measuring the time *t* the current was maintained at a certain potential the electrochemical process can be characterized.[5] This enables to quantify the capacitance C_{GC} of a capacitor (5) but also the kinetics and cyclability can be investigated as a function of current density:[95]

$$C_{GC} = \frac{I * t}{V} \tag{5}$$

GC is also qualified to estimate the internal series resistance R_{ES} of the device. This resistance, resulting from switching the polarity of the electrode, can be retrieved with Ohms law (6) by dividing the drop in voltage U_{IR} by the applied current.[92]

$$R_{ES} = \frac{U_{IR}}{I} \tag{6}$$

Like CV, the GC graph exhibits characteristic shapes, which allow conclusions towards the nature of the system, which again allows a classification of the active material (Fig. 12).[94]

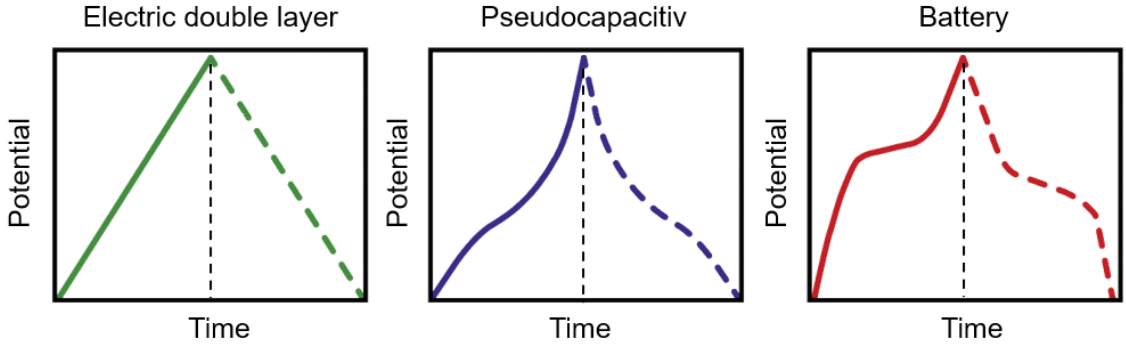

Fig. 12: *Comparison of different charge storage mechanisms and their characteristic shape in GC measurements. Figure modified with permission from ref. [94]*

2.3.3 Electrochemical impedance spectroscopy

Electrochemical impedance spectroscopy (EIS) is another complementary technique, where the applied voltage (or the current) is switched sinusoidally between two set potentials at different frequencies.[97] The impedance of the system is determined from the magnitude and phase shift of the current (or the voltage) response. The frequency dependent impedance spectrum corresponds to characteristic features and processes at the interfaces of the system. The impedance is represented as a complex quantity with a real part Z' and the imaginary part

Z'' of the resistance. The measurement is performed on systems at steady-state conditions and typically evaluated using a Nyquist plot (Fig. 13a) where Z' is plotted versus the Z'' at different frequencies. The Nyquist plot is starting at very high frequencies in the region of MHz, where the cell usually behaves like a resistor. From these high frequencies, the resistance of the system (composed of electrode, electrolyte, contact resistance of electrode and current collector) can be determined (Fig. 13a, position 1).[98-101] When reducing the frequency, the time window is sufficient for processes like charge transfer reactions (Fig. 13a, position 2)[102, 103] and the formation of a double layer (Fig. 13a position 3).[104] Those processes are indicated by a change in system response forming a semi-circle respectively a 45° slope in the Nyquist plot. Again, the shape of the curve can help to identify the nature of the energy storage mechanism (Fig. 13b).[94]

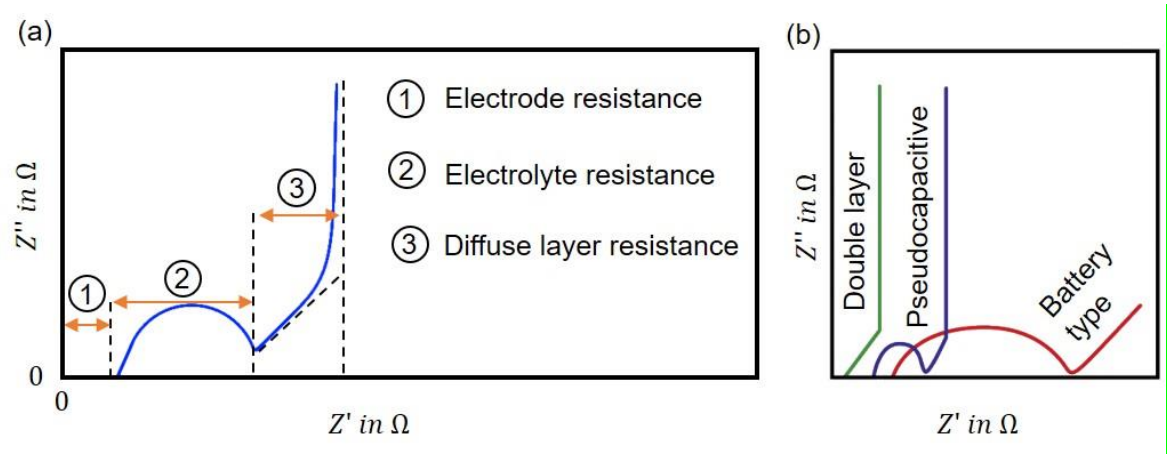

Fig. 13: *(a) Characteristic resistance in electrochemical impedance adapted from.[98] (b) different charge storage mechanism and their characteristic shape in GC measurements. Figure modified with permission from ref. [94]*

2.3.4 Performance Evaluation

The methods of CV, GC and EIS are applied for energy storage applications to determine the performance of the device and to benchmark against other applications (Tab. 1 and Fig. 14). Metrics often used for these purposes are cycling stability, specific capacitance, energy and power density.[92, 105, 106]

Tab. 1: *Performance evaluation metrics and equations for supercapacitors.*

Performance metric	Equation	Ref.
Specific capacitance of the device $C_{sp\,T}$ Total capacitance C_T Total mass of active material m_T	$C_{sp\,T} = \frac{C_T}{m_T}$	(7)
Capacitance of one electrode C_e Specific capacitance of one electrode $C_{sp\,e}$ Active material mass of one electrode m_e	$C_{sp\,e} = \frac{C_e}{m_e} = \frac{4 * C_T}{m_T}$	(8)
Cyclability measured by retained capacitance C_C Initial capacitance C_0 Capacitance after cyclization C_1	$C_C = \frac{C_0}{C_1}$	(9)
Energy density E_D Voltage window $\mathrm{V_0}$	$E_D = \frac{C_T * \mathrm{V}_0^2}{2\,m_T}$	(10)
Power density P_D Internal series resistance R_{ES}	$P_D = \frac{\mathrm{V}_0^2}{4\,m_T * R_{ES}}$	(11)

Cycling stability, which is a parameter to estimate the lifetime of a device, is calculated as the retained capacitance after the capacitor ran through a specific number of cycles performed either in GC or CV mode.[107] The specific capacitance of one electrode or the supercapacitor is calculated based on the amount of active material used. To compare the performance of supercapacitors and batteries, the respective energy density and power density are often reported in a Ragone plot.[108] This plot can also be used to compare other (non-)electrochemical storage applications.[92]

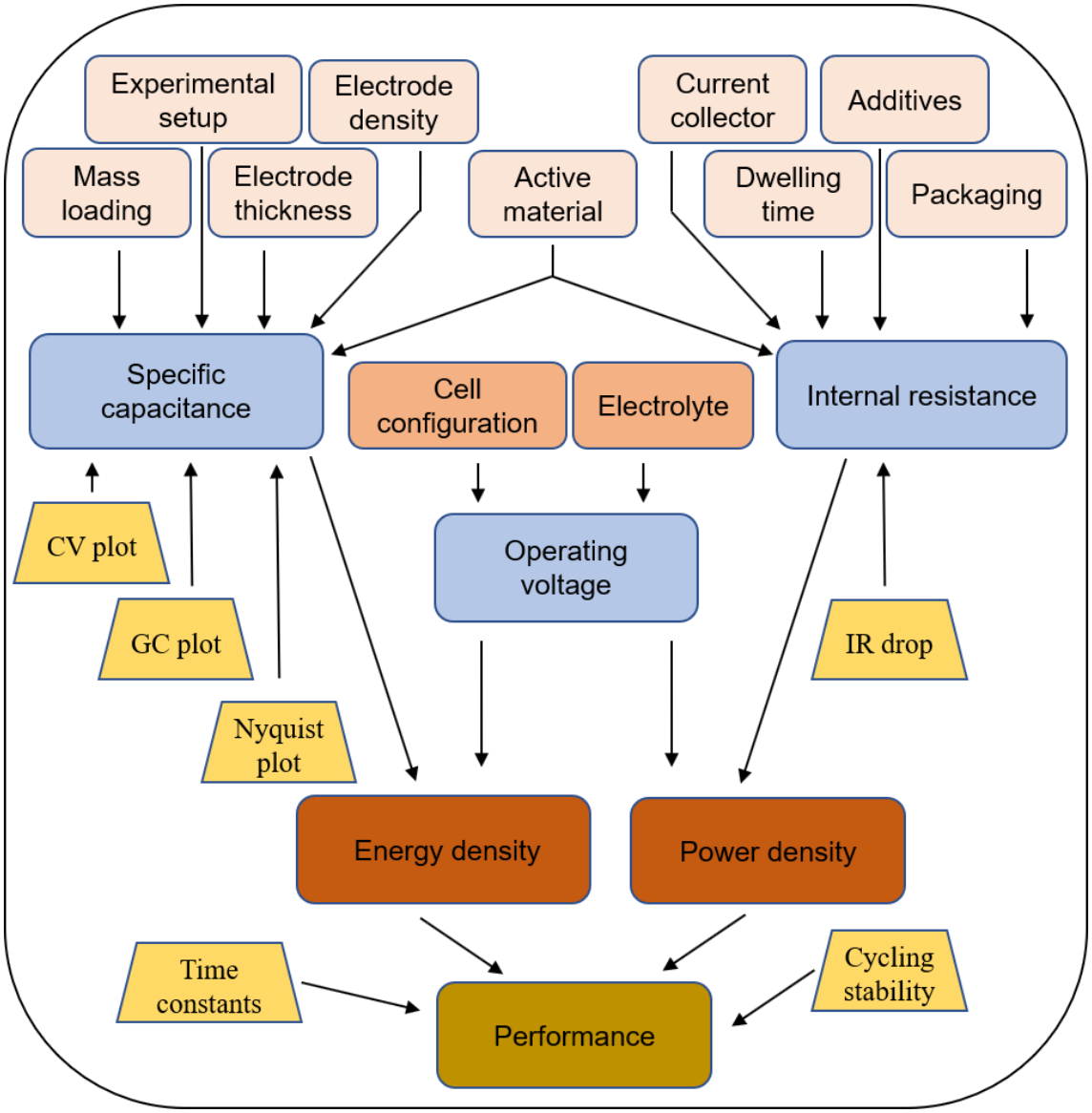

Fig. 14: *Different factors affecting the performance of supercapacitors as well as their measurement techniques. Figure modified with permission from ref. [92]*

However, the performance evaluation of energy storage devices in research is difficult. This is mainly attributed to a lack of a standardized cell setup originating from enormous diversity of active materials with different requirements and availability. Beside the active material itself, also its treatment and processing in the electrode influences the performance.[109] Changes in electrode thickness, density and mass loading can affect the capacitance and ultimately the performance of the supercapacitor. Also, additive materials like binders or conductive agents as well as the current collector, the material and dimensions of the separator and the type of electrolyte which is used, heavily affect the performance of a specific device.[92, 107, 109]

2.4 Structual characterization of the active material

To evaluate and compare the characteristics of different active materials analyses on a nano scale can be performed. To gain structural and morphological information in this range, electron microscopy and X-ray investigations are suited.

2.4.1 Electron microscopy

Scanning (SEM) and high-resolution transmission electron microscopy (HRTEM) are two techniques to reveal nanoscopic structures using a beam of electrons. This high resolution is made possible by the small wavelength corresponding to electrons,[110] a major limiting factor in resolution known as Abbe-limit.[111] The wavelength λ of the electrons is determined according to the wave-particle duality postulated by De Broglie[112] (12) based on the acceleration voltage $U_a$in the electric field, where h is the Planck constant and e and m_e the charge and mass of an electron.[113]

$$\lambda = \frac{h}{\sqrt{2m_e * e * U_a}} \tag{12}$$

The theoretical resolution derived from the wavelength is limited in practice due to interactions of the electrons with the sample material, as an increase in acceleration voltage also increases the depth of penetration into the sample. This results in a prolonged path of the electron in the material from the focus point of the incident electron beam. This local separation of signal and response is blurring the image forming information.[114] On the other side, interactions are essential for scanning electron microscopy as they promote backscattering of primary electrons as well as the formation of secondary electrons, which both can be detected for imaging.[115] According to this tradeoff, the acceleration voltage has to be balanced with regard to the sample material. Typical acceleration voltages for SEM are between 2 and 40 kV.[116] Detecting secondary electrons provides contrast in surface morphology whereas acquired backscattered electrons are capable of showing a contrast in material compositions.[117] The preparation of a conductive sample usually does not include a sputtering step, which is necessary for insulating materials to prevent surface charging otherwise influencing the measurement.[118] SEM measurements require a vacuum atmosphere to ensure a sufficient mean free path for the electrons on their way from source to sample. Otherwise, the collision with air molecules would result in deflected electrons corrupting the measurement.[119] A tight connection to the sample

holder is usually realized with electrically conductive adhesives.[120] Beside morphology and material contrast, SEM measurements, especially in the field of energy research, provide parameters of the electrode cross section like thickness of the active material layer, its particle arrangement, binder or additive distribution and effect of calendaring.[121] Also, measurements before and after cyclization deliver insights on possible rearrangements of the active material and highlight potential problems like the formation of cracks, corrosion of current collector or delamination which all are indicating the deterioration of the electrode.[122]

For high resolution transmission electron microscopy (HRTEM), relying on accelerating voltages up to 1300 kV,[123] the drawback of electron diffusion is bypassed as it is ensured that the sample thickness is so small that the electrons can penetrate it.[124] With this detection method, interactions of electrons and sample material occur to a much lower extent, which results in superior resolution compared to SEM.[125] However, a high accelerating voltage implies electrons with high energy. This energy is introduced into the sample, potentially altering the sample structure, thus decreasing the information value of the measurement. To avoid damage of the sample, the accelerating voltages has to be adjusted for each individual sample.[126] With a superior resolution compared to SEM, HRTEM measurements are focused on processes in discreet active material particles rather than on the entire electrode. HRTEM delivers information about the nanoscopic arrangement of individual particles and can estimate sub-nanometer structural information like the interlayer distance of a carbon material.[126] Structural changes to the particle for example caused by mechanical milling[127] or delamination of the layers [128] due to cyclization can be investigated. Another application of HRTEM is to reveal modifications of the particles by coating or functionalization.[129, 130] The sample preparation of powder active materials is straightforward by dispersing the material in water followed by sieving the solution onto a copper grid, which is coated with a carbon membrane.[131]

2.4.2 X-ray diffraction (XRD)

In contrast to SEM and HRTEM measurements, which provide information about specific particles or small areas of the sample, X-ray diffraction (XRD) delivers an overview over the properties of the entire sample. While the radiation passes through the lattice of the sample particles, X-rays are reflected on atomic cores of the sample. The scattered X-rays are detected at a specific angle after exiting the sample material. If the specimen possesses repetitive ordered

structures, the X-rays can interact with each other, amplifying the signal which is called constructive interference. If the sample is disordered, the X-rays signal is weakened, which is called destructive interference. With the detection angle θ, diffraction order *n* and wavelength λ of the X-ray known, conclusions regarding the structure of the lattice distance d can be deviated according to Braggs law (Fig. 15 and Eq. (13):[132]

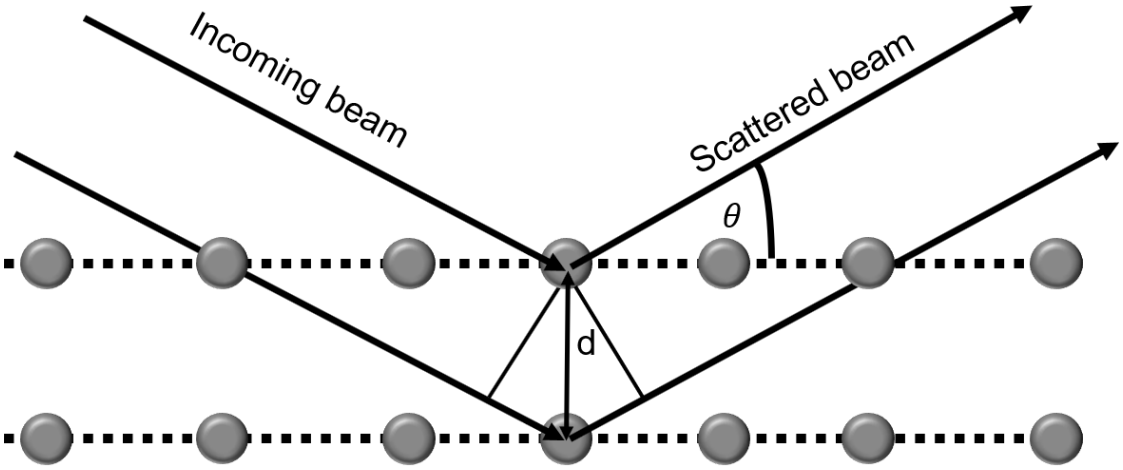

Fig. 15: *Schematic representation of Braggs law. Figure modified with permission from ref. [133]*

$$n\,\lambda = 2d * \sin(\theta) \tag{13}$$

As the particles are randomly distributed in the sample, information over all lattice properties and particles sizes is provided.[134] In contrast to electron microscopy, which only focusses on a small spot of the material, XRD provides information over the entire sample. XRD helps to quickly recognize a promising active material without performing electrochemical testing relying on a complex setup. XRD can help to understand changes of the active material during cyclization,.[135, 136] The measurement itself is nondestructive and does not require special operation.[137] This combination makes XRD a fast and vital tool for active material investigation in the field of energy storage materials. It can for example be used to check the interlayer distance of the sample material and therefore can be used to recognize promising active materials for intercalative energy storage.

2.4.3 References

[1] E. commission, Renewable energy statistics, 2022. https://ec.europa.eu/eurostat/statistics-explained/index.php?title=Renewable_energy_statistics. (Accessed 25.06.2022).

[2] M. Sterner, I. Stadler, Energiespeicher-Bedarf, Technologien, Integration, Springer 2014 605 and 199 ff. https://doi.org/10.1007/978-3-642-37380-0.

[3] M. Sterner, M. Specht, Power-to-gas and power-to-X—the history and results of developing a new storage concept, Energies 14(20) (2021) 6594. https://doi.org/10.3390/en14206594

[4] Y. Balali, S. Stegen, Review of energy storage systems for vehicles based on technology, environmental impacts, and costs, Renew Sust Energ Rev 135 (2021) 110185. https://doi.org/10.1016/j.rser.2020.110185

[5] A. Noori, M. F. El-Kady, M. S. Rahmanifar, R. B. Kaner, M. F. Mousavi, Towards establishing standard performance metrics for batteries, supercapacitors and beyond, Chem Soc Rev 48(5) (2019) 1272-1341. https://doi.org/10.1039/c8cs00581h

[6] N. Zhu, K. Zhang, F. Wu, Y. Bai, C. Wu, Ionic liquid-based electrolytes for aluminum/magnesium/sodium-ion batteries, Energy Material Advances 2021 (2021). https://doi.org/10.34133/2021/9204217

[7] K. Kubota, M. Dahbi, T. Hosaka, S. Kumakura, S. Komaba, Towards K-ion and Na-ion batteries as "beyond Li-ion", The chemical record 18(4) (2018) 459-479. https://doi.org/10.1002/tcr.201700057

[8] M. Zschornak, F. Meutzner, J. Lück, A. Latz, T. Leisegang, J. Hanzig, M. Nentwich, J. Zosel, P. B. Balbuena, Fundamental principles of battery design, Physical Sciences Reviews 3(11) (2018). https://doi.org/10.1515/psr-2017-0111

[9] S. W. Boettcher, S. Z. Oener, M. C. Lonergan, Y. Surendranath, S. Ardo, C. Brozek, P. A. Kempler, Potentially confusing: potentials in electrochemistry, ACS Energy Letters 6(1) (2020) 261-266. https://doi.org/10.1021/acsenergylett.0c02443

[10] A. Dutta, S. Mitra, M. Basak, T. Banerjee, A comprehensive review on batteries and supercapacitors: development and challenges since their inception, Energy Storage (2022) e339. https://doi.org/10.1002/est2.339

[11] K. Yanamandra, D. Pinisetty, A. Daoud, N. Gupta, Recycling of Li-Ion and Lead Acid Batteries: A Review, Journal of the Indian Institute of Science 102(1) (2022) 281-295. https://doi.org/10.1007/s41745-021-00269-7

[12] G. J. May, A. Davidson, B. Monahov, Lead batteries for utility energy storage: A review, Journal of Energy Storage 15 (2018) 145-157. https://doi.org/10.1016/j.est.2017.11.008

[13] J. Zheng, M. S. Kim, Z. Tu, S. Choudhury, T. Tang, L. A. Archer, Regulating electrodeposition morphology of lithium: towards commercially relevant secondary Li metal batteries, Chem Soc Rev 49(9) (2020) 2701-2750. https://doi.org/10.1039/c9cs00883g

[14] M. Li, J. Lu, Z. Chen, K. Amine, 30 Years of Lithium-Ion Batteries, Adv Mater 30(33) (2018) e1800561. https://doi.org/10.1002/adma.201800561

[15] A. Yoshino, The birth of the lithium-ion battery, Angew Chem Int Ed Engl 51(24) (2012) 5798-800. https://doi.org/10.1002/anie.201105006

[16] G. Wang, M. Yu, X. Feng, Carbon materials for ion-intercalation involved rechargeable battery technologies, Chem Soc Rev 50(4) (2021) 2388-2443. https://doi.org/10.1039/d0cs00187b

[17] D. Saurel, B. Orayech, B. W. Xiao, D. Carriazo, X. L. Li, T. Rojo, From Charge Storage Mechanism to Performance: A Roadmap toward High Specific Energy Sodium-Ion Batteries through Carbon Anode Optimization, Advanced Energy Materials 8(17) (2018) 1703268. https://doi.org/10.1002/aenm.201703268

[18] L. J. Xie, C. Tang, Z. H. Bi, M. X. Song, Y. F. Fan, C. Yan, X. M. Li, F. Y. Su, Q. Zhang, C. M. Chen, Hard Carbon Anodes for Next-Generation Li-Ion Batteries: Review and Perspective, Advanced Energy Materials 11(38) (2021) 2101650. https://doi.org/10.1002/aenm.202101650

[19] H. Moriwake, A. Kuwabara, C. A. Fisher, Y. Ikuhara, Why is sodium-intercalated graphite unstable?, RSC Advances 7(58) (2017) 36550-36554. https://doi.org/10.1039/C7RA06777A

[20] J. Xu, Y. Dou, Z. Wei, J. Ma, Y. Deng, Y. Li, H. Liu, S. Dou, Recent Progress in Graphite Intercalation Compounds for Rechargeable Metal (Li, Na, K, Al)-Ion Batteries, Adv Sci (Weinh) 4(10) (2017) 1700146. https://doi.org/10.1002/advs.201700146

[21] D. A. Stevens, J. R. Dahn, High capacity anode materials for rechargeable sodium-ion batteries, Journal of the Electrochemical Society 147(4) (2000) 1271-1273. https://doi.org/10.1149/1.1393348

[22] M. Thompson, Q. Xia, Z. Hu, X. S. Zhao, A review on biomass-derived hard carbon materials for sodium-ion batteries, Materials Advances 2(18) (2021) 5881-5905. https://doi.org/10.1039/D1MA00315A

[23] T. Y. Wang, D. W. Su, D. Shanmukaraj, T. Rojo, M. Armand, G. X. Wang, Electrode Materials for Sodium-Ion Batteries: Considerations on Crystal Structures and Sodium Storage Mechanisms, Electrochemical Energy Reviews 1(2) (2018) 200-237. https://doi.org/10.1007/s41918-018-0009-9

[24] R. A. Adams, A. Varma, V. G. Pol, Carbon Anodes for Nonaqueous Alkali Metal-Ion Batteries and Their Thermal Safety Aspects, Advanced Energy Materials 9(35) (2019) 1900550. https://doi.org/10.1002/aenm.201900550

[25] Y. Li, K. L. Liu, A. M. Foley, A. Zulke, M. Berecibar, E. Nanini-Maury, J. Van Mierlo, H. E. Hoster, Data-driven health estimation and lifetime prediction of lithium-ion batteries: A review, Renew Sust Energ Rev 113 (2019) 109254. https://doi.org/10.1016/j.rser.2019.109254

[26] Z. S. Iro, C. Subramani, S. S. Dash, A Brief Review on Electrode Materials for Supercapacitor, International Journal of Electrochemical Science 11(12) (2016) 10628-10643. https://doi.org/10.20964/2016.12.50

[27] H. Helmholtz, Ueber einige Gesetze der Vertheilung elektrischer Ströme in körperlichen Leitern mit Anwendung auf die thierisch-elektrischen Versuche, Annalen der Physik und Chemie 165(6) (1853) 211-233. https://doi.org/10.1002/andp.18531650603

[28] F. Beguin, V. Presser, A. Balducci, E. Frackowiak, Carbons and electrolytes for advanced supercapacitors, Adv Mater 26(14) (2014) 2219-51, 2283. https://doi.org/10.1002/adma.201304137

[29] W. T. Gu, G. Yushin, Review of nanostructured carbon materials for electrochemical capacitor applications: advantages and limitations of activated carbon, carbide-derived carbon, zeolite-templated carbon, carbon aerogels, carbon nanotubes, onion-like carbon, and graphene,

Wiley Interdisciplinary Reviews-Energy and Environment 3(5) (2014) 424-473. https://doi.org/10.1002/wene.102

[30] Y. Zhu, S. Murali, M. D. Stoller, K. J. Ganesh, W. Cai, P. J. Ferreira, A. Pirkle, R. M. Wallace, K. A. Cychosz, M. Thommes, D. Su, E. A. Stach, R. S. Ruoff, Carbon-based supercapacitors produced by activation of graphene, Science 332(6037) (2011) 1537-41. https://doi.org/10.1126/science.1200770

[31] T. Kim, G. Jung, S. Yoo, K. S. Suh, R. S. Ruoff, Activated Graphene-Based Carbons as Supercapacitor Electrodes with Macro- and Mesopores, Acs Nano 7(8) (2013) 6899-6905. https://doi.org/10.1021/nn402077v

[32] M. Noked, S. Okashy, T. Zimrin, D. Aurbach, Composite carbon nanotube/carbon electrodes for electrical double-layer super capacitors, Angew Chem Int Ed Engl 51(7) (2012) 1568-71. https://doi.org/10.1002/anie.201104334

[33] S. Zhu, J. F. Ni, Y. Li, Carbon nanotube-based electrodes for flexible supercapacitors, Nano Res: Nano Res 13(7) (2020) 1825-1841. https://doi.org/10.1007/s12274-020-2729-5

[34] S. Wen, M. Jung, O. S. Joo, S. I. Mho, EDLC characteristics with high specific capacitance of the CNT electrodes grown on nanoporous alumina templates, Current Applied Physics 6(6) (2006) 1012-1015. https://doi.org/10.1016/j.cap.2005.07.008

[35] Q. T. Jiang, X. Pang, S. T. Geng, Y. H. Zhao, X. M. Wang, H. Qin, B. Liu, J. Zhou, T. Zhou, Simultaneous cross-linking and pore-forming electrospun carbon nanofibers towards high capacitive performance, Applied Surface Science 479 (2019) 128-136. https://doi.org/10.1016/j.apsusc.2019.02.077

[36] X. Liu, A. Roberts, A. Ahmed, Z. X. Wang, X. Li, H. F. Zhang, Carbon nanofibers by pyrolysis of self-assembled perylene diimide derivative gels as supercapacitor electrode materials, Journal of Materials Chemistry A 3(30) (2015) 15513-15522. https://doi.org/10.1039/c5ta03546e

[37] K. Anneser, J. Reichstein, S. Braxmeier, G. Reichenauer, Carbon xerogel based electric double layer capacitors with polymer gel electrolytes–improving the performance by adjusting the type of electrolyte and its processing, Electrochimica Acta 278 (2018) 196-203. https://doi.org/10.1016/j.electacta.2018.05.046

[38] Y. H. Lu, S. L. Zhang, J. M. Yin, C. C. Bai, J. H. Zhang, Y. X. Li, Y. Yang, Z. Ge, M. Zhang, L. Wei, M. X. Ma, Y. F. Ma, Y. S. Chen, Mesoporous activated carbon materials with ultrahigh mesopore volume and effective specific surface area for high performance supercapacitors, Carbon 124 (2017) 64-71. https://doi.org/10.1016/j.carbon.2017.08.044

[39] L. Lv, Y. Fan, Q. Chen, Y. Zhao, Y. Hu, Z. Zhang, N. Chen, L. Qu, Three-dimensional multichannel aerogel of carbon quantum dots for high-performance supercapacitors, Nanotechnology 25(23) (2014) 235401. https://doi.org/10.1088/0957-4484/25/23/235401

[40] O. Mykhailiv, H. Zubyk, M. E. Plonska-Brzezinska, Carbon nano-onions: Unique carbon nanostructures with fascinating properties and their potential applications, Inorganica Chimica Acta 468 (2017) 49-66. https://doi.org/10.1016/j.ica.2017.07.021

[41] M. E. Plonska-Brzezinska, Carbon Nano-Onions: A Review of Recent Progress in Synthesis and Applications, Chemnanomat: Chemnanomat 5(5) (2019) 568-580. https://doi.org/10.1002/cnma.201800583

[42] M. Zeiger, N. Jackel, V. N. Mochalin, V. Presser, Review: carbon onions for electrochemical energy storage, Journal of Materials Chemistry A 4(9) (2016) 3172-3196. https://doi.org/10.1039/c5ta08295a

[43] C. Liu, X. Yan, F. Hu, G. Gao, G. Wu, X. Yang, Toward Superior Capacitive Energy Storage: Recent Advances in Pore Engineering for Dense Electrodes, Adv Mater 30(17) (2018) e1705713. https://doi.org/10.1002/adma.201705713

[44] S. Fleischmann, J. B. Mitchell, R. Wang, C. Zhan, D. E. Jiang, V. Presser, V. Augustyn, Pseudocapacitance: From Fundamental Understanding to High Power Energy Storage Materials, Chem Rev 120(14) (2020) 6738-6782. https://doi.org/10.1021/acs.chemrev.0c00170

[45] C. Choi, D. S. Ashby, D. M. Butts, R. H. DeBlock, Q. L. Wei, J. Lau, B. Dunn, Achieving high energy density and high power density with pseudocapacitive materials, Nature Reviews Materials 5(1) (2020) 5-19. https://doi.org/10.1038/s41578-019-0142-z

[46] Y. Q. Jiang, J. P. Liu, Definitions of Pseudocapacitive Materials: A Brief Review, Energy & Environmental Materials 2(1) (2019) 30-37. https://doi.org/10.1002/eem2.12028

[47] X. T. Hao, J. S. Zhao, Q. Zhang, Temperature-dependent textural and electrochemical properties of a ruthenium oxide capacitor prepared by exchange membrane controlled ion diffusion, Ceramics International 42(7) (2016) 9170-9177. https://doi.org/10.1016/j.ceramint.2016.03.009

[48] S. J. Uke, V. P. Akhare, D. R. Bambole, A. B. Bodade, G. N. Chaudhari, Recent Advancements in the Cobalt Oxides, Manganese Oxides, and Their Composite As an electrode Material for Supercapacitor: A Review, Frontiers in Materials 4 (2017) 21. https://doi.org/10.3389/fmats.2017.00021

[49] B. Y. Chang, E. Ahn, S. M. Park, Real-Time Staircase Cyclic Voltammetry Fourier Transform Electrochemical Impedance Spectroscopic Studies on Underpotential Deposition of Lead on Gold, J Phys Chem C 112(43) (2008) 16902-16909. https://doi.org/10.1021/jp805960j

[50] J. McHardy, Investigation of hydrophobic porous electrodes. II. Pseudocapacitance changes during underpotential copper deposition, Journal of Applied Electrochemistry 7(1) (1977) 57-64. https://doi.org/10.1007/BF00615531

[51] Y. Liu, S. P. Jiang, Z. Shao, Intercalation pseudocapacitance in electrochemical energy storage: recent advances in fundamental understanding and materials development, Materials Today Advances 7 (2020) 100072. https://doi.org/10.1016/j.mtadv.2020.100072

[52] C. M. Proctor, J. Rivnay, G. G. Malliaras, Understanding volumetric capacitance in conducting polymers, (2016). https://doi.org/10.1002/polb.24038

[53] Y. Q. Han, L. M. Dai, Conducting Polymers for Flexible Supercapacitors, Macromolecular Chemistry and Physics 220(3) (2019) 1800355. https://doi.org/10.1002/macp.201800355

[54] H.-W. Chen, C. Li, PEDOT: Fundamentals and Its Nanocomposites for Energy Storage, Chinese Journal of Polymer Science 38(5) (2019) 435-448. https://doi.org/10.1007/s10118-020-2373-2

[55] K. D. Fong, T. Wang, H. K. Kim, R. V. Kumar, S. K. Smoukov, Semi-Interpenetrating Polymer Networks for Enhanced Supercapacitor Electrodes, ACS Energy Lett 2(9) (2017) 2014-2020. https://doi.org/10.1021/acsenergylett.7b00466

[56] G. A. Snook, P. Kao, A. S. Best, Conducting-polymer-based supercapacitor devices and electrodes, Journal of Power Sources 196(1) (2011) 1-12. https://doi.org/10.1016/j.jpowsour.2010.06.084

[57] K. Lota, V. Khomenko, E. Frackowiak, Capacitance properties of poly(3,4-ethylenedioxythiophene)/carbon nanotubes composites, Journal of Physics and Chemistry of Solids 65(2-3) (2004) 295-301. https://doi.org/10.1016/j.jpcs.2003.10.051

[58] Y. Wang, Y. Song, Y. Xia, Electrochemical capacitors: mechanism, materials, systems, characterization and applications, Chem Soc Rev 45(21) (2016) 5925-5950. https://doi.org/10.1039/c5cs00580a

[59] L. Wang, X. Hu, Recent Advances in Porous Carbon Materials for Electrochemical Energy Storage, Chem Asian J 13(12) (2018) 1518-1529. https://doi.org/10.1002/asia.201800553

[60] M. Zeller, V. Lorrmann, G. Reichenauer, M. Wiener, J. Pflaum, Relationship Between Structural Properties and Electrochemical Characteristics of Monolithic Carbon Xerogel-Based Electrochemical Double-Layer Electrodes in Aqueous and Organic Electrolytes, Advanced Energy Materials 2(5) (2012) 598-605. https://doi.org/10.1002/aenm.201100513

[61] K. S. W. Sing, D. H. Everett, R. A. W. Haul, L. Moscou, R. A. Pierotti, J. Rouquerol, T. Siemieniewska, Reporting Physisorption Data for Gas Solid Systems with Special Reference to the Determination of Surface-Area and Porosity (Recommendations 1984), Pure and Applied Chemistry 57(4) (1985) 603-619. https://doi.org/10.1351/pac198557040603

[62] J. F. Ni, Y. Li, Carbon Nanomaterials in Different Dimensions for Electrochemical Energy Storage, Advanced Energy Materials 6(17) (2016) 1600278. https://doi.org/10.1002/aenm.201600278

[63] M. Terrones, A. R. Botello-Mendez, J. Campos-Delgado, F. Lopez-Urias, Y. I. Vega-Cantu, F. J. Rodriguez-Macias, A. L. Elias, E. Munoz-Sandoval, A. G. Cano-Marquez, J. C. Charlier, H. Terrones, Graphene and graphite nanoribbons: Morphology, properties, synthesis, defects and applications, Nano Today 5(4) (2010) 351-372. https://doi.org/10.1016/j.nantod.2010.06.010

[64] D. Ugarte, Curling and closure of graphitic networks under electron-beam irradiation, Nature 359(6397) (1992) 707-9. https://doi.org/10.1038/359707a0

[65] S. Tomita, T. Sakurai, H. Ohta, M. Fujii, S. Hayashi, Structure and electronic properties of carbon onions, J Chem Phys 114(17) (2001) 7477-7482. https://doi.org/10.1063/1.1360197

[66] D. Roy, M. Chhowalla, H. Wang, N. Sano, I. Alexandrou, T. W. Clyne, G. A. J. Amaratunga, Characterisation of carbon nano-onions using Raman spectroscopy, Chemical Physics Letters 373(1-2) (2003) 52-56. https://doi.org/10.1016/S0009-2614(03)00523-2

[67] M. Zeiger, N. Jackel, D. Weingarth, V. Presser, Vacuum or flowing argon: What is the best synthesis atmosphere for nanodiamond-derived carbon onions for supercapacitor electrodes?, Carbon 94 (2015) 507-517. https://doi.org/10.1016/j.carbon.2015.07.028

[68] V. L. Kuznetsov, A. L. Chuvilin, Y. V. Butenko, I. Y. Malkov, V. M. Titov, Onion-Like Carbon from Ultra-Disperse Diamond, Chemical Physics Letters 222(4) (1994) 343-348. https://doi.org/10.1016/0009-2614(94)87072-1

[69] M. Choi, I. S. Altman, Y. J. Kim, P. V. Pikhitsa, S. Lee, G. S. Park, T. Jeong, J. B. Yoo, Formation of shell-shaped carbon nanoparticles above a critical laser power in irradiated acetylene, Advanced Materials 16(19) (2004) 1721-+. https://doi.org/10.1002/adma.200400179

[70] D. Ugarte, Morphology and Structure of Graphitic Soot Particles Generated in Arc-Discharge C60 Production, Chemical Physics Letters 198(6) (1992) 596-602. https://doi.org/10.1016/0009-2614(92)85035-9

[71] X. H. Chen, F. M. Deng, J. X. Wang, H. S. Yang, G. T. Wu, X. B. Zhang, J. C. Peng, W. Z. Li, New method of carbon onion growth by radio-frequency plasma-enhanced chemical vapor deposition, Chemical Physics Letters 336(3-4) (2001) 201-204. https://doi.org/10.1016/S0009-2614(01)00085-9

[72] J. P. Du, R. H. Zhao, Z. P. Zhu, A facile approach for synthesis and in situ modification of onion-like carbon with molybdenum carbide, Phys Status Solidi A 208(4) (2011) 878-881. https://doi.org/10.1002/pssa.201026646

[73] T. H. Mongwe, B. J. Matsoso, B. K. Mutuma, N. J. Coville, M. S. Maubane, Synthesis of chain-like carbon nano-onions by a flame assisted pyrolysis technique using different collecting plates, Diam Relat Mater: Diam Relat Mater 90 (2018) 135-143. https://doi.org/10.1016/j.diamond.2018.10.002

[74] F. Mathieux, F. Ardente, S. Bobba, P. Nuss, G. A. Blengini, P. A. Dias, D. Blagoeva, C. T. de Matos, D. Wittmer, C. Pavel, Critical Raw Materials and the Circular Economy – Background report, (2017). https://doi.org/10.2760/378123

[75] M. Zeiger, N. Jackel, M. Asian, D. Weingarth, V. Presser, Understanding structure and porosity of nanodiamond-derived carbon onions, Carbon 84 (2015) 584-598. https://doi.org/10.1016/j.carbon.2014.12.050

[76] C. Z. Shu, Y. M. Lin, B. S. Zhang, S. B. Abd Hamid, D. S. Su, Mesoporous boron-doped onion-like carbon as long-life oxygen electrode for sodium-oxygen batteries, Journal of Materials Chemistry A 4(17) (2016) 6610-6619. https://doi.org/10.1039/c6ta00901h

[77] N. Jäckel, D. Weingarth, M. Zeiger, M. Aslan, I. Grobelsek, V. Presser, Comparison of carbon onions and carbon blacks as conductive additives for carbon supercapacitors in organic electrolytes, Journal of Power Sources 272 (2014) 1122-1133. https://doi.org/10.1016/j.jpowsour.2014.08.090

[78] K. Pfeifer, S. Arnold, O. Budak, X. L. Luo, V. Presser, H. Ehrenberg, S. Dsoke, Choosing the right carbon additive is of vital importance for high-performance Sb-based Na-ion batteries, Journal of Materials Chemistry A 8(12) (2020) 6092-6104. https://doi.org/10.1039/d0ta00254b

[79] M. E. Plonska-Brzezinska, A. Palkar, K. Winkler, L. Echegoyen, Electrochemical Properties of Small Carbon Nano-Onion Films, Electrochem Solid St 13(4) (2010) K35-K38. https://doi.org/10.1149/1.3299252

[80] E. G. Bushueva, P. S. Galkin, A. V. Okotrub, L. G. Bulusheva, N. N. Gavrilov, V. L. Kuznetsov, S. I. Moiseekov, Double layer supercapacitor properties of onion-like carbon materials, Phys Status Solidi B 245(10) (2008) 2296-2299. https://doi.org/10.1002/pssb.200879608

[81] R. Borgohain, J. C. Li, J. P. Selegue, Y. T. Cheng, Electrochemical Study of Functionalized Carbon Nano-Onions for High-Performance Supercapacitor Electrodes, J Phys Chem C 116(28) (2012) 15068-15075. https://doi.org/10.1021/jp301642s

[82] D. Pech, M. Brunet, P. L. Taberna, P. Simon, N. Fabre, F. Mesnilgrente, V. Conedera, H. Durou, Elaboration of a microstructured inkjet-printed carbon electrochemical capacitor, Journal of Power Sources 195(4) (2010) 1266-1269. https://doi.org/10.1016/j.jpowsour.2009.08.085

[83] R. Borgohain, J. P. Selegue, Y. T. Cheng, Ternary composites of delaminated-MnO2/PDDA/functionalized-CNOs for high-capacity supercapacitor electrodes, Journal of Materials Chemistry A 2(47) (2014) 20367-20373. https://doi.org/10.1039/c4ta04439h

[84] Y. Wang, S. F. Yu, C. Y. Sun, T. J. Zhu, H. Y. Yang, MnO2/onion-like carbon nanocomposites for pseudocapacitors, Journal of Materials Chemistry 22(34) (2012) 17584-17588. https://doi.org/10.1039/c2jm33558a

[85] M. E. Plonska-Brzezinska, M. Lewandowski, M. Blaszyk, A. Molina-Ontoria, T. Lucinski, L. Echegoyen, Preparation and characterization of carbon nano-onion/PEDOT:PSS composites, Chemphyschem 13(18) (2012) 4134-41. https://doi.org/10.1002/cphc.201200789

[86] M. E. Plonska-Brzezinska, D. M. Brus, A. Molina-Ontoria, L. Echegoyen, Synthesis of carbon nano-onion and nickel hydroxide/oxide composites as supercapacitor electrodes, Rsc Advances 3(48) (2013) 25891-25901. https://doi.org/10.1039/c3ra44249g

[87] O. Mykhailiv, M. Imierska, M. Petelczyc, L. Echegoyen, M. E. Plonska-Brzezinska, Chemical versus electrochemical synthesis of carbon nano-onion/polypyrrole composites for supercapacitor electrodes, Chemistry 21(15) (2015) 5783-93. https://doi.org/10.1002/chem.201406126

[88] I. Kovalenko, D. G. Bucknall, G. Yushin, Detonation Nanodiamond and Onion-Like-Carbon-Embedded Polyaniline for Supercapacitors, Advanced Functional Materials 20(22) (2010) 3979-3986. https://doi.org/10.1002/adfm.201000906

[89] D. M. Anjos, J. K. McDonough, E. Perre, G. M. Brown, S. H. Overbury, Y. Gogotsi, V. Presser, Pseudocapacitance and performance stability of quinone-coated carbon onions, Nano Energy 2(5) (2013) 702-712. https://doi.org/10.1016/j.nanoen.2013.08.003

[90] M. Zeiger, D. Weingarth, V. Presser, Quinone-Decorated Onion-Like Carbon/Carbon Fiber Hybrid Electrodes for High-Rate Supercapacitor Applications, Chemelectrochem 2(8) (2015) 1117-1127. https://doi.org/10.1002/celc.201500130

[91] M. V. K. Azhagan, M. V. Vaishampayan, M. V. Shelke, Synthesis and electrochemistry of pseudocapacitive multilayer fullerenes and MnO2nanocomposites, J. Mater. Chem. A 2(7) (2014) 2152-2159. https://doi.org/10.1039/c3ta14076h

[92] S. L. Zhang, N. Pan, Supercapacitors Performance Evaluation, Advanced Energy Materials 5(6) (2015) 1401401. https://doi.org/10.1002/aenm.201401401

[93] C. F. Liu, Y. C. Liu, T. Y. Yi, C. C. Hu, Carbon materials for high-voltage supercapacitors, Carbon 145 (2019) 529-548. https://doi.org/10.1016/j.carbon.2018.12.009

[94] T. S. Mathis, N. Kurra, X. H. Wang, D. Pinto, P. Simon, Y. Gogotsi, Energy Storage Data Reporting in Perspective-Guidelines for Interpreting the Performance of Electrochemical Energy Storage Systems, Advanced Energy Materials 9(39) (2019) 1902007. https://doi.org/10.1002/aenm.201902007

[95] M. D. Stoller, R. S. Ruoff, Best practice methods for determining an electrode material's performance for ultracapacitors, Energy & Environmental Science 3(9) (2010) 1294-1301. https://doi.org/10.1039/c0ee00074d

[96] J. Zhang, X. S. Zhao, On the configuration of supercapacitors for maximizing electrochemical performance, ChemSusChem 5(5) (2012) 818-41. https://doi.org/10.1002/cssc.201100571

[97] Y. Hu, S. Brahim, S. Maat, P. Davies, A. Kundu, T. S. Fisher, Rapid Analytical Instrumentation for Electrochemical Impedance Spectroscopy Measurements, Journal of the Electrochemical Society 167(2) (2020) 027545. https://doi.org/10.1149/1945-7111/ab6ee8

[98] B. A. Mei, O. Munteshari, J. Lau, B. Dunn, L. Pilon, Physical Interpretations of Nyquist Plots for EDLC Electrodes and Devices, J Phys Chem C 122(1) (2018) 194-206. https://doi.org/10.1021/acs.jpcc.7b10582

[99] I. Yang, S. G. Kim, S. H. Kwon, M. S. Kim, J. C. Jung, Relationships between pore size and charge transfer resistance of carbon aerogels for organic electric double-layer capacitor electrodes, Electrochimica Acta 223 (2017) 21-30. https://doi.org/10.1016/j.electacta.2016.11.177

[100] F. Lufrano, P. Staiti, M. Minutoli, Evaluation of nafion based double layer capacitors by electrochemical impedance spectroscopy, Journal of Power Sources 124(1) (2003) 314-320. https://doi.org/10.1016/S0378-7753(03)00589-5

[101] C. H. Lei, F. Markoulidis, Z. Ashitaka, C. Lekakou, Reduction of porous carbon/Al contact resistance for an electric double-layer capacitor (EDLC), Electrochimica Acta 92 (2013) 183-187. https://doi.org/10.1016/j.electacta.2012.12.092

[102] C. L. Liu, W. S. Dong, G. P. Cao, J. R. Song, L. Liu, Y. S. Yang, Influence of KOH followed by oxidation pretreatment on the electrochemical performance of phenolic based activated carbon fibers, Journal of Electroanalytical Chemistry 611(1-2) (2007) 225-231. https://doi.org/10.1016/j.jelechem.2007.09.003

[103] J. Gamby, P. L. Taberna, P. Simon, J. F. Fauvarque, M. Chesneau, Studies and characterisations of various activated carbons used for carbon/carbon supercapacitors, Journal of Power Sources 101(1) (2001) 109-116. https://doi.org/10.1016/S0378-7753(01)00707-8

[104] R. Kötz, M. Carlen, Principles and applications of electrochemical capacitors, Electrochimica acta 45(15-16) (2000) 2483-2498. https://doi.org/10.1016/S0013-4686(00)00354-6

[105] A. Laheäär, P. Przygocki, Q. Abbas, F. Béguin, Appropriate methods for evaluating the efficiency and capacitive behavior of different types of supercapacitors, Electrochemistry Communications 60 (2015) 21-25. https://doi.org/10.1016/j.elecom.2015.07.022

[106] J. Li, C. Arbizzani, S. Kjelstrup, J. Xiao, Y. Y. Xia, Y. Yu, Y. Yang, I. Belharouak, T. Zawodzinski, S. T. Myung, R. Raccichini, S. Passerini, Good practice guide for papers on batteries for the Journal of Power Sources, Journal of Power Sources 452 (2020) 227824. https://doi.org/10.1016/j.jpowsour.2020.227824

[107] C. Arbizzani, Y. Yu, J. Li, J. Xiao, Y. Y. Xia, Y. Yang, C. Santato, R. Raccichini, S. Passerini, Good practice guide for papers on supercapacitors and related hybrid capacitors for the Journal of Power Sources, Journal of Power Sources 450 (2020) 227636. https://doi.org/10.1016/j.jpowsour.2019.227636

[108] R. Vicentini, J. P. Aguiar, R. Beraldo, R. Venâncio, F. Rufino, L. M. Da Silva, H. Zanin, Ragone Plots for Electrochemical Double-Layer Capacitors, Batteries & Supercaps 4(8) (2021) 1291-1303. https://doi.org/10.1002/batt.202100093

[109] Y. Gogotsi, P. Simon, Materials science. True performance metrics in electrochemical energy storage, Science 334(6058) (2011) 917-8. https://doi.org/10.1126/science.1213003

[110] B. R. Masters, History of the electron microscope in cell biology, eLS (2009). https://doi.org/10.1002/9780470015902.a0021539

[111] E. Abbe, Beiträge zur Theorie des Mikroskops und der mikroskopischen Wahrnehmung, Archiv für mikroskopische Anatomie 9(1) (1873) 413-468. https://doi.org/BF02956173

[112] L. De Broglie, Recherches sur la théorie des quanta, (1924). https://doi.org/10.1051/anphys/192510030022

[113] E. M. Slayter, H. S. Slayter, Light and electron microscopy, Cambridge University Press (1992). p.17

[114] K. Akhtar, S. A. Khan, S. B. Khan, A. M. Asiri, Scanning electron microscopy: principle and applications in nanomaterials characterization, Handbook of materials characterization (2018) 119 ff. https://doi.org/10.1007/978-3-319-92955-2_4

[115] R. F. Egerton, The scanning electron microscope, Physical principles of electron microscopy (2005) 124 ff. https://doi.org/10.1007/0-387-26016-1_5

[116] K. Vernon-Parry, Scanning electron microscopy: an introduction, III-Vs Review 13(4) (2000) 40-44. https://doi.org/10.1016/S0961-1290(00)80006-X

[117] M. Suga, S. Asahina, Y. Sakuda, H. Kazumori, H. Nishiyama, T. Nokuo, V. Alfredsson, T. Kjellman, S. M. Stevens, H. S. Cho, M. Cho, L. Han, S. N. Che, M. W. Anderson, F. Schuth, H. X. Deng, O. M. Yaghi, Z. Liu, H. Y. Jeong, A. Stein, K. Sakamoto, R. Ryoo, O. Terasaki, Recent progress in scanning electron microscopy for the characterization of fine structural details of nano materials, Progress in Solid State Chemistry 42(1-2) (2014) 1-21. https://doi.org/10.1016/j.progsolidstchem.2014.02.001

[118] J. Cazaux, Charging in scanning electron microscopy "from inside and outside", Scanning 26(4) (2004) 181-203. https://doi.org/10.1002/sca.4950260406

[119] A. Mohan, N. Khanna, J. Hwu, D. C. Joy, Secondary electron imaging in the variable pressure scanning electron microscope, Scanning 20(6) (1998) 436-441. https://doi.org/10.1002/sca.1998.4950200603

[120] J. N. T. Nguyen, A. M. Harbison, Scanning electron microscopy sample preparation and imaging, Molecular Profiling, Springer2017, pp. 71-84.

[121] F. Orsini, A. Du Pasquier, B. Beaudoin, J. M. Tarascon, M. Trentin, N. Langenhuizen, E. De Beer, P. Notten, In situ Scanning Electron Microscopy (SEM) observation of interfaces within plastic lithium batteries, Journal of Power Sources 76(1) (1998) 19-29. https://doi.org/10.1016/S0378-7753(98)00128-1

[122] N. Lin, Z. Jia, Z. H. Wang, H. Zhao, G. Ai, X. Y. Song, Y. Bai, V. Battaglia, C. D. Sun, J. Qiao, K. Wu, G. Liu, Understanding the crack formation of graphite particles in cycled commercial lithium-ion batteries by focused ion beam - scanning electron microscopy, Journal of Power Sources 365 (2017) 235-239. https://doi.org/10.1016/j.jpowsour.2017.08.045

[123] M. A. O'Keefe, “Resolution” in high-resolution electron microscopy, Ultramicroscopy 47(1-3) (1992) 282-297. https://doi.org/10.1016/0304-3991(92)90203-V

[124] R. F. Egerton, Choice of operating voltage for a transmission electron microscope, Ultramicroscopy 145 (2014) 85-93. https://doi.org/10.1016/j.ultramic.2013.10.019

[125] F. Ernst, M. Ruhle, Present developments in high-resolution transmission electron microscopy, Curr Opin Solid St M 2(4) (1997) 469-476. https://doi.org/10.1016/S1359-0286(97)80092-7

[126] P. J. Harris, Transmission electron microscopy of carbon: a brief history, C 4(1) (2018) 4. https://doi.org/10.3390/c4010004

[127] F. Salver-Disma, J. M. Tarascon, C. Clinard, J. N. Rouzaud, Transmission electron microscopy studies on carbon materials prepared by mechanical milling, Carbon 37(12) (1999) 1941-1959. https://doi.org/10.1016/S0008-6223(99)00059-7

[128] S. Bhattacharya, A. R. Riahi, A. T. Alpas, A transmission electron microscopy study of crack formation and propagation in electrochemically cycled graphite electrode in lithium-ion cells, Journal of Power Sources 196(20) (2011) 8719-8727. https://doi.org/10.1016/j.jpowsour.2011.05.079

[129] D. N. Qian, C. Ma, K. L. More, Y. S. Meng, M. F. Chi, Advanced analytical electron microscopy for lithium-ion batteries, Npg Asia Materials 7(6) (2015) e193-e193. https://doi.org/10.1038/am.2015.50

[130] X. Z. Liu, L. Gu, Advanced Transmission Electron Microscopy for Electrode and Solid-Electrolyte Materials in Lithium-Ion Batteries, Small Methods 2(8) (2018) 1800006. https://doi.org/10.1002/smtd.201800006

[131] L. E. Franken, E. J. Boekema, M. C. A. Stuart, Transmission Electron Microscopy as a Tool for the Characterization of Soft Materials: Application and Interpretation, Advanced Science 4(5) (2017) 1600476. https://doi.org/10.1002/advs.201600476

[132] J. Epp, X-ray diffraction (XRD) techniques for materials characterization, Materials characterization using nondestructive evaluation (NDE) methods (2016) 84ff. https://doi.org/10.1016/B978-0-08-100040-3.00004-3

[133] M. A. Moram, M. E. Vickers, X-ray diffraction of III-nitrides, Reports on Progress in Physics 72(3) (2009) 036502. https://doi.org/10.1088/0034-4885/72/3/036502

[134] A. Chauhan, P. Chauhan, Powder XRD technique and its applications in science and technology, J Anal Bioanal Tech 5(5) (2014) 1-5. https://doi.org/10.4172/2155-9872.1000212

[135] T. Placke, G. Schmuelling, R. Kloepsch, P. Meister, O. Fromm, P. Hilbig, H. W. Meyer, M. Winter, In situ X-ray Diffraction Studies of Cation and Anion Intercalation into Graphitic Carbons for Electrochemical Energy Storage Applications, Zeitschrift Fur Anorganische Und Allgemeine Chemie 640(10) (2014) 1996-2006. https://doi.org/10.1002/zaac.201400181

[136] M. Morcrette, Y. Chabre, G. Vaughan, G. Amatucci, J. B. Leriche, S. Patoux, C. Masquelier, J. M. Tarascon, In situ X-ray diffraction techniques as a powerful tool to study battery electrode materials, Electrochimica Acta 47(19) (2002) 3137-3149. https://doi.org/10.1016/S0013-4686(02)00233-5

[137] A. A. Bunaciu, E. G. Udristioiu, H. Y. Aboul-Enein, X-ray diffraction: instrumentation and applications, Crit Rev Anal Chem 45(4) (2015) 289-99. https://doi.org/10.1080/10408347.2014.949616

3 Results

The research findings in this work using carbon materials for energy storage are divided into four chapters. The first chapter explains how to build a performant supercapacitor with onion-like carbon in an aqueous process, using a sustainable binder. To improve the sustainability of onion-like carbon (OLC) based electrodes, the structure of the OLC agglomerates is investigated, revalued and discussed. The second chapter involves research on pseudocapacitors, using OLC in order to achieve superior capacitance. In contrast to the first chapter, here OLC are used as a template, decorated with conductive polymers to increase the capacitance of the electrode. A big part of the research was attributed to dispersibility issues of the starting materials. A synergistic approach improving both connectivity during reaction and conductivity in the device was the main objective. The third chapter is dedicated to find a new production method for OLC supercapacitor electrodes using a stable dispersion of OLC, which can be inkjet printed. The last chapter deals with the issue of OLC integration into a sodium ion battery. Thereby, composition and configuration issues are solved regarding the electrolyte and electrode. Especially, the role of OLC was reiterated and thus shifted from active material to conductive agent.

3.1 Supercapacitors with onion-like carbon

Parts of this chapter are based on the publication: Bauer, C., Bilican, A., Braxmeier, S., Reichenauer, G., & Krueger, A. (2022). Sustainable supercapacitor electrodes based on preagglomerated carbon onions and a green binder. Carbon, 197, 555-562.

The first topic of this work investigates secondary OLC particles, which are formed by the agglomeration of primary OLC. This zoom-out, from primary particle to agglomerate, enabled a critical rework of the interaction between bigger particles and the binder, which eventually is affecting the properties of the macroscopic electrode. The key task was to enhance the sustainability of the system without a loss in performance. Therefore, fluorinated polymers, which are widely used as binder, should be replaced by the sustainable carboxymethyl cellulose (CMC). Problems of a high content of CMC were targeted by a pre-agglomeration step of the OLC material. Pre-agglomeration of OLC solved the underlying contradiction as it reduces the specific volume of the agglomerate while maintaining the specific surface. The result was surprising, as agglomeration of nanoparticles is expected alongside a reduction of the specific surface of the active material. The potential of this finding was identified and utilized in supercapacitor electrodes, which were characterized electrochemically and showed a capacitance of 56 F/g.

3.1.1 Introduction

Growing ecological awareness is accelerating the demand for eco-friendly supply and storage of energy. The application potential of regenerative but intermittent energy sources is tightly linked to the capacity as well as to the flexibility of the energy storage grid.[1] Besides systems with a high energy density like batteries, reactive systems are required to compensate fluctuations of renewable energy sources. Supercapacitors can fulfill this role, as they provide superior power density and cyclability.[2, 3] For a throughout sustainable energy supply chain sustainable storage devices are integral to close the gap between energy demand and supply. Thus, the provision of environmentally friendly supercapacitors is an important cornerstone of a sustainable power grid.

A key component of a supercapacitor is the active material of the electrode. Typically, sp^2 carbon is used mainly in the form of activated biomaterial,[4] but also carbon nanotubes or graphene are applied.[5] Here, we report on the use of onion-like carbon (OLC), a spherical form of carbon mainly composed of sp^2 hybridized carbon atoms arranged in concentric layers,

initially described in 1992 by Ugarte.[6] These fullerene layers stack in a way that the eponymous onion-like structure of this zero dimensional nanomaterial is formed.[5]

OLC can be produced in high yield by a simple and easily scalable, high temperature treatment of detonation nanodiamond (DND) (Kuznetsov method),[7] acetylene black [8] or by ball milling of graphite.[9] Unlike natural graphite, considered as critical raw material by the European union,[10] detonation diamonds are an artificial carbon source. The detonation method does not require external energy input and yields detonation diamonds from e.g. waste explosives.[11] Even though OLC show a smaller specific surface area compared to activated carbon,[4] but consist of primary particles with low variation in size and shape in contrast to common carbon materials derived from biomaterials.[12] These characteristics build an interesting platform with four key properties to qualify OLC as a promising active material for electrochemical double layer capacitors:

- **i)** open porous structure: enabling a high accessibility for the electrolyte [13, 14]
- **ii)** high external specific surface: suited to form a large double layer [3]
- **iii)** electric conductivity: enabling fast and efficient polarization of the material [15]
- **iv)** low content of micropores: mesopore surfaces are providing the sites especially relevant for organic electrolytes [16, 17]

The first supercapacitor based on OLC as active material and 15 wt% polytetrafluoroethylene (PTFE) as binder was reported more than a decade ago.[18] Since then, OLC-based supercapacitors have seen intense research activity and significant improvement.[19, 20] OLCs have been already investigated in different electrode setups such as on-chip electrodeposited OLC films,[21] cavity micro electrodes,[22] PTFE bound free-standing films [23] and OLC-dispersion coated glassy carbon electrodes.[24] To increase the capacitance of OLC, conditions during synthesis like atmosphere[25] and temperature of the furnace[13] were examined, targeting the porosity of the active material. In addition, numerous post-synthetic approaches like functionalization, oxidation or coating of the OLC have been investigated to improve the electrochemical performance.[26-33]

Beside the active material, a supercapacitor consists of a current collector, a binder, a separator and conductive additives. The binder forms a matrix for the active material and allows establishing contact with the current collector, thus providing mechanical durability. It must be electrochemically stable, insoluble in the electrolyte and needs to be evenly distributed in the slurry. Many supercapacitor applications rely on fluorinated polymers like PTFE as binders.

[27, 33-39] Even though fluorinated polymers are still considered as “polymer of low concern”,[40] they require wetting agents or organic solvents during processing and residual fluorinated monomers and fragments have undesired health and environmental effects.[41] Additionally, fluorinated polymers are highly persistent in nature and release toxic decomposition products upon recycling.[41]

Only an optimal combination of all components leads to an environmentally sustainable supercapacitor which up to day presents a key development target.[15] Here, we report on an approach for the production of a supercapacitor based on OLC using an aqueous preparation method combined with a sustainable binder material while maintaining high electrochemical performance. The following challenges are addressed: i) increasing the surface area of the OLC without compromising the mesoporous character of the primary structure; ii) implementing an environmentally and economically sustainable binder based on carboxymethyl cellulose, while limiting the total amount of the binder to 10%; iii) develop a method to produce a thin homogenous active material coating with sufficient ad- and cohesion to enable fast cyclization over a wide range of scan rates and more than 5000 cycles.

3.1.2 Experimental section

Synthesis of the active material

Purified detonation nanodiamond (*Gansu Lingyun Corp., China*) was used without further purification as a precursor. The phase transition to **OLC** was performed by thermal annealing in vacuum (~1 mbar starting from Ar atmosphere) using a tube furnace (STF 16/450, Carbolite Gero GmbH, Germany), temperature modulation was adjusted with a build in digital temperature controller (3216 P1, Eurotherm). A heating rate of 5 K min^{-1} was applied until the plateau temperature of 1500 °C was reached which was held for two hours.[18] After cooling to room temperature (5 °K min^{-1}), the **OLC** were transferred into a preheated muffle furnace (KL 04/12M, Thermconcept LAC GmbH). An activation step at 600 °C in air for 30 minutes was carried out to increase the specific surface area (SSA) of the active material and to obtain **aOLC**.

X-ray Diffraction and Raman spectroscopy

The X-ray diffraction pattern of the powder OLC samples was recorded with a D8 Discovery Diffractometer (Bruker, USA) using Cu-Kα radiation (wavelength: 1.53 Å). The Raman

spectrum of OLC powders was measured with a DXR Raman Microscope (Thermo Fisher Scientific Inc., USA) using a laser power of 0.2 mW and an excitation wavelength of 532 nm.

Electron microscopy of the active material

To prepare the sample for high resolution electron transmission microscopy (HRTEM), OLC powder was sonicated in water. The resulting dispersion was drop casted onto a lacey carbon copper grid (Plano GmbH, Germany). The measurement was conducted with a FEI Titan 80-300 (Thermo Fischer Scientific Inc., USA) using an operating voltage of 300 kV. Scanning electron microscopy (SEM) images of the electrodes were recorded at an operating voltage of 5 kV using a Gemini Fe-SEM Ultra-Plus Zeiss field emission scanning electron microscope (Carl Zeiss Microscopy Deutschland GmbH, Germany). For this analysis, the electrodes were contacted using conductive carbon tapes and directly investigated without further preparation.

N_2 adsorption analysis

The nitrogen adsorption isotherms at 77 K were recorded using a commercial volumetric analyzer (ASAP2020 by Micromeritics Inc., USA). Prior to analysis, the powder sample (about 100 mg) was degassed under vacuum for 24 hours at 300 °C. The isotherm was evaluated with respect to the specific BET surface area S_{BET} following the IUPAC recommendations for microporous materials to adapt the pressure range used to determinate the linear slope in the BET-plot.[42] The data at relative gas pressures below the onset of the isotherm hysteresis were analyzed with respect to the external surface area S_{ext} and the micropore volume with the t-plot using the data of Magee as a reference.[43] For further analysis of the materials the pore size distribution was evaluated by means of nonlocal density function theory (NLDFT). Thereby a set of theoretical sorption isotherms (= kernel) calculated for N_2 on carbon with slit shaped micropores at 77 K are numerically fitted to the measured isotherms. Details about the theoretical models can be found in literature.[44-47] All data evaluation was performed using the Software *Microactive* (Micromeritics Inc., Norcross)

Slurry and electrode preparation

The slurry for the electrode preparation, referred to as **apOLC-CMC**, consisted of deionized water as solvent, activated and agglomerated active material (**apOLC)**, carboxymethyl cellulose (CMC) as binder (degree of substitution: 1.2; molar mass: 250 kg mol^{-1}, Acros organics) and carbon black (Super C65; Imerys Graphite & Carbon, Belgium). For the pre-agglomeration step (see below), **aOLC** powder was sonicated in ethanol for 30 minutes. After the complete evaporation of ethanol under ambient conditions, the brittle **paOLC** cake was

ground to fine powder in a mortar. For the system with PVDF binder, referred to as **paOLC-PVDF,** water was replaced by *N*,*N*-dimethylacetamide (TCI, Germany) and CMC by polyvinylidene fluoride (SOLEF PVDF, Solvay Belgium).

For the preparation of the respective slurries, all components were mixed together in the mass ratio 30:10:1:1 for solvent: **paOLC** : binder : carbon black and vigorously stirred for 72 hours using a magnetic stirrer. All coatings were produced by doctor blading the slurry onto a carbon coated aluminum (Zflo 2653, Transcontinental Advanced Coatings, USA) current collector with an active material loading of around 1.5 mg cm^{-2} and a thickness of around 20 μm. After drying at ambient conditions, round electrodes with a diameter of 18 mm were die cut with a punching iron and pressed with ~0.2 GPa, using a hydraulic press. SEM images of the electrodes are shown in the supporting information (Fig. S1 and Fig. S2).

Electrochemical characterization

For the electrochemical measurements of the die cut electrodes, symmetrical cells (Fig. S3) were produced using a stainless-steel test cell separated by a glass fiber membrane with 1.55 mm thickness (ECC-Ref, El-Cell, Germany). The electrolyte was prepared as a 1 M solution of tetraethylammonium tetra-fluoroborate ($TEABF_4$; TCI, Germany) in acetonitrile (Sigma Aldrich). For each system (**paOLC-PVDF** and **paOLC-CMC**), three test cells were assembled in the absence of humidity (<1 ppm) and oxygen (<1 ppm) using a glovebox (N_2, Labmaster 130, M. Braun Inertgas-Systeme, Germany).

Constant current charging/discharging (CCCD) as well as cyclic voltammetry (CV) were carried out with a potentio-/galvanostat (VMP300 Bio-Logic, France). CCCD measurements were carried out between 0 and 2.5 V using different current densities reaching from 0.15 A g^{-1} up to 10 A g^{-1}. The capacitance was calculated with consideration of the voltage drop V_{IR}[48] caused by the internal resistance during discharging using Eq. 1:

$$C_{CCCD} = \frac{I_{dis} * t_{dis}}{V - V_{IR}} \quad (1)$$

where C_{CCCD} is the total capacitance of the device and I_{dis} the discharging current, during discharging of the cell starting from the charged potential V. CV measurements were carried out between -2.5 and 2.5 V, before and after 5000 cycles of the endurance test for different scan rates reaching from 10 mV s^{-1} to 50 V s^{-1}. The gravimetric capacitance of the total device

(C_{CV}) and the specific capacitance of one electrode (C_E) [48] was calculated based on Eq. 2 and Eq. 3:

$$C_{CV} = \frac{\int_{t_0}^{t_1} I\,(t) * dt}{2 * \Delta V} \tag{2}$$

$$C_E = \frac{4 * C}{m} \tag{3}$$

where m is the total mass of the active material and C the capacitance of the device. The endurance test was carried out over 5000 cycles and a scan rate of 2.5 V s^{-1}.

3.1.3 Results and discussion

Structural characterization of the active material

To investigate the conversion of the detonation diamond to OLC and the structure of the active material aOLC, Raman spectroscopy (Fig. 1A), X-ray diffraction (Fig. 1B) HRTEM (Fig. 1C and D), and nitrogen adsorption analysis were evaluated (Fig. S4).

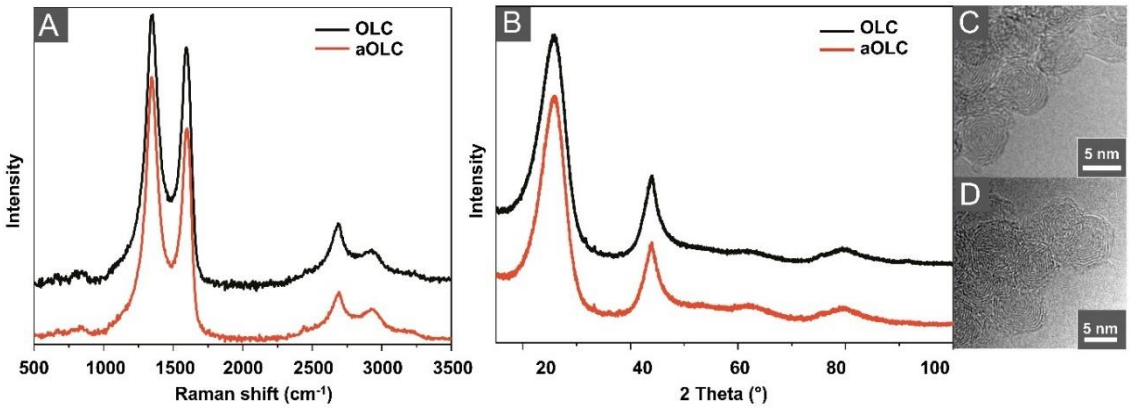

Fig. 1: *Comparison of the active material onion-like carbon before (OLC) and after air activation (aOLC): (A) Raman spectra, (B) powder X-ray diffractograms and transmission electron micrographs for OLC (C) and aOLC (D). Curves are vertically shifted relative to each other for better comparison.*

The Raman spectra exhibit peaks typical for onion-like carbon as explained in detail elsewhere. [49-55] Briefly, the G-mode (around 1600 cm^{-1}) is characteristic for sp^2 carbon,[53] the D-mode (around 1345 cm^{-1}) indicates disorder in the graphitic structure.[55] The symmetric shape of the 2D-mode at around 2690 cm^{-1} is caused by turbostratic stacking of the graphitic

layers.[56] The Raman spectra before and after air activation show comparable structural features (Fig. 1A). The shape of neither the D nor G-mode changes during air activation indicating the absence of a significant structural rearrangement. Changes in the primary structure of **OLC** in general, observed upon annealing in argon or nitrogen atmosphere, would translate into a shoulder in the D-mode in the region of 1600 cm^{-1} of the Raman spectrum.[55] This fact supports the suggestion in [13] that the recorded mass loss of around 20 % during air activation results from the combustion of outer shells and amorphous carbon and does not affect the primary onion structure. This conclusion is also in line with the fact that the primary structure seen in the HRTEM micrograph (Fig. 1 C and D) of **OLC** has not changed.

The X-ray diffraction (Fig. 1 B) shows two pronounced reflexes. The first signal at 26 ° represents perpendicular stacking of the graphitic planes corresponding to the primitive reciprocal vector (002).[57] Utilizing the Bragg equation [58] the interlayer or intershell distance can be calculated as 3.4 Å indicating a turbostratic stacking of the graphitic layers, which is in line with the results from Raman spectroscopy. Two carbon phases contribute to the signal at 44 °. First, the graphitic phase, expressed by the reflex of the primitive reciprocal vector (100) and secondly, the (111) reflex pertaining to the diamond phase which can be explained by a residual diamond core of not fully graphitized particles.[59] The specific BET surface area (SSA) of the active material as derived from nitrogen adsorption analysis is 389 $m^2\ g^{-1}$ for **OLC** (Fig. S4) and increased by 35 % to 527 $m^2\ g^{-1}$ for **aOLC** as a result of the air activation. With 366 (94 %) and 453 $m^2\ g^{-1}$(85 %), respectively, the contribution of the specific external surface area is dominating in both cases.

Preagglomeration of OLC

Several steps are necessary to obtain a mechanically resistant electrode when working with **OLC** carbon as active material. While the activation of **OLC** increases the specific surface as shown by adsorption measurements it also removes interparticle connections.[13]. For the electrode the connection between the particles has to be assured by binder, whose amount in the supercapacitor has to be tailored. High binder incorporation adds deadweight to the system and could block access to the storage sites, ultimately deteriorating the performance of the device. This problem is well known for supercapacitors combining CMC and activated carbon.[60] With an agglomeration step for the active material prior to the addition of any additives we resolved the issue of contradicting requirements of a firmly connected active material and minimal binder usage. This approach ensures high accessibility of the surface area for the electrolyte. Therefore, **aOLC** was sonicated in ethanol and dried completely under

ambient conditions to obtain **paOLC**; this step reduced the volume of the sample significantly (Fig. 2) due to the formation of agglomerates.

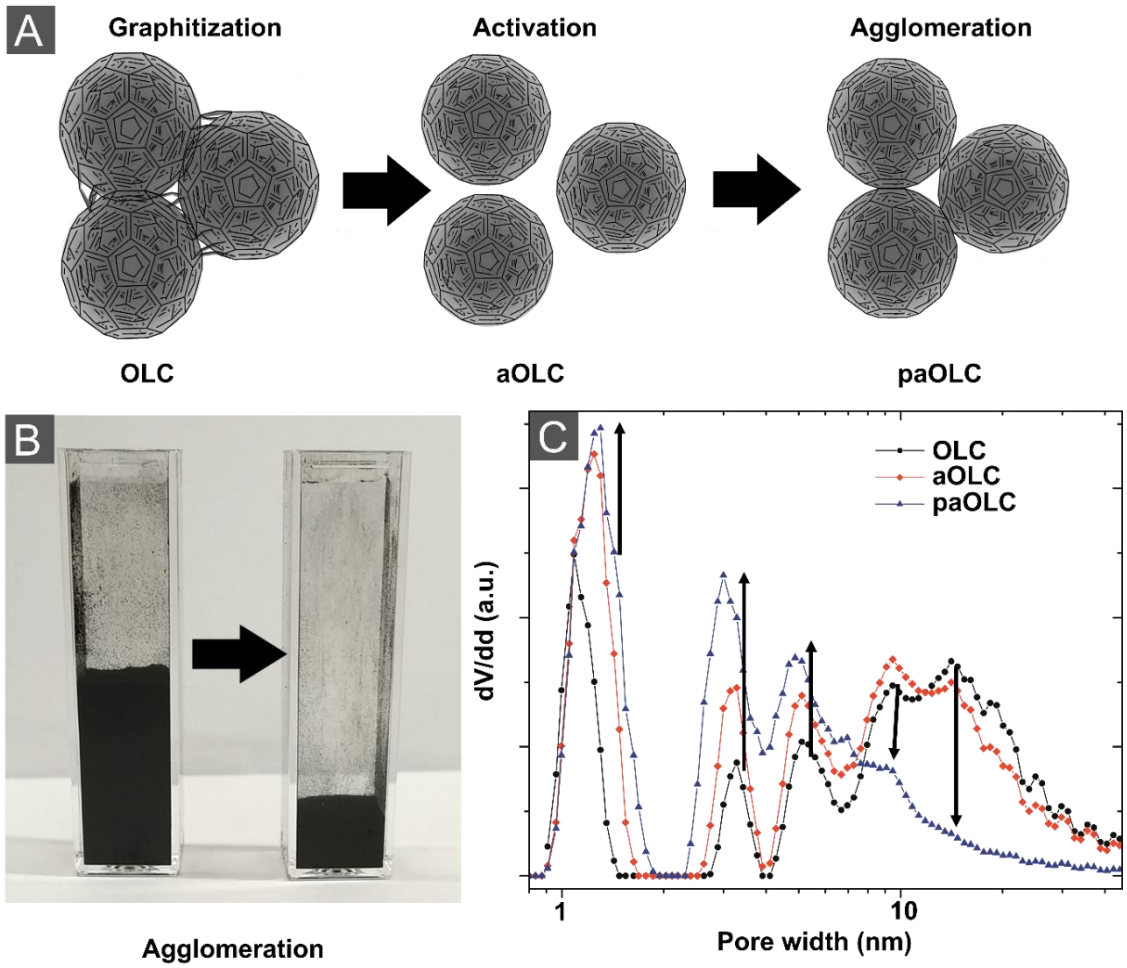

Fig. 2: *Overview for the activation and agglomeration steps of the graphitized onion-like carbon prior to electrode production (A). The picture in B shows the volume reduction of the samples before (**aOLC**) and after agglomeration and drying (**paOLC**) and C tracks changes of the pore size distribution alongside the treatment.*

After this treatment, the number of small particles was reduced in favor of bigger rearranged agglomerates featuring less large interparticle voids. The rearrangement is observable on a macroscopic scale as the volume of the sample shrinks considerable (Fig. 2A) but also on nanoscale when comparing the pore size distribution of **OLC**, **aOLC** and **paOLC** (Fig. 2C). The increase in small pores (1-10 nm) obtained during air activation is further consolidated with the agglomeration step by reducing pores above 10 nm. A model developed by Presser et al. suggests these pores (>10 nm) as interparticle voids.[13] We can confirm these considerations as our measurements show a significant reduction of those pores after the agglomeration step, without changing the BET surface area (SSA) (Fig. S4A and Tab. S1).

Sorption measurements also show that the external surface does not decrease during agglomeration (Tab. S1). This is desirable as the external surface of OLC is considered highly accessible for the electrolyte, enabling fast electrochemical charging and discharging when used as active material in electrodes.[15] Regarding the production of electrodes, the absence of additional smaller particles (like e.g. in carbon black or binder) in the agglomerates precludes any blocking of mesopores inside the close-packing of equal spheres. The big agglomerates now facilitated the usage of binder especially for CMC, which tends to accumulate between active material areas rather than coating the entire surface like PVDF.[61] With the agglomeration approach, it was possible to decrease the CMC content to 10% while still forming a robust electrode (Fig. 3).

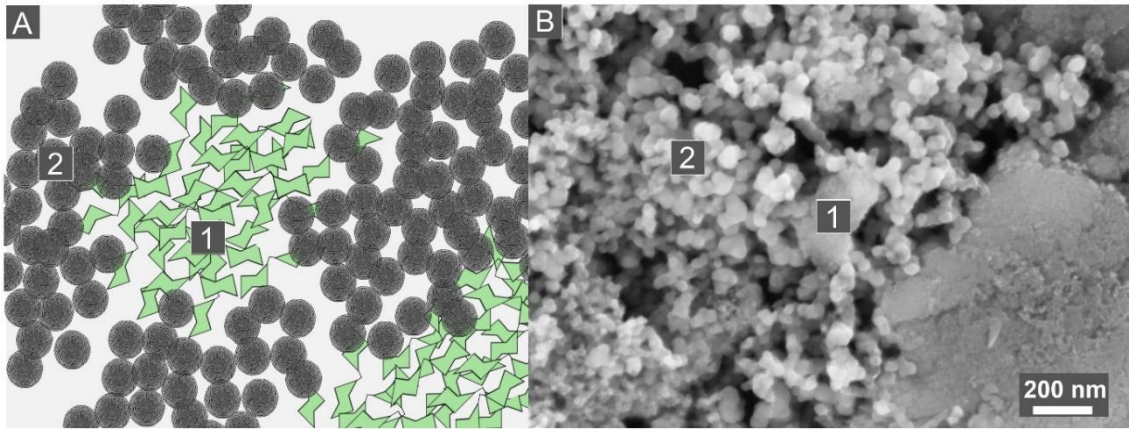

Fig. 3*: Scheme (A) and SEM image (B) for the interaction between* ***paOLC*** *and cellulose based binder in the electrode. The green armchair structures in (A) represent the cellulose related saccharide moieties. Numbers in (B) indicate binder (1) and* ***paOLC*** *agglomerates (2).*

For the processing of the slurry, the size of the agglomerates was found to be optimal below a diameter of 30 μm. Bigger agglomerates were observed to be associated with the formation of highly inhomogeneous coatings. Additionally, they initiated cracks in the layer resulting in a delamination of the coating during drying. For the aqueous slurry, an addition of ethanol (5-10%) prior to **paOLC** deposition by doctor-blading increased the homogeneity of the coating by improving wetting (by reduced surface tension) and by reduction of capillary stress during drying.[53] This step prevents delamination, especially at high specific mass loadings. Since the stress during drying increases with the thickness of the coating. cohesion between substrate and coating remains constant.

Electrochemical Performance of the Supercapacitor

Within the framework of the electrochemical analysis, the performance of the supercapacitors was evaluated using constant current charging/discharging (CCCD) (Fig. 4A) and cyclic

voltammetry (CV) (Fig. 4B) in a two-electrode cell configuration. Both methods were evaluated over a wide range of scan rates according to [48] and [62] to calculate the corresponding capacitance related to the mass of OLC according to Eq. 1 and Eq. 3. These measurements were performed for **paOLC-CMC** and also for **paOLC-PVDF** using non-aqueous preparation in both cases. The comparison of these binders is of particular interest because they offer different binding mechanisms due to their morphology which can be seen by the comparison of the SEM measurements provided in the supplementary information (Fig. S1 and S2); the effects are also described in literature where PVDF develops net like structures and CMC fills interparticle voids.[61]

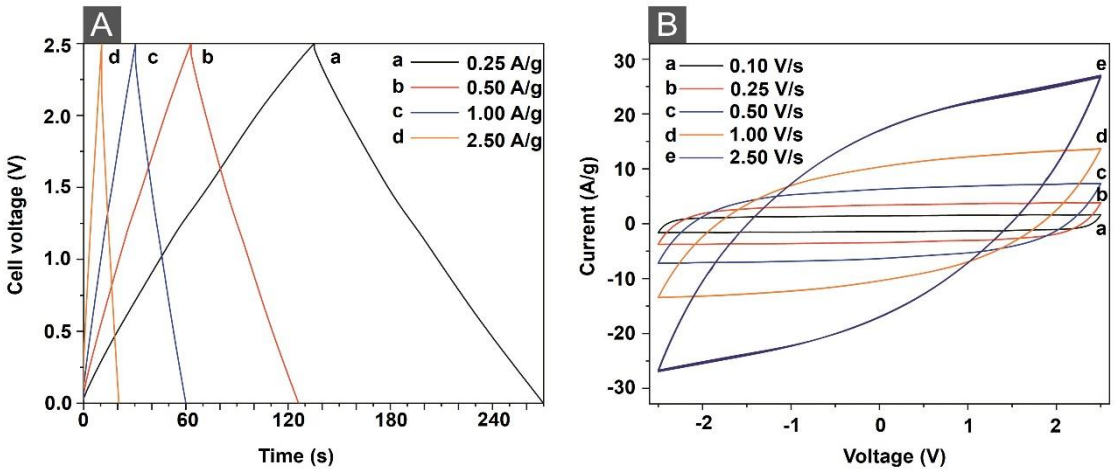

Fig. 4: *Electrochemical characterization of **paOLC-CMC** based electrodes. (A) CCCD for electrodes at different current densities between 0.25 A g^{-1} and 2.5 A g^{-1}, (B) CV for electrodes using different scan rates between 0.10 V s^{-1} and 2.5 V s^{-1}*

For the CCCD, the charging and discharging times decreases at higher current densities (Fig. 4 A). The shape of the cyclic voltammogram (Fig. 4B) changes from a narrow quasi-rectangle at low scan rates to an ellipsoid at high scan rates. Considering these observations and taking into account that the stored energy is proportional to the integrated area in the cyclic voltammogram as well as for the CCCD graph, it is evident that the capacitance of the device decreases with a higher frequency of charging/discharging. In general, this observation is common for supercapacitors and is found as well for **paOLC-PVDF** (Fig. S5 and Fig. S6). Accordingly, the highest capacitance is measured at low scan rates. In this case at 10 mV s^{-1}, a capacitance of 56 F g^{-1} (**paOLC-CMC**) and 44 F g^{-1} (**paOLC-PVDF**) was measured. At given binder content, the electrode relying on PDVF as binder offers 23 % less specific capacitance compared to the electrode with CMC as binder. Obviously, the higher capacitance for the CMC based binder electrodes indicates that filling the voids between the agglomerates with CMC is

blocking less surface than coating large parts of the OLC surface with PVDF. N_2 adsorption analysis performed on the two respective electrodes shows about the same relation in the total surface area as detected for the respective capacitances. Obviously, the higher capacitance for the CMC based binder electrodes indicates that filling the voids between the agglomerates with CMC is blocking less surface than coating with PVDF. This can be seen by comparing the SEM measurements of the electrodes (Fig. S1). In the case of PVDF, the active material seems to be completely covered by the binder, thus a lower accessibility is to be expected. Both systems feature the desired quasi-rectangular shape for CV- and equilateral triangles for CCCD measurements, which indicates an excellent reactance without irreversible reactions like decomposition of the electrolyte. To further investigate the electrochemical performance of both types of electrodes, the capacitance was plotted over a wide range of scan and charging rates (Fig. 5).

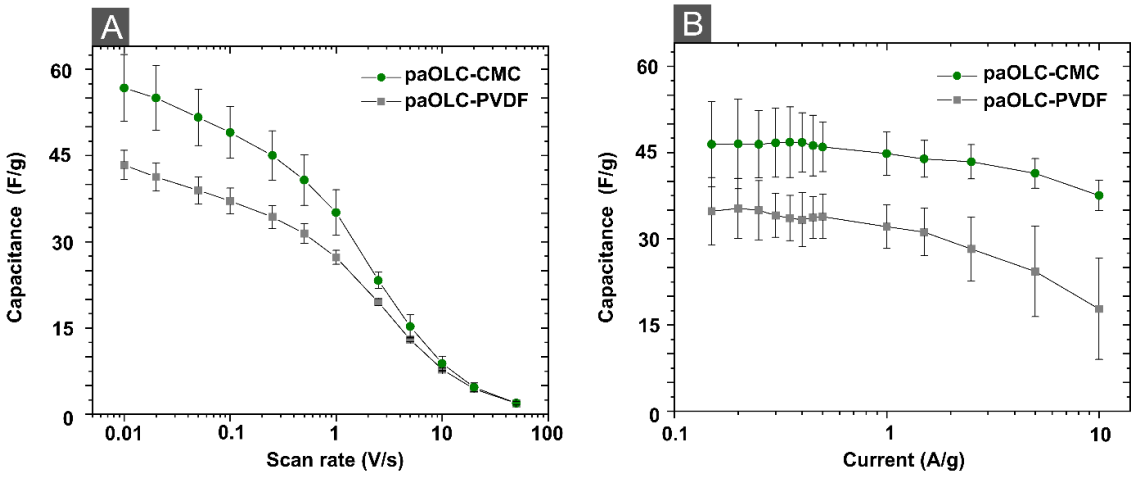

Fig. 5: *Comparison of the specific capacitance and relative capacitance retention between* ***paOLC****-electrodes with PDVF and CMC binders, respectively, as a function of (A) scan rate, and (B) current density.*

As expected, the capacitance decreased with increasing scan rate. The supercapacitor retains ca. 70 % of its capacitance when increasing the scan rate from 10 mV s^{-1} to 500 mV s^{-1}. A further increase to 50 V s^{-1} decreases the capacitance significantly to around 3 F g^{-1}. The porous network provides surface to form an electrical double layer but also tortuosity which induces diffusional resistance for the electrolyte. Hence, the surface can only be utilized partially to form an electric double layer before reversing the voltage, resulting in a lower capacitance at higher scan rates. As shown in Fig. 5A, the capacitance is not saturating even at the smallest scan-rates investigated. These characteristics are observed independently of the used binder in both systems. However, the system with CMC offers higher maximal capacitance, which

indicates that in our experiments the combination of **paOLC** with CMC is favorable over using PVDF. The capacitance measured by CCCD at different charging rates between 0.15 A g^{-1} and 10 A g^{-1} (Fig. 5 B) confirms these considerations. The experimental results propose that the **paOLC-CMC** system provides superior capacitance compared to the **paOLC-PVDF**, an observation that correlates with the specific surface area of the respective binder electrodes accessible to N_2 system. Independent from the capacitance, the charging kinetics are comparable; this can be explained by the higher amount of accessible surface area in the case of the CMC binder at similar transport porosity.

Other OLC-based systems with organic electrolyte reveal a similar power handling,[35], but lower specific capacitance (ca. 40 F g^{-1} at 0.3 A g^{-1})[18], for a better comparison we also included a Ragone plot (Fig. S7).[63, 64] To our knowledge significantly higher values were only reached by functionalization or coating of the onion-like carbon.[30, 38] With activated carbon and organic electrolytes capacitances in range of 100 F g^{-1} are characteristic due to their high specific surface typically in the range of 1000-3000 m^2 g^{-1}.[65] However, a direct comparison of the maximum specific capacitance of the active material can be misleading because of different current densities, scan rates or parameters within the cell setup, such as thickness, mass loading of the electrode and electrolyte composition.[66]

As the combination of onion-like carbon as active material and CMC as eco-friendly binder in a thin film electrode was successful, the frequency response behavior of the different electrodes by electrochemical impedance spectroscopy (EIS, 1 Mhz-100 mHz) as well as their stability after 5000 cycles was compared (Fig. 6).

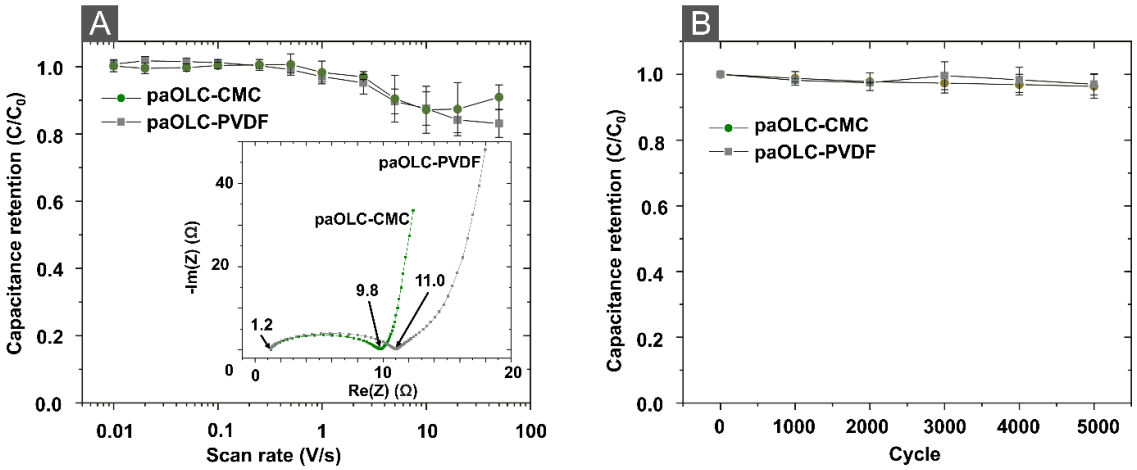

Fig. 6: *Comparison between* ***paOLC*** *electrodes with PVDF and CMC (A) capacitance retention after 5000 cycles as a function of scan rate with an insert showing EIS data, (B) capacitance retention during 5000 cycle test.*

The Nyquist plots (Fig. 6A) feature a similar equivalent series resistance (ESR) of 1.2 Ω at a high frequency for both systems. The charge transfer resistance represented by the semicircle at medium frequencies as well as the equivalent distributed resistance in the slow the frequency regime is shifted towards a higher real resistance for the PVDF compared to the CMC system. According to literature, this frequency behavior suggests a lower ion diffusion resistance and superior pore accessibility for the CMC based electrode. [67]

The capacitance retention (C/C_0) after 5000 cycles was determined over a wide range of scan rates for both systems (Fig. 6). High retentions could be attained over the entire range of scan rates (Fig. 6A) showing excellent durability of the binder electrode's integrity for both systems. During the 5000 cycles at a scan rate of 2.5 V s^{-1}, the electrodes with CMC and PVDF preserved ~96 % of their initial capacitance C_0 (Fig. 6B). It was also shown that power handling was not altered after 5000 cycles (Fig. S8 and Fig. S9).

3.1.4 Conclusion

In summary, the combination of an active material based on OLC and a green binder in an aqueous slurry approach enabled the production of very efficient thin film electrodes for supercapacitors. The use of preagglomerated OLC particles as active material with high surface, mesoporosity, monodispersity, and an environmentally friendly, sustainable binder and a water-based preparation led to the easily scalable production of a competitive carbon-based supercapacitor. The electrochemical measurements of the device provide convincing

results regarding capacitance and power performance over a wide range of scan rates as well as a convincing stability of the electrode's integrity. The viability of the water based **paOLC-CMC** system regarding performance and sustainability is highlighted by comparing it with the **paOLC-PVDF** electrode where an organic solvent based slurry and PVDF as binder was used, thus enabling the production of performant and at the same time sustainably producible devices.

The presented electrode production with **paOLC-CMC** can be easily expanded either in a top-down approach where the electrodes act as template to adsorb pseudocapacitive substances or as a bottom-up solution using the technique to assemble performant and sustainable electrodes.

3.1.5 Supporting information

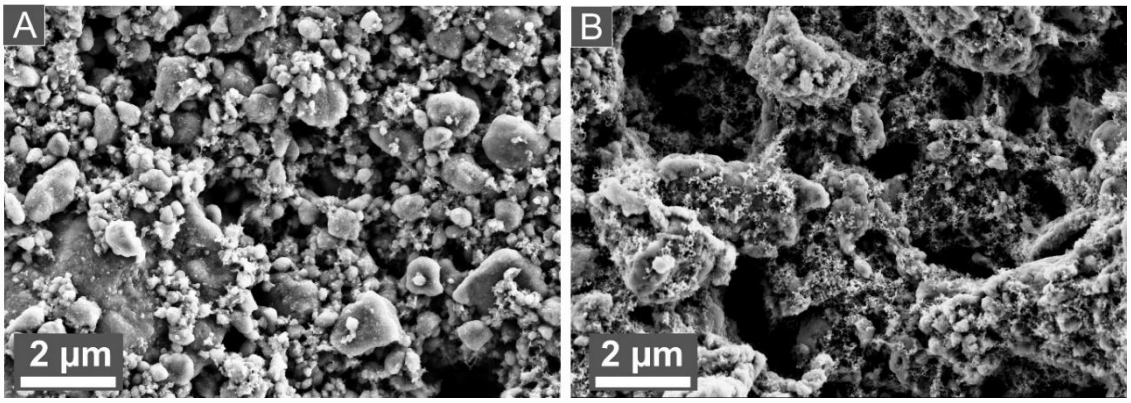

Fig. S1*: SEM image of the surface of the produced electrode before pressing and cycling of paOLC-PVDF (A) and paOLC-CMC (B)*

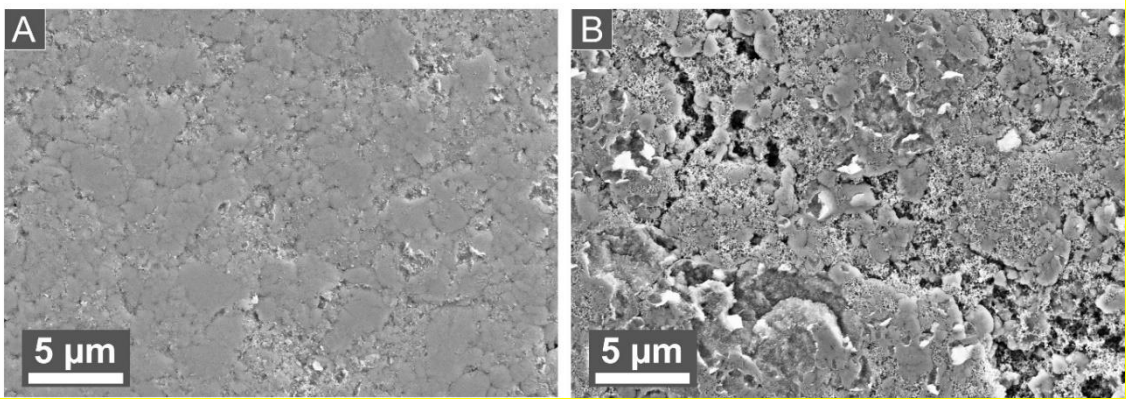

Fig. S2*: SEM image of the surface of the produced electrode after pressing and before cycling of paOLC-PVDF (A) and paOLC-CMC (B)*

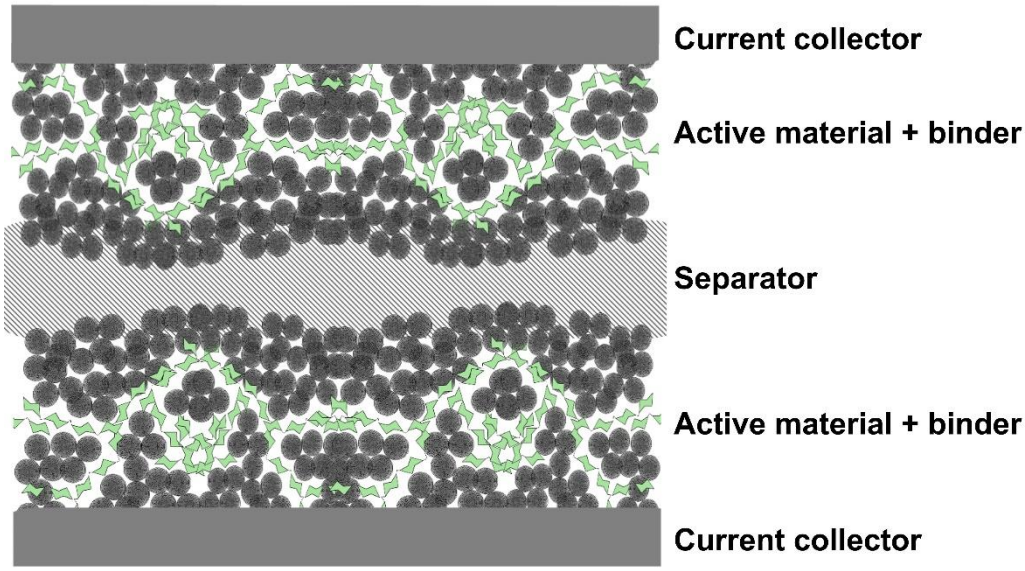

***Fig. S3**: Scheme of the symmetrical supercapacitor cell*

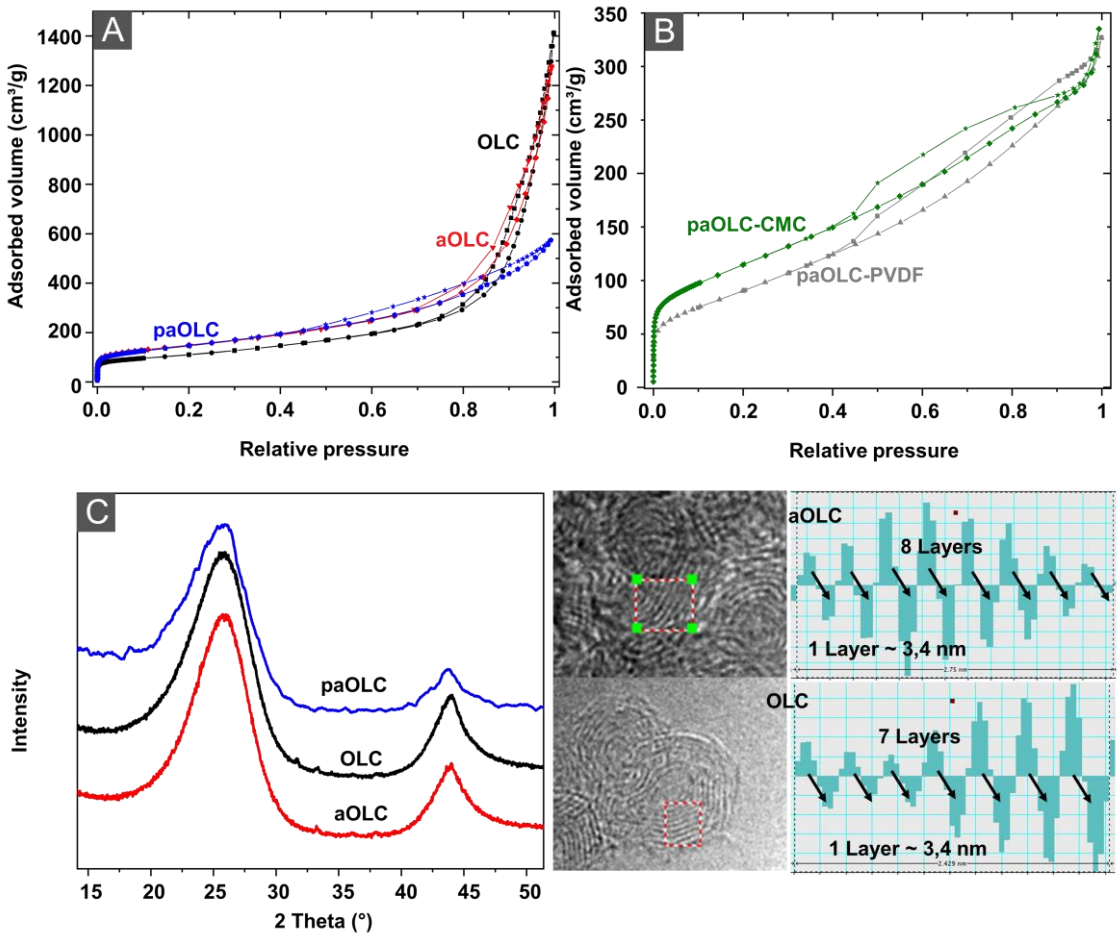

***Fig. S4:** N_2 adsorption-isotherm of OLC aOLC and paOLC (A) as well as of paOLC-CMC and paOLC-PVDF (B)*

Tab. S1: *Comparison of structural parameters derived from sorption analysis.*

	S_{BET} (m^2/g)	S_{ext} (m^2/g)	S_{ext}/S_{BET} (%)
OLC	389	340	87
aOLC	527	453	86
paOLC	527	508	96

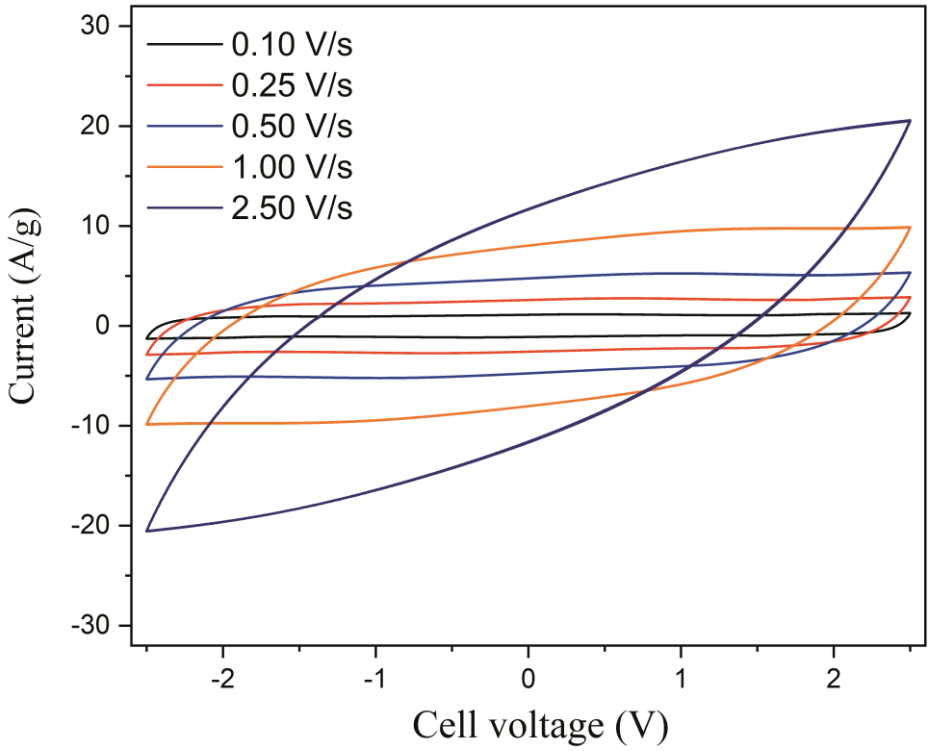

Fig. S5*: Cyclic voltammogram of paOLC-based electrodes with PVDF binder using different scan rates between 0.10 V* s^{-1} *up to 2.5 V* s^{-1}*.*

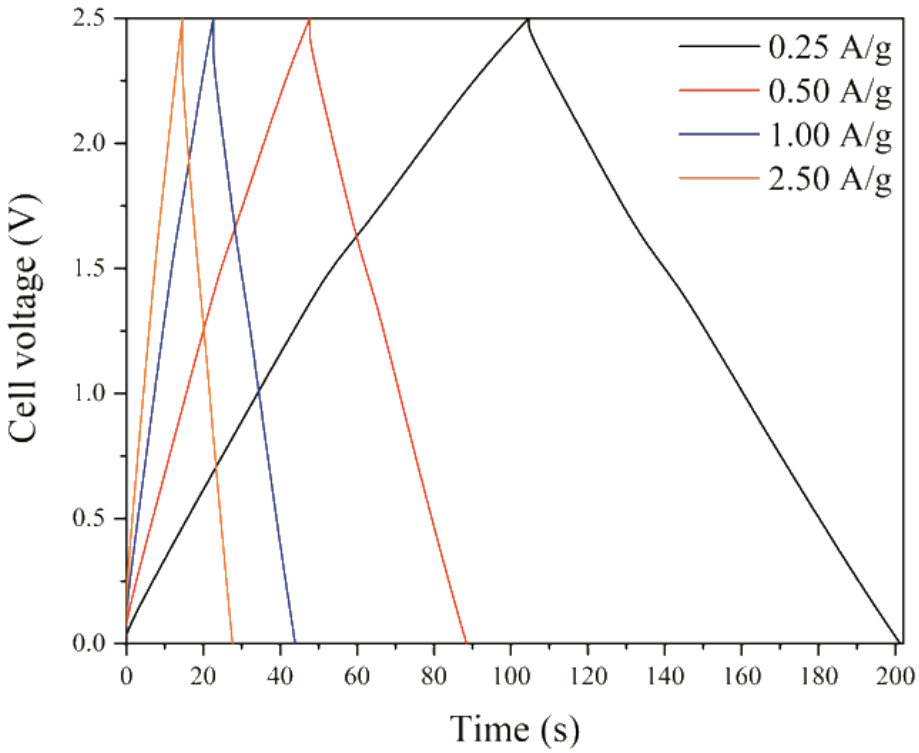

***Fig. S6**: CCCD measurements of paOLC-based electrodes with PVDF binder using different current densities.*

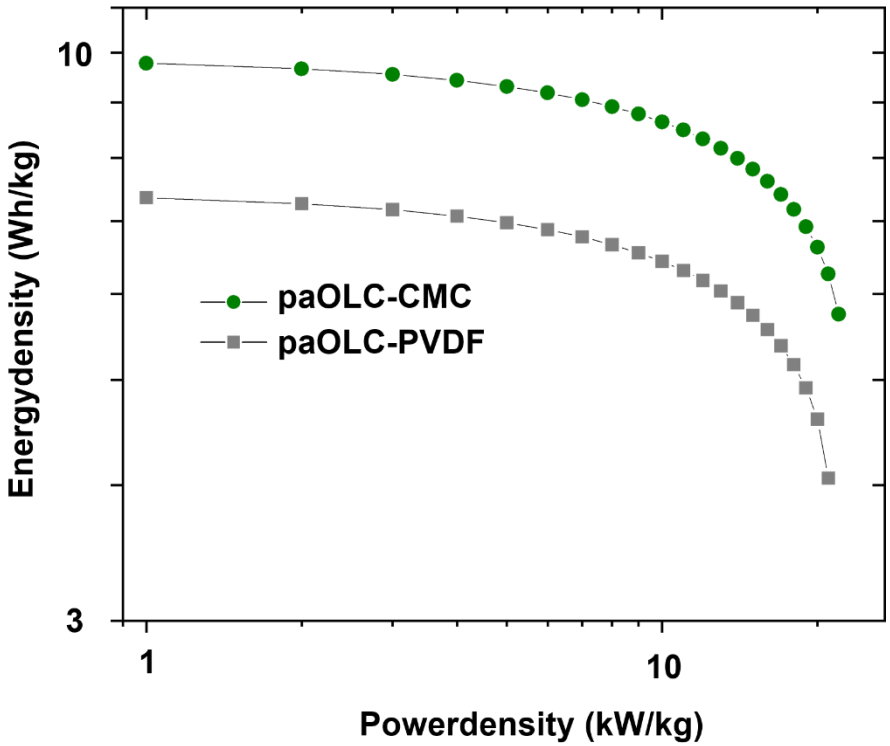

***Fig. S7**: Ragone plot for the paOLC-based device with PVDF and CMC as binder based on the total active material of the device.*

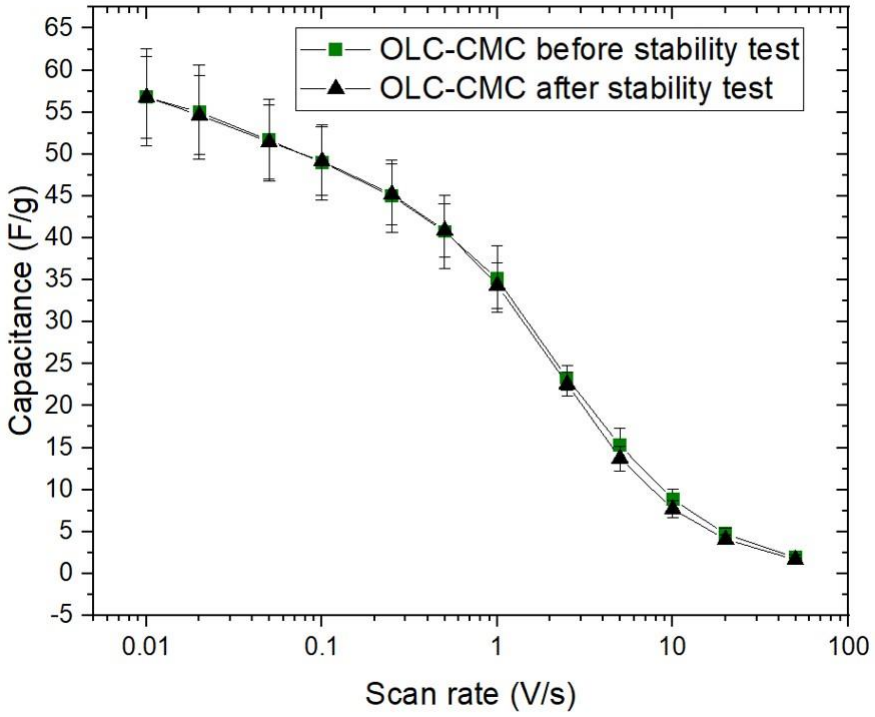

Fig. S8: *Comparison of Capacitance of paOLC-based electrodes with CMC before and after the stability test as binder using different scan rates between 0.10 V s^{-1} up to 2.5 V s^{-1}*

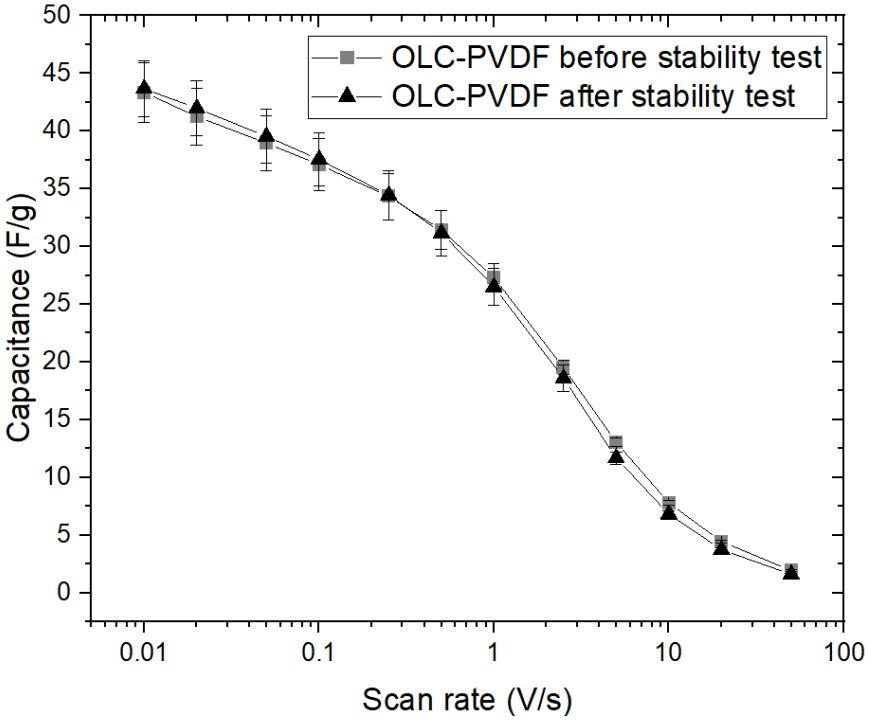

Fig. S9: *Comparison of Capacitance of paOLC-based electrodes with PVDF before and after the stability test as binder using different scan rates between 0.10 V s^{-1} up to 2.5 V s^{-1}*

3.1.6 Refernces

[1] Z. Yang, J. Zhang, M.C. Kintner-Meyer, X. Lu, D. Choi, J.P. Lemmon, J. Liu, Electrochemical energy storage for green grid, Chem. Rev. 111(5) (2011) 3577-3613. https://doi.org/10.1021/cr100290v

[2] J. R. Miller, P. Simon, Electrochemical capacitors for energy management, Science 321(5889) (2008) 651-652. https://doi.org/10.1126/science.1158736

[3] A. M. Saleem, V. Desmaris, P. Enoksson, Performance enhancement of carbon nanomaterials for supercapacitors, J. Nanomater. 2016 (2016). https://doi.org/10.1155/2016/1537269

[4] L. Weinstein, R. Dash, Supercapacitor carbons, Mater Today 10(16) (2013) 356-357. https://doi.org/10.1016/j.mattod.2013.09.005

[5] G. S. d. Reis, S. H. Larsson, H. P. d. de Oliveira, M. Thyrel, E.C. Lima, Sustainable Biomass Activated Carbons as Electrodes for Battery and Supercapacitors–A Mini-Review, Nanomaterials 10(7) (2020) 1398. https://doi.org/10.3390/nano10071398

[6] D. Ugarte, Curling and closure of graphitic networks under electron-beam irradiation, Nature 359(6397) (1992) 707-709. https://doi.org/10.1038/359707a0

[7] V. L. Kuznetsov, A. L. Chuvilin, Y. V. Butenko, I. Y. Mal'kov, V. M. Titov, Onion-like carbon from ultra-disperse diamond, Chem. Phys. Lett. 222(4) (1994) 343-348. https://doi.org/10.1016/0009-2614(94)87072-1

[8] W. Lian, H. Song, X. Chen, L. Li, J. Huo, M. Zhao, G. Wang, The transformation of acetylene black into onion-like hollow carbon nanoparticles at 1000 C using an iron catalyst, Carbon 46(3) (2008) 525-530. https://doi.org/10.1016/j.carbon.2007.12.024

[9] X. Chen, H. Yang, G. Wu, M. Wang, F. Deng, X. Zhang, J. Peng, W. Li, Generation of curved or closed-shell carbon nanostructures by ball-milling of graphite, J. Cryst. Growth 218(1) (2000) 57-61. https://doi.org/10.1016/S0022-0248(00)00486-3

[10] F. Mathieux, F. Ardente, S. Bobba, P. Nuss, G.A. Blengini, P.A. Dias, D. Blagoeva, C.T. de Matos, D. Wittmer, C. Pavel, Critical Raw Materials and the Circular Economy – Background report, in: F. Mathieux (Ed.) Luxembourg, 2017. https://doi.org/10.2760/378123

[11] V. Yu. Dolmatov, A. N. Ozerin, I. I. Kulakova, O. O. Bochchka, N. M. Lapchuk, V. Myllimäki, A. Vehanen, Detonation nanodiamonds: new aspects in the theory and practice of synthesis, properties and applications, Russ. Chem. Rev. 89 (2020) 1428-1462.

[12] S. Tomita, T. Sakurai, H. Ohta, M. Fujii, S. Hayashi, Structure and electronic properties of carbon onions, J. Chem. Phys. 114(17) (2001) 7477-7482. https://doi.org/10.1063/1.1360197

[13] M. Zeiger, N. Jäckel, M. Aslan, D. Weingarth, V. Presser, Understanding structure and porosity of nanodiamond-derived carbon onions, Carbon 84 (2015) 584-598. https://doi.org/10.1016/j.carbon.2014.12.050

[14] M. Hantel, V. Presser, J. McDonough, G. Feng, P. T. Cummings, Y. Gogotsi, R. Kötz, In situ electrochemical dilatometry of onion-like carbon and carbon black, J. Electrochem. Soc. 159(11) (2012) A1897-A1903. https://doi.org/10.1149/2.006212jes

[15] M. Zeiger, N. Jaeckel, V. N. Mochalin, V. Presser, Review: carbon onions for electrochemical energy storage, J. Mater. Chem. A 4(9) (2016) 3172-3196. https://doi.org/10.1039/C5TA08295A

[16] Z. Yu, L. Tetard, L. Zhai, J. Thomas, Supercapacitor electrode materials: nanostructures from 0 to 3 dimensions, Energy Environ. Sci. 8(3) (2015) 702-730. https://doi.org/10.1039/c4ee03229b

[17] M. Zeller, V. Lorrmann, G. Reichenauer, M. Wiener, J. Pflaum, Relationship Between Structural Properties and Electrochemical Characteristics of Monolithic Carbon Xerogel-Based Electrochemical Double-Layer Electrodes in Aqueous and Organic Electrolytes, Adv. Energy Mater. 2(5) (2012) 598-605. https://doi.org/10.1002/aenm.201100513

[18] C. Portet, G. Yushin, Y. Gogotsi, Electrochemical performance of carbon onions, nanodiamonds, carbon black and multiwalled nanotubes in electrical double layer capacitors, Carbon 45(13) (2007) 2511-2518. https://doi.org/10.1016/j.carbon.2007.08.024

[19] M. Zeiger, N. Jäckel, V. N. Mochalin, V. Presser, carbon onions for electrochemical energy storage, J. Mater. Chem. A 4(9) (2016) 3172-3196. https://doi.org/10.1039/c5ta08295a

[20] M. E. Plonska-Brzezinska, L. Echegoyen, Carbon nano-onions for supercapacitor electrodes: recent developments and applications, J. Mater. Chem. A 1(44) (2013) 13703-13714. https://doi.org/10.1039/c3ta12628e

[21] P. H. Huang, D. Pech, R.Y. Lin, J.K. McDonough, M. Brunet, P.L. Taberna, Y. Gogotsi, P. Simon, On-chip micro-supercapacitors for operation in a wide temperature range, Electrochem. commun. 36 (2013) 53-56. https://doi.org/10.1016/j.elecom.2013.09.003

[22] C. Portet, J. Chmiola, Y. Gogotsi, S. Park, K. Lian, Electrochemical characterizations of carbon nanomaterials by the cavity microelectrode technique, Electrochim. Acta 53(26) (2008) 7675-7680. https://doi.org/10.1016/j.electacta.2008.05.019

[23] D. Weingarth, M. Zeiger, N. Jäckel, M. Aslan, G. Feng, V. Presser, Graphitization as a universal tool to tailor the potential-dependent capacitance of carbon supercapacitors, Adv. Energy Mater. 4(13) (2014) 1400316. https://doi.org/10.1002/aenm.201400316

[24] M. E. Plonska-Brzezinska, A. Palkar, K. Winkler, L. Echegoyen, Electrochemical properties of small carbon nano-onion films, Electrochem. Solid-State Lett. 13(4) (2010) K35-K38. https://doi.org/10.1149/1.3299252

[25] M. Zeiger, N. Jäckel, D. Weingarth, V. Presser, Vacuum or flowing argon: What is the best synthesis atmosphere for nanodiamond-derived carbon onions for supercapacitor electrodes?, Carbon 94 (2015) 507-517. https://doi.org/10.1016/j.carbon.2015.07.028

[26] O. Butsyk, P. Olejnik, E. Romero, M.E. Plonska-Brzezinska, Postsynthetic treatment of carbon nano-onions: Surface modification by heteroatoms to enhance their capacitive and electrocatalytic properties, Carbon 147 (2019) 90-104. https://doi.org/10.1016/j.carbon.2019.02.063

[27] M. Zeiger, D. Weingarth, V. Presser, Quinone-Decorated Onion-Like Carbon/Carbon Fiber Hybrid Electrodes for High-Rate Supercapacitor Applications, Chemelectrochem 2(8) (2015) 1117-1127. https://doi.org/10.1002/celc.201500130

[28] R. Borgohain, J. Li, J.P. Selegue, Y. T. Cheng, Electrochemical Study of Functionalized Carbon Nano-Onions for High-Performance Supercapacitor Electrodes, J. Phys. Chem. C 116(28) (2012) 15068-15075. https://doi.org/10.1021/jp301642s

[29] M. E. Plonska-Brzezinska, M. Lewandowski, M. Blaszyk, A. Molina-Ontoria, T. Lucinski, L. Echegoyen, Preparation and Characterization of Carbon Nano-Onion/PEDOT:PSS Composites, ChemPhysChem. 13(18) (2012) 4134-4141. https://doi.org/10.1002/cphc.201200789

[30] O. Mykhailiv, M. Imierska, M. Petelczyc, L. Echegoyen, M.E. Plonska-Brzezinska, Chemical versus Electrochemical Synthesis of Carbon Nano-onion/Polypyrrole Composites for Supercapacitor Electrodes, Chem. Eur. J. 21(15) (2015) 5783-5793. https://doi.org/10.1002/chem.201406126

[31] I. Kovalenko, D. G. Bucknall, G. Yushin, Detonation Nanodiamond and Onion-Like-Carbon-Embedded Polyaniline for Supercapacitors, Adv. Funct. Mater. 20(22) (2010) 3979-3986. https://doi.org/10.1002/adfm.201000906

[32] M. E. Plonska-Brzezinska, D. M. Brus, A. Molina-Ontoria, L. Echegoyen, Synthesis of carbon nano-onion and nickel hydroxide/oxide composites as supercapacitor electrodes, RSC Adv. 3(48) (2013) 25891-25901. https://doi.org/10.1039/c3ra44249g

[33] G. Moussa, C. Matei Ghimbeu, P.-L. Taberna, P. Simon, C. Vix-Guterl, Relationship between the carbon nano-onions (CNOs) surface chemistry/defects and their capacitance in aqueous and organic electrolytes, Carbon 105 (2016) 628-637. https://doi.org/10.1016/j.carbon.2016.05.010

[34] B. Zhang, D. Wang, B. Yu, F. Zhou, W. Liu, Candle soot as a supercapacitor electrode material, RSC Adv. 4(6) (2014) 2586-2589. https://doi.org/10.1039/c3ra42507j

[35] M. Zeiger, N. Jaeckel, D. Weingarth, V. Presser, Vacuum or flowing argon: What is the best synthesis atmosphere for nanodiamond-derived carbon onions for supercapacitor electrodes?, Carbon 94 (2015) 507-517. https://doi.org/10.1016/j.carbon.2015.07.028

[36] D. Weingarth, M. Zeiger, N. Jackel, M. Aslan, G. Feng, V. Presser, Graphitization as a Universal Tool to Tailor the Potential-Dependent Capacitance of Carbon Supercapacitors, Adv. Energy Mater. 4(13) (2014). https://doi.org/10.1002/aenm.201400316

[37] Y. Wang, S. F. Yu, C.Y. Sun, T.J. Zhu, H. Y. Yang, MnO2/onion-like carbon nanocomposites for pseudocapacitors, J. Mater. Chem. A 22(34) (2012) 17584-17588. https://doi.org/10.1039/c2jm33558a

[38] K. L. Van Aken, K. Maleski, T.S. Mathis, J. P. Breslin, Y. Gogotsi, Processing of Onion-like Carbon for Electrochemical Capacitors, ECS J. Solid State Sci. Technol. 6(6) (2017) M3103-M3108. https://doi.org/10.1149/2.0181706jss

[39] O. Mykhailiv, K. Brzezinski, B. Sulikowski, Z. Olejniczak, M. Gras, G. Lota, A. Molina-Ontoria, M. Jakubczyk, L. Echegoyen, M.E. Plonska-Brzezinska, Boron-Doped Polygonal Carbon Nano-Onions: Synthesis and Applications in Electrochemical Energy Storage, Chem. Eur. J. 23(29) (2017) 7132-7141. https://doi.org/10.1002/chem.201700914

[40] B. J. Henry, J. P. Carlin, J. A. Hammerschmidt, R. C. Buck, L. W. Buxton, H. Fiedler, J. Seed, O. Hernandez, A critical review of the application of polymer of low concern and regulatory criteria to fluoropolymers, Integr. Environ. Assess. Manag. 14(3) (2018) 316-334. https://doi.org/10.1002/ieam.4035

[41] D. Bresser, D. Buchholz, A. Moretti, A. Varzi, S. Passerini, Alternative binders for sustainable electrochemical energy storage–the transition to aqueous electrode processing and bio-derived polymers, Energy Environ. Sci. 11(11) (2018) 3096-3127. https://doi.org/10.1039/c8ee00640g

[42] M. Thommes, K. Kaneko, A. V. Neimark, J.P. Olivier, F. Rodriguez-Reinoso, J. Rouquerol, K.S. Sing, Physisorption of gases, with special reference to the evaluation of surface area and pore size distribution (IUPAC Technical Report), Pure Appl. Chem. 87(9-10) (2015) 1051-1069. https://doi.org/10.1515/pac-2014-1117

[43] R. Magee, Evaluation of the external surface area of carbon black by nitrogen adsorption, Rubber Chem. Technol. 68(4) (1995) 590-600. https://doi.org/10.5254/1.3538760

[44] P. Tarazona, A density functional theory of melting, Mol. Phys. 52(1) (1984) 81-96. https://doi.org/10.1080/00268978400101071

[45] J.P. Olivier, Modeling physical adsorption on porous and nonporous solids using density functional theory, J. Porous Mater. 2(1) (1995) 9-17. https://doi.org/10.1007/BF00486565

[46] M. Maddox, J. Olivier, K. Gubbins, Characterization of MCM-41 using molecular simulation: heterogeneity effects, Langmuir 13(6) (1997) 1737-1745. https://doi.org/10.1021/la961068o

[47] J. P. Olivier, Improving the models used for calculating the size distribution of micropore volume of activated carbons from adsorption data, Carbon 36(10) (1998) 1469-1472. https://doi.org/10.1016/S0008-6223(98)00139-0

[48] S. Zhang, N. Pan, Supercapacitors performance evaluation, Adv. Energy Mater. 5(6) (2015) 1401401. https://doi.org/10.1002/aenm.201401401

[49] A.C. Ferrari, Raman spectroscopy of graphene and graphite: disorder, electron–phonon coupling, doping and nonadiabatic effects, Solid State Commun. 143(1-2) (2007) 47-57. https://doi.org/10.1016/j.ssc.2007.03.052

[50] V. Mennella, G. Monaco, L. Colangeli, E. Bussoletti, Raman spectra of carbon-based materials excited at 1064 nm, Carbon 33(2) (1995) 115-121. https://doi.org/10.1016/0008-6223(94)00113-E

[51] V. Mochalin, S. Osswald, Y. Gogotsi, Contribution of functional groups to the Raman spectrum of nanodiamond powders, Chem. Mater. 21(2) (2009) 273-279. https://doi.org/10.1021/cm802057q

[52] M. E. Plonska-Brzezinska, A.T. Dubis, A. Lapinski, A. Villalta-Cerdas, L. Echegoyen, Electrochemical Properties of Oxidized Carbon Nano-Onions: DRIFTS-FTIR and Raman Spectroscopic Analyses, ChemPhysChem. 12(14) (2011) 2659-2668. https://doi.org/10.1002/cphc.201100198

[53] D. Roy, M. Chhowalla, H. Wang, N. Sano, I. Alexandrou, T. Clyne, G. Amaratunga, Characterisation of carbon nano-onions using Raman spectroscopy, Chem. Phys. Lett. 373(1-2) (2003) 52-56. https://doi.org/10.1016/S0009-2614(03)00523-2

[54] P. Tan, S. Dimovski, Y. Gogotsi, Raman scattering of non–planar graphite: arched edges, polyhedral crystals, whiskers and cones, Philos. Trans. Royal Soc. A 362(1824) (2004) 2289-2310. https://doi.org/10.1098/rsta.2004.1442

[55] K. Bogdanov, A. Fedorov, V. Osipov, T. Enoki, K. Takai, T. Hayashi, V. Ermakov, S. Moshkalev, A. Baranov, Annealing-induced structural changes of carbon onions: high-resolution transmission electron microscopy and Raman studies, Carbon 73 (2014) 78-86. https://doi.org/10.1016/j.carbon.2014.02.041

[56] L. Malard, M. Pimenta, G. Dresselhaus, M. Dresselhaus, Raman spectroscopy in graphene, Phys. Rep. 473(5-6) (2009) 51-87. https://doi.org/10.1016/j.physrep.2009.02.003

[57] S. Tomita, A. Burian, J. C. Dore, D. LeBolloch, M. Fujii, S. Hayashi, Diamond nanoparticles to carbon onions transformation: X-ray diffraction studies, Carbon 40(9) (2002) 1469-1474. https://doi.org/10.1016/S0008-6223(01)00311-6

[58] W. H. Bragg, W. L. Bragg, The reflection of X-rays by crystals, Proc. Math. Phys. Eng. 88(605) (1913) 428-438. https://doi.org/10.1098/rspa.1913.0040

[59] O. O. Mykhaylyk, Y. M. Solonin, D. N. Batchelder, R. Brydson, Transformation of nanodiamond into carbon onions: a comparative study by high-resolution transmission electron microscopy, electron energy-loss spectroscopy, X-ray diffraction, small-angle X-ray scattering, and ultraviolet Raman spectroscopy, Int. J. Appl. Phys. 97(7) (2005) 074302. https://doi.org/10.1063/1.1868054

[60] L. Bonnefoi, P. Simon, J. Fauvarque, C. Sarrazin, J. Sarrau, A. Dugast, Electrode compositions for carbon power supercapacitors, J. Power Sources 80(1-2) (1999) 149-155. https://doi.org/10.1016/S0378-7753(99)00069-5

[61] T. Zhao, Y. Meng, R. Ji, F. Wu, L. Li, R. Chen, Maintaining structure and voltage stability of Li-rich cathode materials by green water-soluble binders containing Na+ ions, J Alloy Compd 811 (2019) 152060. https://doi.org/10.1016/j.jallcom.2019.152060

[62] M .D. Stoller, R. S. Ruoff, Best practice methods for determining an electrode material's performance for ultracapacitors, Energy Environ. Sci. 3(9) (2010) 1294-1301. https://doi.org/10.1039/c0ee00074d

[63] Y. Gao, Y. S. Zhou, M. Qian, X. N. He, J. Redepenning, P. Goodman, H. M. Li, L. Jiang, Y.F. Lu, Chemical activation of carbon nano-onions for high-rate supercapacitor electrodes, Carbon 51 (2013) 52-58. https://doi.org/10.1016/j.carbon.2012.08.009

[64] R. Vicentini, J. P. Aguiar, R. Beraldo, R. Venâncio, F. Rufino, L.M. Da Silva, H. Zanin, Ragone Plots for Electrochemical Double-Layer Capacitors, Batter. Supercaps 4(8) (2021) 1291-1303. https://doi.org/10.1002/batt.202100093

[65] A. Divyashree, G. Hegde, Activated carbon nanospheres derived from bio-waste materials for supercapacitor applications–a review, RSC Adv. 5(107) (2015) 88339-88352. https://doi.org/10.1039/c5ra19392c

[66] Y. Gogotsi, P. Simon, True performance metrics in electrochemical energy storage, Science 334(6058) (2011) 917-918. https://doi.org/10.1126/science.1213003

[67] B.-A. Mei, O. Munteshari, J. Lau, B. Dunn, L. Pilon, Physical interpretations of Nyquist plots for EDLC electrodes and devices, J. Phys. Chem. C 122(1) (2018) 194-206. https://doi.org/10.1021/acs.jpcc.7b10582

3.2 Pseudocapacitor with onion-like carbon

Parts of this chapter are based on the manuscript: In situ polymerization of EDOT onto sulfonated onion-like carbon for pseudocapacitor electrodes by C. Bauer, M. Kirchner, A. Krueger.

For the second chapter, the basic objective was to enhance the capacitance of the device by a pseudocapacitance functionalization using the knowledge from the first chapter and the active material OLC as a platform. Many state of the art pseudocapacitors rely on aqueous systems featuring a narrow potential window.[1] These designs maximize the specific capacitance with little regard towards power density. For the presented pseudocapacitors, a different strategy was aspired. The following investigation targeted to increase the strong aspects of the OLC material rather than counterbalancing the weakness of the system. As the accessibility of the external surface was identified as an outstanding property, a pseudocapacitive functionalization was chosen with high charging and discharging kinetics. This role was fulfilled by PEDOT, which was mechanically supported and electrically connected by OLC. The main problem was to ensure an even distribution and tight connection of PEDOT onto the surface of the OLC material. This problem was caused by the indispersibility of both starting materials in any common solvents. Therefore, the goal was to develop a system, which is soluble (during production) but also insoluble (as electrode). The inspiration for this research was knowledge derived from the PEDOT:PSS system,[2] which has been integrated into various nanomaterials.[3]

3.2.1 Introduction

Conductive polymers (CPs) are used as active material for supercapacitors due to their convenient synthesis, electrochemical stability, and intrinsic capacitance.[4] The charge storage capability of CPs originates mainly from faradaic but also from non-faradaic processes. The formation of a double layer at the solid-liquid interface between the CP and the electrolyte represents the non-faradaic part. The faradaic component, also called pseudocapacitance, is attributed to redox reactions of the CPs. Due to limited specific porosity of CPs, the contribution of pseudocapacitance towards energy storage exceeds the non-faradaic component.[5] In this context, CPs such as polyaniline (PANI), polypyrrole (PPy), and poly(3,4-ethylenedioxythiophene) (PEDOT), are often used for pseudocapacitor applications. Among these CPs, PEDOT offers a superior cyclic stability and an outstanding resilience of its oxidized state, which enables application in a wide potential window.[4]

Despite their electrochemical stability, CPs lack inherent mechanical strength. When used in electrodes for supercapacitors, swelling and shrinking induced by cycling initiates crack formation resulting in degrading capacitance.[6] This drawback is often addressed by the addition of nanoparticles, which act as a framework to provide mechanical strength and space for swelling due to open porosity. For this purpose, various nanoparticles like MXenes,[7] ZnO nanowires,[8] nanofibers,[9] carbon nanotubes,[10] graphene[11] and onion-like carbon[12] have been combined with CPs. Carbon particles are ideal because of their sustainability, abundance, electrical conductivity and capability to contribute non-faradaic capacitance.[6]

To yield a superior composite electrode, the contradicting requirements of a stable coupling between PEDOT and carbon particle while maintaining their dispersibility during the formation of the composite. Both requirements are vital, with the tight interconnection between the particles as a gateway for the electrical current and their dispersibility assuring percolation of the PEDOT network throughout the forming composite. However, neither carbon nanoparticles nor PEDOT are easily dispersible.[6]

The most convenient approach to enable PEDOT dispersibility is to link it ionically with polystyrene sulfonate (PSS).[6] These PEDOT:PSS micelles can be used to adsorb onto the carbon particle, which was reported for onion-like carbon (OLC) by Plonska-Brzezinska *et al*., enabling the application in electrodes for supercapacitors with a maximum capacitance of 75 F/g.[12] However, as the charge of PEDOT is neutralized by the interaction with sulfonic acid groups of PSS, excess amounts of the latter are required to maintain dispersibility of PEDOT:PSS.[6]

Another possibility is to establish CP monomers at the surface of the carbon material prior to polymerization. This in situ approach can either be promoted by electrodeposition or by chemical reactions. Electrodeposition is well controllable but also requires charged carbon particles for co-deposition and a specialized setup.[11] Chemical oxidation is a more facile method that does not need specific equipment, additionally offering high yields but also requiring a stable carbon dispersion.[6]

Here we report an efficient approach to integrate and connect PEDOT with carbon particles to form a composite suitable for the application in supercapacitor electrodes. Inspired by the functionality of PEDOT:PSS, we designed carbon nanoparticles directly decorated with benzenesulfonic groups. Sulfonation of carbon onions provides not only superior dispersibility but also the binding sites for PEDOT formed upon oxidative in situ polymerization of EDOT.

This enables the template assisted precipitation of the PEDOT molecules and thus a homogeneous distribution in the composite without the formation of insulating PSS domains. In the electrode, the OLC template offers accessible surface area and mechanical stability while PEDOT enhances the specific capacitance and connects OLC agglomerates. Based on these findings the composite can be used as active material for supercapacitor electrodes without additional binder.

3.2.2 Experimental section

Sulfonation of OLC and Composite formation

OLC was obtained by thermal annealing of detonation nanodiamond (Gansu Lingyun Corp.) in vacuum (~1 mbar) for two hours at 1500 °C (heating rate 5 K min^{-1}) using a tube furnace (STF 16/450, Carbolite Gero GmbH).[13]

For the functionalization with phenyl groups, OLC (2.39 g) was pre-dried at 350 °C for three hours in air and then dispersed in dried toluene (100 mL) via sonication. Dibenzoyl peroxide (DBPO, 5.22 g, 21.55mmol) was added and the dispersion was heated to 80 °C in an ultrasonic bath. After two hours of sonication, more DBPO (5.18 g, 21.38 mmol) was added and sonication continued for two hours at 80 °C. After another addition of DBPO (5.07 g, 20.93 mmol), sonication continued for 8 h. To end the reaction, water (15 mL) was added. The particles were separated from the reaction mixture by centrifugation (6000 rpm, 20 minutes). The phenylated OLC particles (**POLC**) were then washed four times with THF. Each time the particles were first dispersed in THF (15 mL) via sonication and then centrifuged (6000 rpm, 20 minutes).

POLC (1.80 g) were then combined with oleum (3.0 mL, 30 wt% SO_3), dispersed in an ultrasonic bath and heated to 80 °C for four hours. To finish the reaction, water (5 mL) was added. The sulfonated OLC (**SPOLC**) were separated by centrifugation (6000 rpm, 20 min). Afterwards, the supernatant was removed and the residue was dispersed in water via sonication, then centrifuged again (6000 rpm, 20 minutes). The functionalization steps were executed according to a modified procedure reported by Palkar *et al*.[14] Here, ultrasonication was used to increase the reactivity.

Composite Formation

The onion-like carbon material was then used to form composites with PEDOT. To vary the content of benzenesulfonic acid moieties in the composite, **SPOLC**, pristine OLC as well as a

mixture of both was used as carbon template. Based on these templates, three composites **PEDOT@OLC** (Fig. 1A) **PEDOT@SPOLC** (Fig. 1B) and **PEDOT@SPOLC/OLC** (Fig. 1C) were produced. A detailed synthetic procedure for the different composites can be found in the SI.

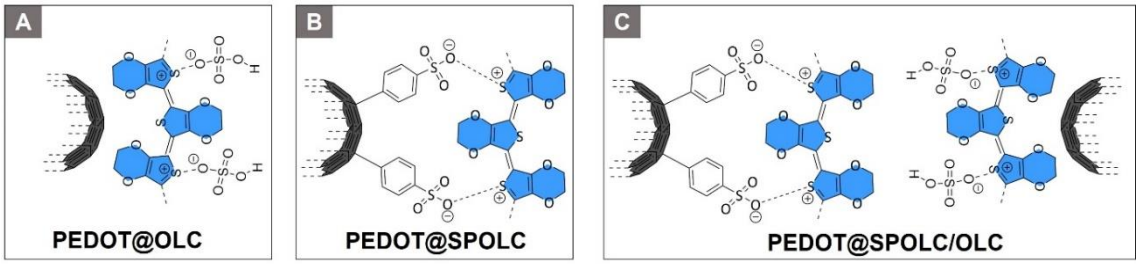

***Fig. 1**: Schematic overview of the three synthesized composites.*

Fabrication of electrodes and supercapacitors

For the slurry, 50 mg of washed **PEDOT@SPOLC, PEDOT@SPOLC/OLC** or **PEDOT@OLC** precipitate was stirred with water (100 mg). To obtain electrodes, the respective slurry was doctor bladed onto a carbon coated aluminum foil (Zflo 2653, Transcontinental Advanced Coatings), dried at ambient conditions for 15 minutes and transferred into a drying furnace (130 °C) for about 12 hours. Round electrodes with a diameter of 16 mm were die cut with a punching iron and pressed with a hydraulic press (ca. 0.2 GPa). Symmetrical cells were produced using a stainless-steel test cell separated by a polymer membrane (Cellgard 2325, El-Cell). The electrolyte was prepared as a 1 M solution of tetraethylammonium tetra-fluoroborate ($TEABF_4$; TCI) in acetonitrile (Sigma Aldrich). Three test cells for each system were assembled in the absence of humidity (<1 ppm) and oxygen (<1 ppm) using a glovebox (N_2, Labmaster 130, M. Braun Inertgas-Systeme).

Characterization

The Raman spectra were acquired with a DXR Raman Microscope (Thermo Fisher Scientific Inc.) using a laser power of 0.2 mW and an excitation wavelength of 532 nm. Thermogravimetric analysis (TGA) was carried out with a STA 6000 (Perkin Elmer) using nitrogen as purge gas (20 L/min), a heating rate of 5 K min^{-1} and a plateau phase of 30 minutes at 130 °C to remove residual water. HRTEM was conducted with a FEI Titan 80-300 (Thermo Fischer Scientific Inc.) using an operating voltage of 300 kV. Scanning electron microscopy (SEM) images were measured at an operating voltage of 5 kV using a Gemini Fe-SEM Ultra-Plus Zeiss field emission scanning electron microscope (Carl Zeiss Microscopy Deutschland

GmbH). Cyclic voltammetry measurements (CV) were carried out with a potentio-/galvanostat (VMP300 Bio-Logic). Electrochemical measurements were conducted in a symmetrical supercapacitor setup. Every composite system was measured in three test cells at ambient conditions. For each applied scan rate the arithmetic average of ten consecutive cycles was used to calculate the total capacitance of the device C_{CV} as well as the specific capacitance for one electrode C_E where *m* is the combined mass of carbon material and PEDOT, *I* the current and V_0 the potential window and *v* the scan rate.

One cycle consists of a charge and a discharge process for every electrode, achieved by a repolarization between $-V_0$ and V_0.

$$C_{CV} = \frac{\int I \, dV}{2 * 2\, V_0 * v} \tag{4}$$

$$C_E = \frac{4 * C_{CV}}{m} \tag{5}$$

3.2.3 Results and discussion

Characterization of the composite material

Raman spectroscopy

Functionalization of carbon particles is vital to ensure their dispersibility in aqueous media as well as for in situ incorporation of EDOT. Surface functionalization with benzenesulfonic acid groups meets both criteria, as the hydrophilic character of the sulfonic acid stabilizes the particles in aqueous media and the anionic charge electrostatically attracts PEDOT tightly to the surface of the OLC particle. As the functionalization occurs on carbon surfaces, Raman microscopy is well suited to identify these changes due to characteristic modes (Fig. 2; Tab. 1).

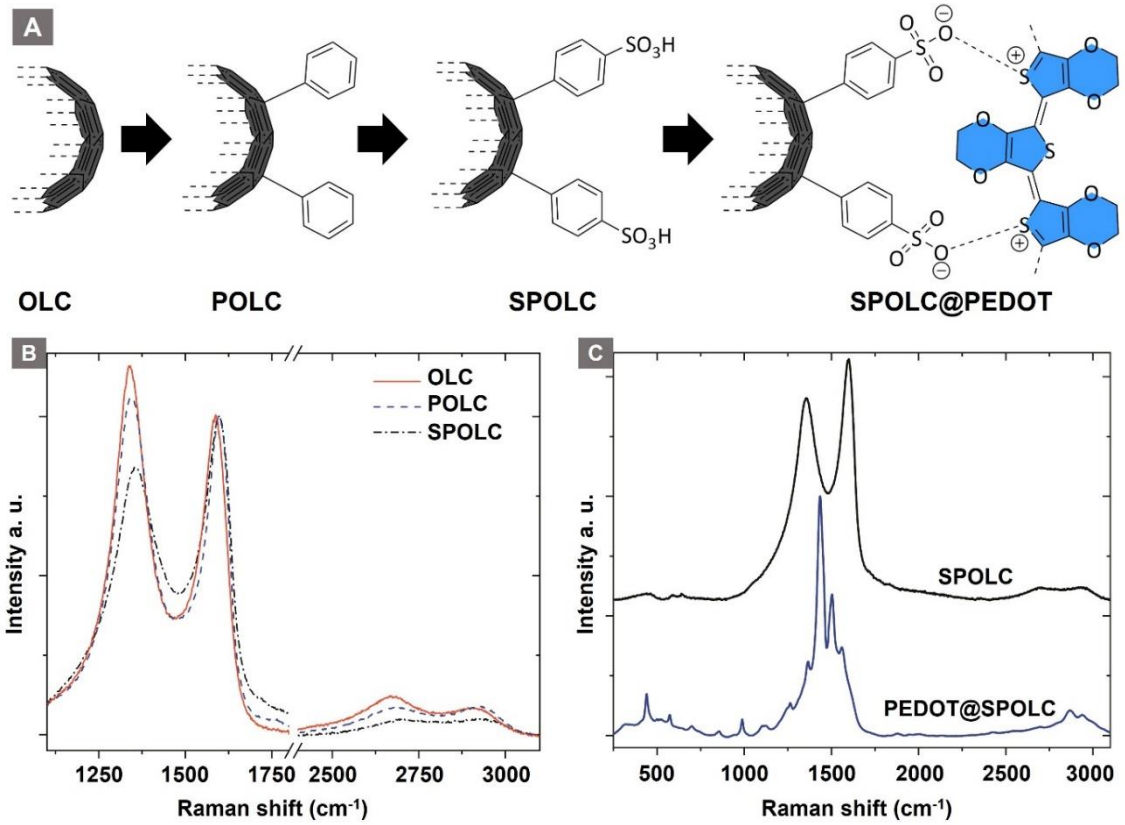

Fig. 2: *Schematic overview for the precursor functionalization (A) as well as Raman shift of the particles before (B) and after (C) PEDOT functionalization.*

Tab: 1: *Raman shifts of G-, D- and 2D-mode and D/G intensity ratios of OLC, POLC and SPOLC.*

	G-mode (1/cm))	D-mode (1/cm)	2D-mode (1/cm)	I_D/I_G	I_{2D}/I_G
OLC	1588	1338	2670	1.17	0.12
POLC	1598	1345	2681	1.06	0.09
SPOLC	1600	1357	2684	0.84	0.05

The structural changes after each functionalization step are observable by Raman spectroscopy in the characteristic modes for sp^2 carbon, i.e. D, G and 2D bands. The G-mode is characteristic for the graphitic structure of the material, whereas the D-mode indicates disorder in the graphitic structure. During surface functionalization of OLC, the intensity ratio of D/G decreases with the surface functionalization of OLC (I_D/I_G = 1.17) to POLC (I_D/I_G = 1.06) and SPOLC (I_D/I_G = 0.84) indicating an influence of functional groups. The change in intensity ratio was already reported for other covalent OLC functionalizations which included phenolic

groups.[15] The 2D-modeits symmetric shape of the 2D-mode, indicates the typical turbostratic stacking of the graphitic layers in OLC.[16]

Unlike the starting material (OLC) and POLC, SPOLC was highly dispersible in water due to its hydrophilic functionalization, forming a concentrated black, ink-like suspension. For the formation of the composites, PEDOT was established at the carbon particles OLC and SPOLC and a mixture of SPOLC/OLC by addition of EDOT and its in situ polymerization yielding the composites PEDOT@OLC, PEDOT@SPOLC and PEDOT@SPOLC/OLC. The successful formation of PEDOT at the carbon surfaces is apparent by very intense signals in the Raman spectra, overshadowing characteristic signals for SPOLC (Fig. 2B), PEDOT without carbon additive and the three composites PEDOT@OLC (Fig. 1 A), PEDOT@SPOLC (Fig. 1 B) and PEDOT@SPOLC/OLC (Fig. 1C) showed no significant difference in Raman shift (Fig. S1, Tab. S1).

To explain the scaffolding effect which is responsible for the different arrangements of PEDOT in the SPOLC and unfunctionalized OLC, HRTEM measurements were conducted for both composites (Fig. 3).

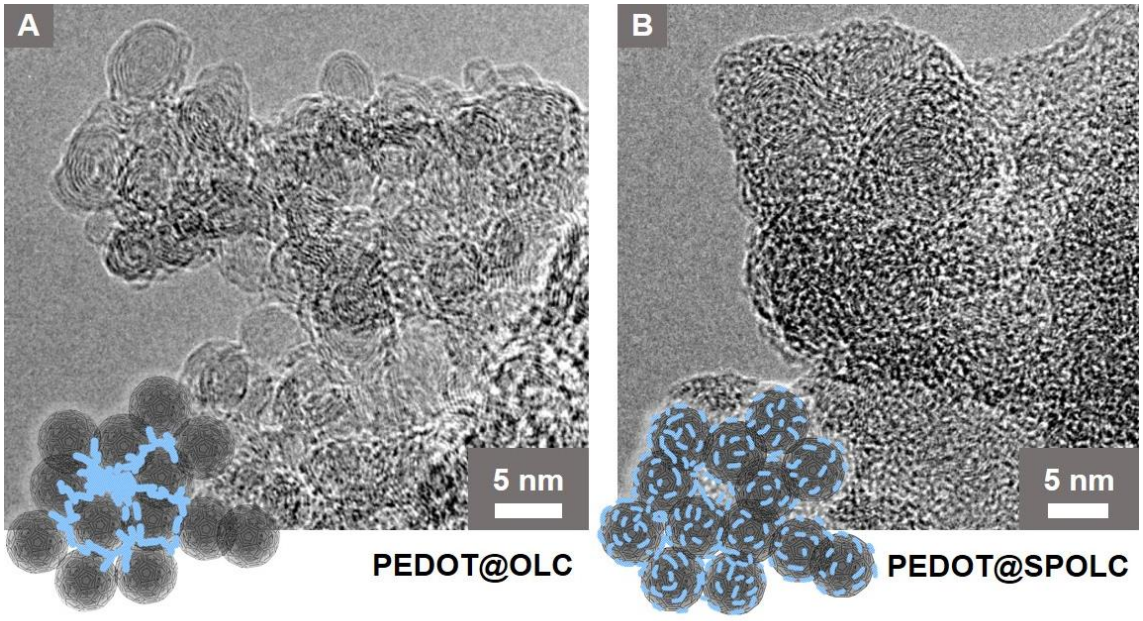

Fig. 3: *HRTEM micrographs of A: PEDOT@OLC, B: PEDOT@SPOLC and schematic interpretation, blue structures represent PEDOT.*

In **PEDOT@OLC**, the PEDOT is concentrated heterogeneously in bigger bulks between voids in the agglomerate leaving single OLC primary participles widely uncoated (Fig. 3A). In contrast, functionalized particles of **SPOLC** are evenly coated with PEDOT (Fig. 3B). However, as the typical domain size of PEDOT amounts to only several nm,[2] the non-

uniform coating was not detectable using SEM or Raman microscopy. Consequently, EDX mapping, performed to trace PEDOT, also showed a largely homogeneous sulfur distribution (Fig. S2).

The difference in morphology between **PEDOT@OLC** and **PEDOT@SPOLC** visible in the HRTEM measurements can be explained by the mechanism of the reaction. Like PEDOT:PSS, oxidized PEDOT oligomers are attracted by counterions during polymerization.[17] For the **PEDOT@SPOLC** system, benzenesulfonic acid moieties present at the surface of the carbon onions act as counterion, binding the PEDOT oligomer alongside the carbon particle electrostatically and thus inducing a "guiding or scaffolding effect" for the polymerization. Thus, after polymerization, **SPOLC** agglomerates are homogeneously covered with PEDOT. The interaction with the functional surface groups neutralizes the charge of the composite leading to its precipitation.

For the **PEDOT@OLC** this electrostatic interaction between SO_3^- and PEDOT is not possible, as the carbon particle lacks counterions at its surface. Instead, PEDOT oligomers interact with sulfonic acid anions, provided by the decomposition of the oxidative agent (sodium persulfate) during the oxidation of EDOT. Benzenesulfonic acid stabilized PEDOT particles grow in solution, eventually co-precipitating with the agglomerates of OLC. Precipitation eventually occurs for the **PEDOT@OLC** system because unfunctionalized OLC particles are generally unable to form stable aqueous dispersions. For the mixed composite consisting of functionalized and unfunctionalized OLC particles (**PEDOT@SPOLC/OLC**) it follows that both types of PEDOT deposition take place.

While PEDOT:PSS systems in the literature retain their dispersibility in aqueous media due to excess benzenesulfonic acid groups, all our composites were precipitating in water forming viscoelastic pastes. This property was beneficial since the composite pastes could be used for electrode production by doctor blading without further processing or the addition of thickening agents like binders.

Besides, the mechanical properties of **PEDOT@SPOLC** electrodes showed superior stability during electrode manufacturing. Processing of **PEDOT@OLC** on the other hand, was unsatisfying due to the formation of cracks and delamination of the coating (Fig. S3). These drawbacks were observed neither for **PEDOT@SPOLC** nor for **PEDOT@SPOLC/OLC** composites, although, for the latter, functionalized and unfunctionalized OLC were mixed in equal amounts prior to the polymerization of EDOT.

This can be explained by the morphology of PEDOT at the surface of carbon particles, or more

precisely at the surface of their agglomerates. In **PEDOT@SPOLC,** PEDOT is evenly distributed over the whole surface and can interact with other neighboring agglomerates, especially while the coating is drying and compressed. The result is a superior inter-agglomerate binding compared to **PEDOT@OLC**, where PEDOT is concentrated in voids of agglomerates, which hinders inter-agglomerate linkage. Therefore, **PEDOT@OLC** is not suitable for electrode production due to the formation of cracks. These findings show that the quality of the composite is determined rather by the interaction and distribution of PEDOT and the carbon particles than by its actual relative content. This is not only of importance for a system where PEDOT serves as capacitive enhancing additive, but also in case of its application as a conductive binder,[18] where a tailored distribution and superior connection can reduce its content to a minimum.

Thermal analysis

The thermal stability of the composite is an important parameter influencing the possible operating temperature for the intended application. In order to test the thermal properties of the composite, thermogravimetric analysis (TGA) was performed in nitrogen atmosphere (Fig. 4).

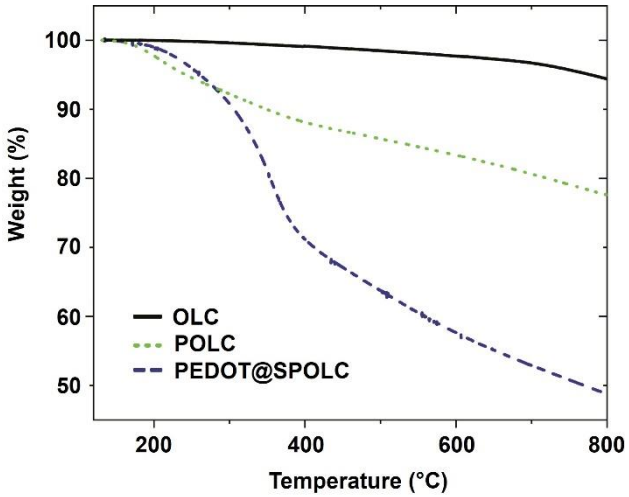

Fig. 4: *Thermogravimetric analysis of OLC, POLC and composite PEDOT@SPOLC.*

A significant loss in weight for **PEDOT@SPOLC,** was recorded between 260 and 400 °C, representing the degradation typically observed in composites of PEDOT films and carbon.[19-21] No weight loss was observed for the starting material OLC, as expected by the absence of surface groups and the temperature resistance of OLC in nitrogen atmosphere. Given this reasonable thermal stability, **PEDOT@SPOLC** is useable for various applications including electrodes for supercapacitors.[22]

Electrochemical characterization

The functionalization of OLC is not only beneficial for mechanical but also for electrical interaction between PEDOT and the carbon material. The homogeneous distribution of PEDOT and its tight connection to carbon particles influences energy storage as well as performance capabilities.[1] These properties were investigated by cyclic voltammetry measurements for **PEDOT@SPOLC** and **PEDOT@SPOL/OLC**, which feature functional groups. With **PEDOT@OLC**, eligible electrodes could not be produced due to its unsatisfactory mechanical properties (see above).

A cyclic voltammogram for pristine PEDOT consists of a capacitive and pseudocapacitive current, explained in detail by Volkov *et al*.[2] The pseudocapacitance in CPs originates from redox reactions, where cations are replaced by holes for an anodic scan and vice versa for the cathodic reversal. The non-faradaic contribution is caused by the formation of a double layer at the interface of electrolyte and particle surface.

In our composites, faradaic and non-faradaic contributions resulting from PEDOT, as well as the non-faradaic current originating from OLC are super-positioned. OLC does not show pseudocapacitance due to the lack of redox active functional groups at the surface. However, OLC offers a high external surface and is therefore used for electrical double layer capacitor (EDLC) applications.[23, 24] Due to the mesoporous character, OLC is a suitable template to host a variety of pseudocapacitive additives.[1] Especially for PEDOT, the porosity of OLC offers space for volume changes of the CPs during cycling. To investigate the stability of the composite, we decided to charge and discharge both electrodes in each cycle, which is achieved by reversing the polarity of the electrodes.

CV measurements of both composites show a quasi-rectangular shape when cycled using a symmetrical cell setup (Fig. S4) between 1 and -1 V (Fig. 5A). At high scan rates, the shape turns into an ellipsoid (Fig. 5B). This can be observed for the **PEDOT@SPOLC** and **PEDOT@SPOLC/OLC** (Fig. S5) system.

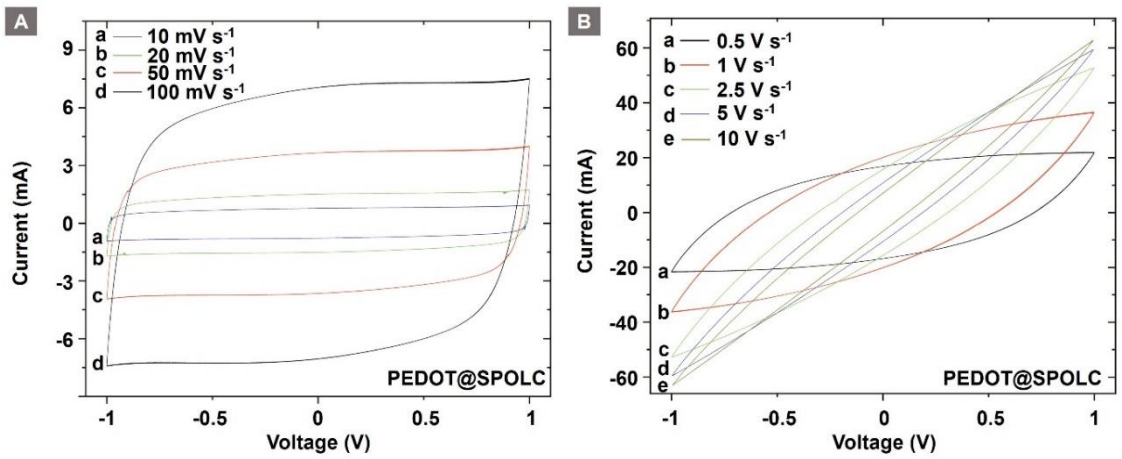

Fig. 5: *Cyclic voltammogram of* ***PEDOT@SPOLC*** *at low (A) and high (B) scan rates.*

The change in shape can be explained by kinetic limitations of the time sensitive electrochemical processes at the interface of OLC and conductive polymers. These incomplete processes result in a decreased stored charge.

Differences between both composites arise when the voltage window is increased. This investigation was possible due to the excellent electrochemical stability of PEDOT and the usage of an organic electrolyte (Fig. 6). A widening of the voltage range revealed a superior connection between CP and the carbon material for **PEDOT@SPOLC** (Fig. 6 A and B) when compared with **PEDOT@SPOLC/OLC** (Fig. 6 C and D).

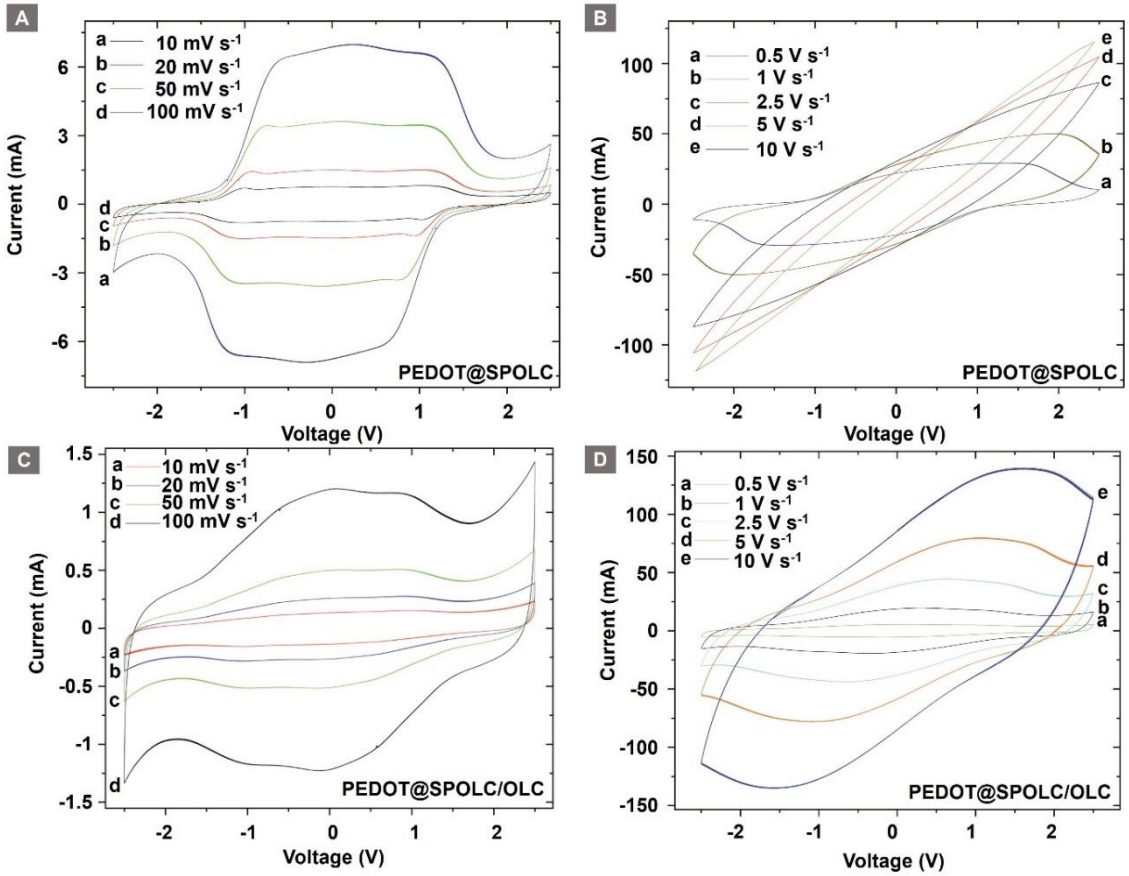

Fig. 6: *Comparison of cyclic voltammograms of* ***PEDOT@SPOLC*** *(A: high, B: low scan rates) and* ***PEDOT@SPOLC/OLC*** *(C: high, D: low scan rates).*

The CV curve for both composites shows a characteristic shape for systems using PEDOT as pseudocapacitive active material.[10] A drop in current starting at around 1 V indicates that the maximal pseudocapacitance is reached and PEDOT is completely doped. The subsequent decrease in current is more pronounced for **PEDOT@SPOLC** compared with **PEDOT@SPOLC/OLC**. The slower pseudocapacitive processes for **PEDOT@SPOLC/OLC**, expressed in flattened slopes in the cyclic voltammogram, support the idea of a more disadvantageous distribution and connection of PEDOT and carbon template.

Faster pseudocapacitive processes for **PEDOT@SPOLC** (Fig. 6A) indicate a superior electrochemical interaction between PEDOT and OLC in the composite relying on a functionalized template. As ten overlapping cycles are presented for each scan rate (Fig. 6) the excellent reversibility of the system is shown. Especially the redoping of PEDOT works without problems even after the electrodes were repolarized and reduced to -2.5 V.

These experiments support the idea of an electrical mediation between PEDOT and OLC in the presence of benzenesulfonic acid groups. To show this trend over a wide range of scan rates, the specific capacitance of the composites was compared for both potential ranges (Fig. 7).

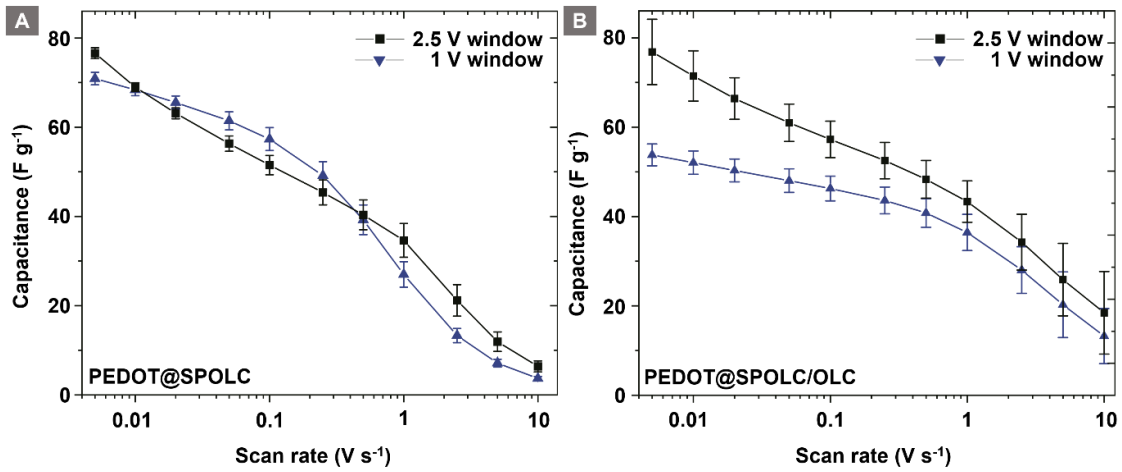

Fig. 7:*Comparison of specific capacitance between 1 V and 2.5 V windows for* ***PEDOT@SPOLC*** *(A) and* ***PEDOT@SPOLC/OLC*** *(B).*

For **PEDOT@SPOLC**, a specific capacitance of 77 F/g has been observed at a scan rate of 5 mV/s and an operating potential window of 2.5 V. Roughly the same capacitance (76 F/g) was obtained in a 1 Vpotential window. Increasing the scan rate did not influence the difference of specific capacitance for both potential windows. In this context, **PEDOT@SPOLC** shows an independence of the selected voltage windows regarding its specific capacitance. In contrast, for the system in which sulfonated and pristine OLC were mixed (**PEDOT@SPOLC/OLC**), the specific capacitance is influenced by the voltage window (Fig. 7A). Especially at low scan rates, where time sensitive processes determine the capacitance, a certain potential is required to exhaust pseudocapacitive charge storage. This potential is provided by a large voltage window of 2.5 V (Fig. 7B).

This phenomenon underlines the importance of the morphology of the system. Superior performance can be observed for the specifically incorporated PEDOT compared to the partly functionalized system especially at low scan rates where capacitance is dominated by pseudocapacitive processes.

With an increasing scan rate, the specific capacitance decreases for both systems. **PEDOT@SPOLC/OLC** maintains 19 F/g of its specific capacitance, whereas **PEDOT@SPOLC** retains only 6 F/g at a scan rate of 10 V/s. The difference in specific capacitance regarding the two voltage windows fades for both composites at high scan rates,

indicating a rise in influence of the non-faradaic processes over the slower faradaic pseudocapacitive processes.

At high scan rates, **PEDOT@SPOLC/OLC** delivers higher specific capacitance since less open porosity is blocked by PEDOT offering higher accessible surface to form an electrical double layer to store energy. Regarding the design of the composites, a different level of surface covering seems to offer the possibility for tuning the balance between faradaic and non-faradaic capacitance.

When compared to related materials, the maximal capacitance of **PEDOT@SPOLC** (77 F/g at 5 mV/s) significantly exceeds the capacitance of pure PEDOT:PSS electrodes (29 F/g at 5 mV/s)[22] and supercapacitors based on pure OLC (up to 52 F/g).[1] Supercapacitors relying on organic solvents and nanofibrillar, structured PEDOT electrodes (70 F/g at 2 mV/s)[25] or reduced graphene oxide combined with PEDOT:PSS (81 F/g at 5 mV/s) offer specific capacitances in the same range. For other PEDOT carbon composites, especially those using solvents with small diameters like aqueous electrolytes, values over 180 F/g have been reported.[8, 26] However, water only allows a much narrower potential window and therefore limits the power density for the supercapacitor. For the combination of OLC and PEDOT:PSS, a comparable specific capacitance of 75 F/g was reported,[12] but could not be maintained in long-term measurements (see below).

Cyclability and capacitance retention are important metrics to evaluate the performance of a supercapacitor. To evaluate the capacitance retention, electrodes of **PEDOT@SPOLC** were chosen over **PEDOT@SPOLC/OLC** on the basis of their superior electrochemical connection between carbon material and PEDOT. The electrodes were cycled 70000 times with a fast scan rate of 2.5 V/s. Between segments, ten cycles at 5 mV/s were performed to increase the visibility of any impacts on pseudocapacitive processes (Fig. 8A). After this first test, a second series with a slow scan rate of 20 mV/s, focusing mainly on the pseudocapacitance, was performed for 7500 cycles (Fig. 8B).

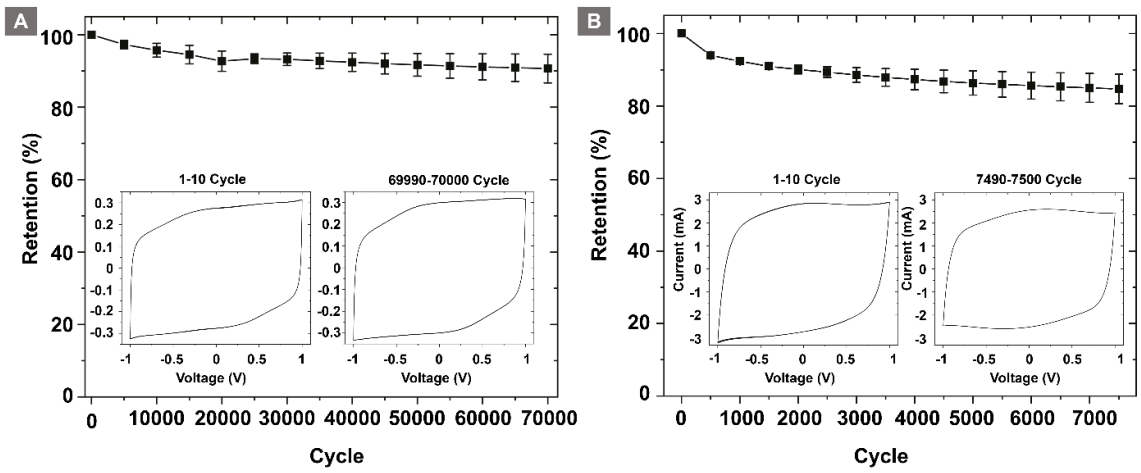

Fig. 8: *Retention of capacitance during the stability test of PEDOT@SPOLC using a fast scan rate of 2.5 V/s (A) and slow scan rate of 20 mV/s (B), the inserts show the first and last cycles of the test.*

For the fast cycling, 91 % of the capacitance was retained after 70000 cycles while 85 % of the initial capacitance was reached after 7500 cycles with a scan rate of 20 mV/s. The major factor for damage and degrading capacitance in PEDOT:PSS systems are swelling induced cracks[27] promoted by the pseudocapacitive current prominent at slow scan rates. **SPOLC** templates enable swelling of PEDOT into the open porous structure, reducing stress which subsequently suppresses the formation of cracks. At fast scan rates mostly non-faradaic processes take place, which are less demanding for the integrity of the composite. In total, the system could retain a high share of its initial capacitance, proving an excellent stability of the composite in both tests. High retention was also reported for other composites where PEDOT was combined with carbon nanotubes (10000 cycles at 80 mV/s, retention 95-98%)[11] or with graphene (2000 cycles, retention 82%)[9] underlining the suitability of carbon:PEDOT composites. However, depending on the manufacturing method, the degradation of the initial capacitance of these composites can be substantial, i.e. the combination of OLC and PEDOT:PSS showed a loss of 19 % of its initial capacitance already after 300 cycles.[12]

This is where our approach based on the template assisted ionic attraction of PEDOT onto functionalized OLC improves the capacitance retention of the device significantly. It combines a wide potential window and long-term stability. These results reflect the importance of the morphology of PEDOT in the carbon template. Besides, benzenesulfonic acid emerged as a vital component to dispersing carbon in aqueous media and to attracting and integrating PEDOT in the composite.

3.2.4 Conclusion

Sulfonated onion-like carbon (**SPOLC**) was used as a template for electrostatically guided in situ polymerization of 3,4-ethylenedioxythiophene (EDOT) to form an active material for supercapacitor electrodes. The composite material combines the pseudocapacitive and binding capabilities of PEDOT with the mechanical stability of OLC while overcoming the problem of indispersible starting materials. Key element to reach a stable dispersion was the covalent functionalization of OLC with benzenesulfonic acid groups whose anionic charge also attracts and locks PEDOT tightly at the surface of the modified OLC (**SPOLC**) particles. While the PEDOT deposition was proven by Raman and TGA data for all composites, differences in morphology of PEDOT and OLC have been revealed by HRTEM. Electrochemical characterization of the composite showed a maximal capacitance of 77 F/g at a scan rate of 5 mV/s. A superior electrical connection of the functionalized composite was concluded as a result of the performance in cyclic voltammetry measurements. In long term stability tests with over 70000 cycles, 91% of the initial capacitance could be retained, demonstrating the mechanical stability of the connection between PEDOT and **SPOLC**.

In perspective, **PEDOT@SPOLC** could be also used as additive for sodium ion cathodes, where PEDOT adopts the role of the binder and OLC serves as a spherical conductive additive whose structural integrity prevents trapping of sodium ions currently posing a problem for many commercial conductive additives.[28]

3.2.5 Supplementary material

EDOT was distilled in vacuo prior to use. To produce **PEDOT@SPOLC**, EDOT (288 mg) was dispersed in aqueous **SPOLC** suspension (4 mL, 576 mg, 14 wt%) after the addition of ethanol (3 mL). For **PEDOT@OLC**, pristine OLC (1 g) and EDOT (570 mg) was dispersed in a mixture of water (4 mL) and ethanol (3 mL). For **PEDOT@SPOLC/OLC**, EDOT (575 mg) and pristine **OLC** (570 mg) was dispersed in aqueous **SPOLC** (4 mL, 576 mg, 14 wt%) with the addition of ethanol (3 mL).

To polymerize EDOT, an aqueous solution of sodium persulfate $Na_2S_2O_8$ (2.4 M) was added dropwise to a solution with an EDOT:$Na_2S_2O_8$ ratio of 1:2. After 24 hours of vigorous stirring using a hand-held coiled wire stirrer" (i.e. a cappucino creamer). The resulting mixture was centrifuged (6000 rpm, 20 minutes) and the supernatant subsequently removed. The particles

were redispersed and centrifuged six more times, alternating between ethanol and water as solvents.

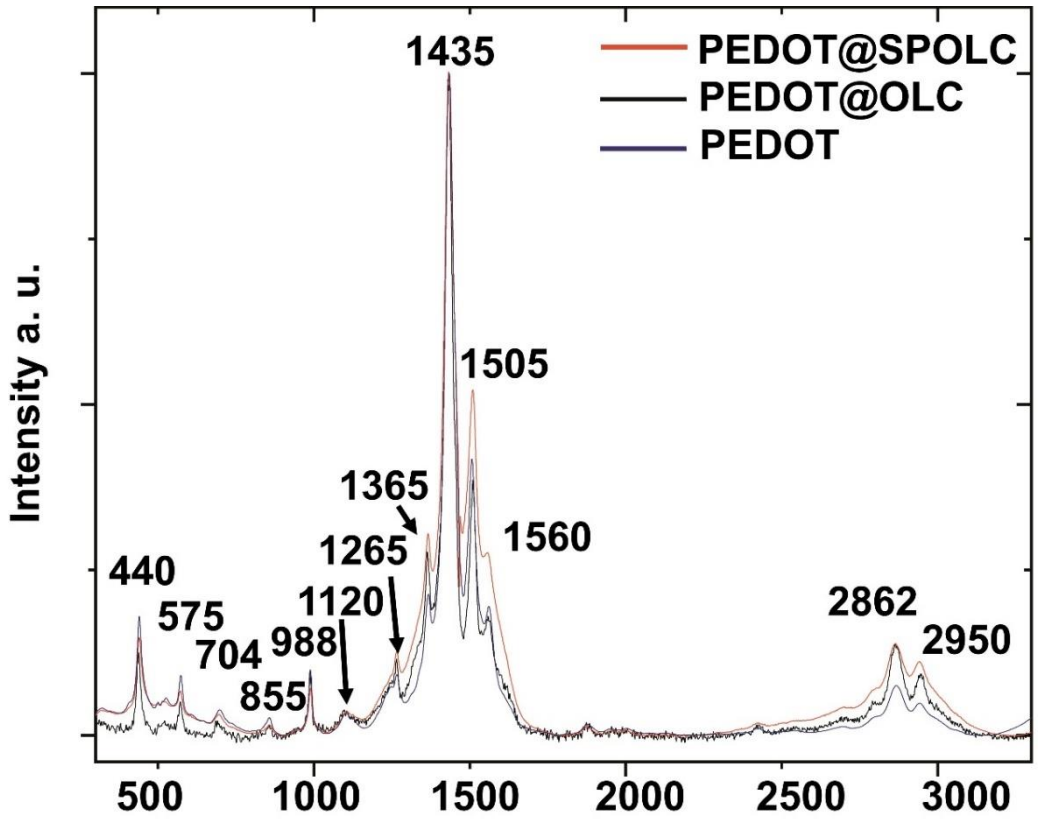

Fig. S1: *Raman spectra of* ***PEDOT@SPOLC****,* ***PEDOT@OLC*** *and PEDOT (excitation wavelength: 532 nm).*

Tab. S1: *Assignment of Raman modes for functional groups of PEDOT*

Raman shifts (cm^{-1})	Assignment
440, 575, 988	oxy- ethylene ring CO deformation
1128	C-O-C deformation
1265	CαCα stretching and CH bending
1435, 1405, 1560	symmetric and asymmetric C=C stretching
1365	thiophene ring CβCβ stretching
2870, 2965	OH and CH stretching

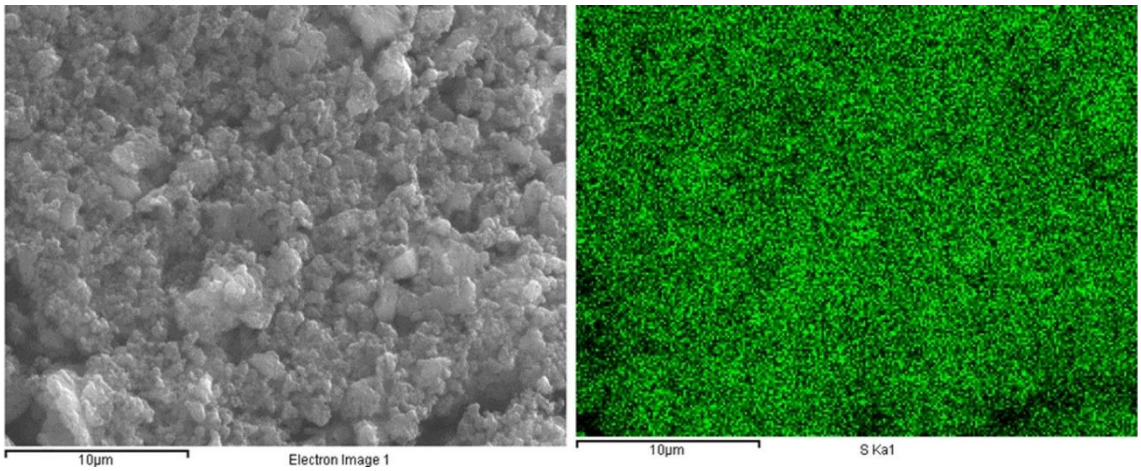

Fig. S2: *SEM picture (left) and its corresponding EDX measurement (tracking sulfur) for the* ***PEDOT@SPOLC*** *composite.*

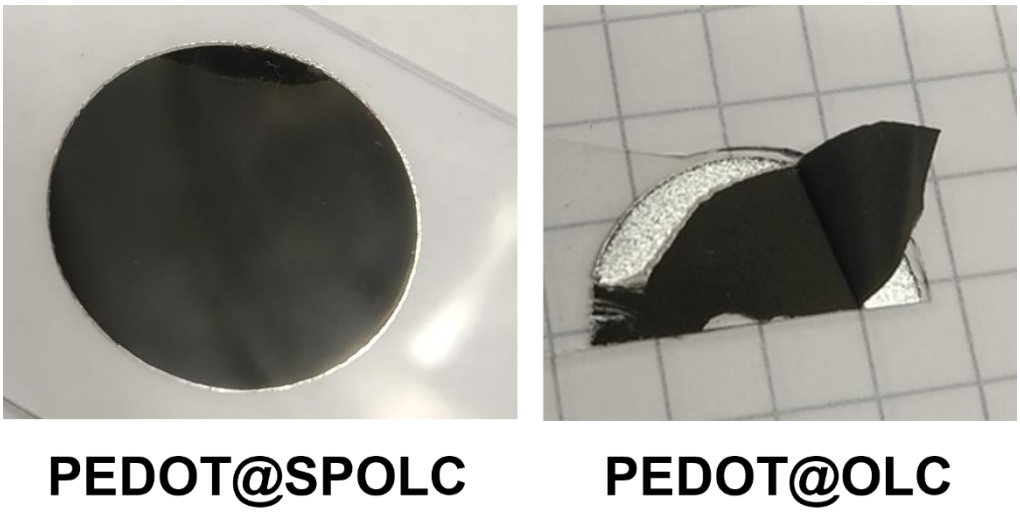

Fig. S3: *Differences in electrode manufacturing of* ***PEDOT@SPOLC*** *and* ***PEDOT@OLC****, where* ***PEDOT@OLC*** *shows delamination despite the identical electrode manufacturing procedure. Variations also did not lead to improved electrode characteristics.*

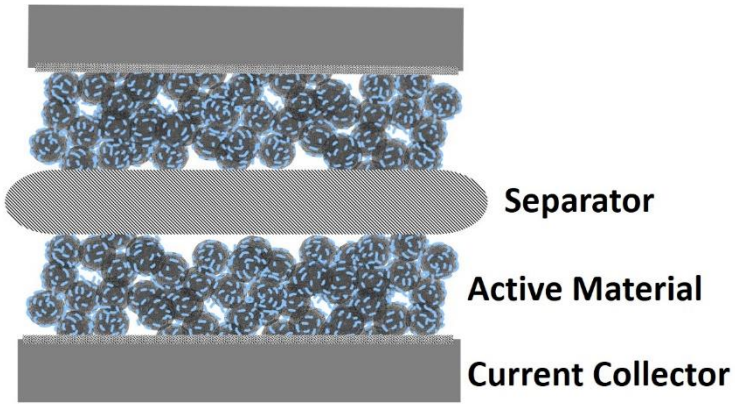

Fig. S4: *Schematic overview of* ***a*** *symmetric supercapacitor setup with separator, active material and current collector.*

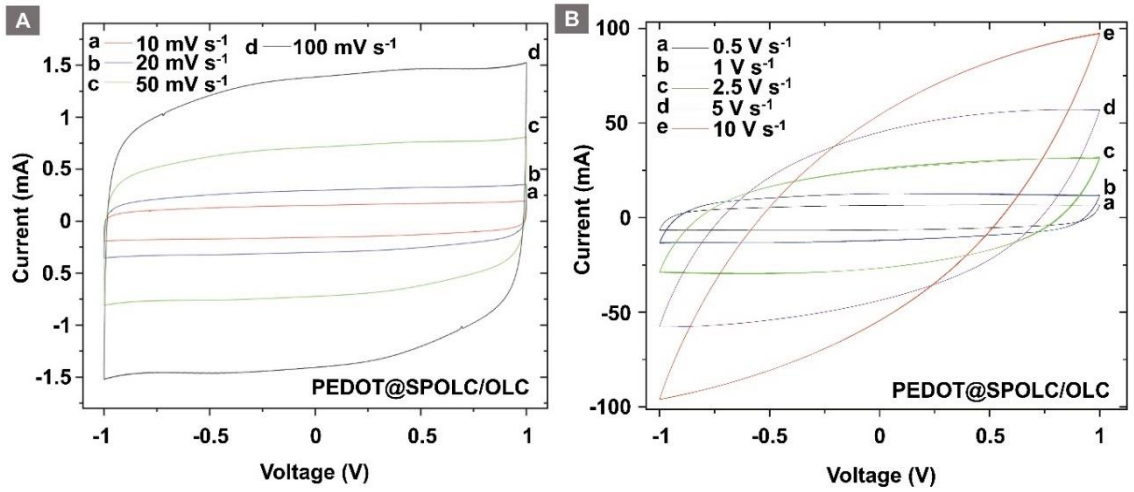

Fig. S5: *Cyclic voltammogram with 1 V potential window of* ***PEDOT@SPOLC/OLC*** *at low (A) and high (B) scan rates.*

3.2.6 References

[1] M. Zeiger, N. Jackel, V. N. Mochalin, V. Presser, Review: carbon onions for electrochemical energy storage, Journal of Materials Chemistry A 4(9) (2016) 3172-3196. https://doi.org/10.1039/c5ta08295a

[2] A. V. Volkov, K. Wijeratne, E. Mitraka, U. Ail, D. Zhao, K. Tybrandt, J. W. Andreasen, M. Berggren, X. Crispin, I. V. Zozoulenko, Understanding the Capacitance of PEDOT:PSS, Advanced Functional Materials 27(28) (2017) 1700329. https://doi.org/10.1002/adfm.201700329

[3] H.-W. Chen, C. Li, PEDOT: fundamentals and its nanocomposites for energy storage, Chinese Journal of Polymer Science 38(5) (2020) 435-448.

[4] H.-W. Chen, C. Li, PEDOT: Fundamentals and Its Nanocomposites for Energy Storage, Chinese Journal of Polymer Science 38(5) (2019) 435-448. https://doi.org/10.1007/s10118-020-2373-2

[5] R. A. Fisher, M. R. Watt, W. J. Ready, Functionalized Carbon Nanotube Supercapacitor Electrodes: A Review on Pseudocapacitive Materials, Ecs Journal of Solid State Science and Technology 2(10) (2013) M3170-M3177. https://doi.org/10.1149/2.017310jss

[6] G. J. Adekoya, R. E. Sadiku, S. S. Ray, Nanocomposites of PEDOT:PSS with Graphene and its Derivatives for Flexible Electronic Applications: A Review, Macromolecular Materials and Engineering 306(3) (2021) 2000716. https://doi.org/10.1002/mame.202000716

[7] M. Boota, Y. Gogotsi, MXene-Conducting Polymer Asymmetric Pseudocapacitors, Advanced Energy Materials 9(7) (2019) 1802917. https://doi.org/10.1002/aenm.201802917

[8] F. Niu, R. Guo, L. Q. Dang, J. Sun, Q. Li, X. X. He, Z. H. Liu, Z. B. Lei, Coral-like PEDOT Nanotube Arrays on Carbon Fibers as High-Rate Flexible Supercapacitor Electrodes, Acs Applied Energy Materials 3(8) (2020) 7794-7803. https://doi.org/10.1021/acsaem.0c01202

[9] M. A. A. M. Abdah, N. A. Zubair, N. H. N. Azman, Y. Sulaiman, Fabrication of PEDOT coated PVA-GO nanofiber for supercapacitor, Mater Chem Phys; Mater Chem Phys 192 (2017) 161-169. https://doi.org/10.1016/j.matchemphys.2017.01.058

[10] D. X. Wang, C. Lu, J. J. Zhao, S. Han, M. H. Wu, W. Chen, High energy conversion efficiency conducting polymer actuators based on PEDOT:PSS/MWCNTs composite electrode, Rsc Advances 7(50) (2017) 31264-31271. https://doi.org/10.1039/c7ra05469f

[11] H. H. Zhou, X. M. Zhi, Ternary composite electrodes based on poly(3,4-ethylenedioxythiophene)/carbon nanotubes-carboxyl graphene for improved electrochemical capacitive performances, Synthetic Metals 234 (2017) 139-144. https://doi.org/10.1016/j.synthmet.2017.10.011

[12] M. E. Plonska-Brzezinska, M. Lewandowski, M. Blaszyk, A. Molina-Ontoria, T. Lucinski, L. Echegoyen, Preparation and characterization of carbon nano-onion/PEDOT:PSS composites, Chemphyschem 13(18) (2012) 4134-41. https://doi.org/10.1002/cphc.201200789

[13] C. Portet, G. Yushin, Y. Gogotsi, Electrochemical performance of carbon onions, nanodiamonds, carbon black and multiwalled nanotubes in electrical double layer capacitors, Carbon 45(13) (2007) 2511-2518. https://doi.org/10.1016/j.carbon.2007.08.024

[14] A. Palkar, F. Melin, C. M. Cardona, B. Elliott, A. K. Naskar, D. D. Edie, A. Kumbhar, L. Echegoyen, Reactivity differences between carbon nano onions (CNOs) prepared by different methods, Chem Asian J 2(5) (2007) 625-33. https://doi.org/10.1002/asia.200600426

[15] J. D. Velasquez, M. Tomczykowa, M. E. Plonska-Brzezinska, M. N. Chaur, Evaluation of the Covalent Functionalization of Carbon Nano-Onions with Pyrene Moieties for Supercapacitor Applications, Materials (Basel) 13(5) (2020) 1141. https://doi.org/10.3390/ma13051141

[16] K. Bogdanov, A. Fedorov, V. Osipov, T. Enoki, K. Takai, T. Hayashi, V. Ermakov, S. Moshkalev, A. Baranov, Annealing-induced structural changes of carbon onions: High-resolution transmission electron microscopy and Raman studies, Carbon 73 (2014) 78-86. https://doi.org/10.1016/j.carbon.2014.02.041

[17] P. Sakunpongpitiporn, K. Phasuksom, N. Paradee, A. Sirivat, Facile synthesis of highly conductive PEDOT:PSS via surfactant templates, Rsc Adv 9(11) (2019) 6363-6378. https://doi.org/10.1039/c8ra08801b

[18] X. Liu, J. Zai, A. Iqbal, M. Chen, N. Ali, R. Qi, X. Qian, Glycerol-crosslinked PEDOT:PSS as bifunctional binder for Si anodes: Improved interfacial compatibility and conductivity, J Colloid Interface Sci 565 (2020) 270-277. https://doi.org/10.1016/j.jcis.2020.01.028

[19] B. Friedel, P. E. Keivanidis, T. J. K. Brenner, A. Abrusci, C. R. McNeill, R. H. Friend, N. C. Greenham, Effects of Layer Thickness and Annealing of PEDOT:PSS Layers in Organic Photodetectors, Macromolecules 42(17) (2009) 6741-6747. https://doi.org/10.1021/ma901182u

[20] J. A. Luceno Sanchez, R. Pena Capilla, A. M. Diez-Pascual, High-Performance PEDOT:PSS/Hexamethylene Diisocyanate-Functionalized Graphene Oxide Nanocomposites: Preparation and Properties, Polymers (Basel) 10(10) (2018) 1169. https://doi.org/10.3390/polym10101169

[21] Y. F. Xu, Y. Wang, J. J. Liang, Y. Huang, Y. F. Ma, X. J. Wan, Y. S. Chen, A Hybrid Material of Graphene and Poly (3,4-ethyldioxythiophene) with High Conductivity, Flexibility, and Transparency, Nano Res: Nano Res 2(4) (2009) 343-348. https://doi.org/10.1007/s12274-009-9032-9

[22] Y. Liu, B. Weng, J. M. Razal, Q. Xu, C. Zhao, Y. Hou, S. Seyedin, R. Jalili, G. G. Wallace, J. Chen, High-Performance Flexible All-Solid-State Supercapacitor from Large Free-Standing Graphene-PEDOT/PSS Films, Sci Rep 5 (2015) 17045. https://doi.org/10.1038/srep17045

[23] V. Dhand, M. Yadav, S. H. Kim, K. Y. Rhee, A comprehensive review on the prospects of multi-functional carbon nano onions as an effective, high- performance energy storage material, Carbon 175 (2021) 534-575. https://doi.org/10.1016/j.carbon.2020.12.083

[24] M. Zeiger, N. Jackel, D. Weingarth, V. Presser, Vacuum or flowing argon: What is the best synthesis atmosphere for nanodiamond-derived carbon onions for supercapacitor electrodes?, Carbon 94 (2015) 507-517. https://doi.org/10.1016/j.carbon.2015.07.028

[25] J. M. D'Arcy, M. F. El-Kady, P. P. Khine, L. Zhang, S. H. Lee, N. R. Davis, D. S. Liu, M. T. Yeung, S. Y. Kim, C. L. Turner, A. T. Lech, P. T. Hammond, R. B. Kaner, Vapor-phase polymerization of nanofibrillar poly(3,4-ethylenedioxythiophene) for supercapacitors, ACS Nano 8(2) (2014) 1500-10. https://doi.org/10.1021/nn405595r

[26] M. Rajesh, C. J. Raj, R. Manikandan, B. C. Kim, S. Y. Park, K. H. Yu, A high performance PEDOT/PEDOT symmetric supercapacitor by facile in-situ hydrothermal polymerization of PEDOT nanostructures on flexible carbon fibre cloth electrodes, Materials Today Energy 6 (2017) 96-104. https://doi.org/10.1016/j.mtener.2017.09.003

[27] M. Modarresi, A. Mehandzhiyski, M. Fahlman, K. Tybrandt, I. Zozoulenko, Microscopic Understanding of the Granular Structure and the Swelling of PEDOT:PSS, Macromolecules 53(15) (2020) 6267-6278. https://doi.org/10.1021/acs.macromol.0c00877

[28] K. Pfeifer, S. Arnold, O. Budak, X. L. Luo, V. Presser, H. Ehrenberg, S. Dsoke, Choosing the right carbon additive is of vital importance for high-performance Sb-based Na-ion batteries, Journal of Materials Chemistry A 8(12) (2020) 6092-6104. https://doi.org/10.1039/d0ta00254b

3.3 Printing electrodes with onion-like carbon

Parts of this chapter are based on the manuscript: Functional ink with onion-like carbon for energy storage by C. Bauer, T. Neff, A. Day, A. Krueger

For the third chapter, a manufacturing technique for supercapacitor electrodes was researched. The aim was to fabricate thin film electrodes for energy storage using OLC ink as active material in an innovative process. The driving force for the project was the versatility of printing techniques, as the shape and electrode thickness can easily be modified. A key challenge for this project was to increase the dispersibility of OLC in water, which was chosen as solvent due to its sustainability. Another factor for the ink was a small particle size of the OLC agglomerates, vital for the stability of the ink and to avoid clogging of the inkjet nozzle. Furthermore, the search for an electrochemically stable additive, which prevents precipitation of the OLC, was substantial. Therefore, the goal was to produce a stable ink with an OLC particle dispersion.

3.3.1 Introduction

The digital transformation with its accelerating number of decentralized electronic devices is powered by individual energy storage solutions.[1] Printing of those key parts enables customized design and can be integrated into the manufacturing process for the entire application.[2-5] Recently, functional inks were used to manufacture various devices like photodetectors,[6, 7] gas and humidity sensors,[8, 9] solar cells,[10] field effect transistors[11] as well as supercapacitors.[12-14]

In supercapacitors, energy is stored in an electric double layer formed between the electrolyte and an active material. This active material must be electrochemically stable and offer a high specific surface in combination with an open porosity to grant accessibility for the electrolyte.[15] Materials based on sp^2-hybridized carbon fulfill these requirements while maintaining a high degree of electric conductivity, necessary to deliver charge to the electrode surface, where the energy is stored in an electric field between the charged electrode and a layer of solvated ions.[16]

In this work, onion-like carbon (OLC) was chosen as active material due to its conductivity and open mesoporous structure which enables accessibility for the electrolyte even at elevated

charging rates. OLC can be produced at large scale [17] and is considered biocompatible[18] due to its low toxicity.

To print electrodes, carbon materials need to be dispersed in the form of an ink, forming a colloidal suspension in which the solid particles are evenly distributed in the liquid phase. Solvating carbon particles like OLC using common solvents is a challenge, because of interparticle interactions which promote agglomeration. Additionally, the absence of functional groups which could interact with solvents or repulse other particles hinders suspension or solvation of OLC. [19-21]

Here we report on the production of a stable, environmentally friendly, water-based functional ink for the production of supercapacitor electrodes using OLC as active material. The ink dispersion is designed to be stable for years. It was studied by high resolution transmission electron microscopy, dynamic light scattering and Raman microscopy. With inkjet printing and spray deposition we report two different printing techniques to obtain thin film supercapacitor electrodes. The electrochemical performance and stability of the electrodes was demonstrated by cyclic voltammetry in a wide potential window and over 5000 cycles.

3.3.2 Experimental section

Active material production and milling

The active material OLC was obtained after thermal annealing of detonation nanodiamond (Gansu Lingyun Corp.) in vacuum (~1 mbar) for two hours at 1500 °C in a tube furnace (STF 16/450, Carbolite Gero GmbH).[22] Prior to milling, OLC (3.0 g) and 1.8 g sodium dodecyl sulfate (SDS) were dispersed in water (130.0 g) using an ultra-sonic bath for 30 minutes. Milling of the dispersion was conducted for two hours with an attrition mill (minicer, Netzsch) with a circumferential velocity of 10 m s^{-1} using zirconia milling beads (30-50 µm, Tosoh Corp.).[23] Particle size given as intensity distribution was obtained by dynamic light scattering (Zetasizer Nano ZS, Malvern) using the Marquardt method.

Ink preparation

For the spray printing the OLC dispersion (2.0 g) and deionized water (4.0 g) were mixed. For electrode production, the ink was sprayed onto carbon coated aluminum foil (Zflo 2653, Transcontinental Advanced Coatings) which was kept at 100 °C using a small piezoceramic atomizer with a mesh size of 10 µm operated at 110 KHz using a small driver board (300 mA and 5 V).

To yield the dispersion for inkjet printing, the OLC dispersion (2.0 g), deionized water (4.0 g) and DMSO (0.2 g) were mixed. The ink was printed onto carbon coated aluminum foil (Zflo 2653, Transcontinental Advanced Coatings, USA) which was attached to a DIN A4 paper using a conventional ink jet printer (MFC 290C, Brother), with a nozzle diameter of 30 µm. The deposition pattern was controlled by a computer. The viscosity of both inks was determined with a rolling-ball viscosimeter (Lovis 2000 ME, Anton Paar).

Substrates coated by both techniques were die cut with a punching iron and pressed with a hydraulic press (ca. 0.2 GPa) yielding round electrodes (16 mm diameter).

All electrodes were transferred into a drying furnace (130 °C). For electrochemical measurements, symmetrical supercapacitors were built using a stainless-steel test cell separated by a polymer membrane (Cellgard 2325, El-Cell, Germany). For the electrolyte, a 1 M solution of tetraethyl ammonium tetra-fluoroborate ($TEABF_4$; TCI) in acetonitrile (CH_3CN, Sigma Aldrich) was used. For each deposition technique, three test cells were assembled in the absence of humidity (<1 ppm) and oxygen (<1 ppm) using a glovebox (N_2, Labmaster 130, M.Braun Inertgas-Systeme, Germany. For each applied scan rate the arithmetic average of ten consecutive cycles was used to calculate the total capacitance of the device C_{CV} (Eq. 1) as well as the specific capacitance for one electrode C_E (Eq. 2), where *a* is the area of one electrode, *I* the current, *v* the scan rate and V_0 the potential window:

$$C_{CV} = \frac{\int_0^{V_0} I\,(t) * dV}{2 * V_0 * v} \tag{6}$$

$$C_E = \frac{2 * C_{CV}}{a} \tag{7}$$

For high resolution electron transmission microscopy (HRTEM), the ink was drop casted onto a copper grid coated with lacey carbon (Plano GmbH). The measurement was conducted using a FEI Titan 80-300 (Thermo Fischer Scientific Inc.) with an operating voltage of 300 kV. Scanning electron microscopy (SEM) images were recorded at an operating voltage of 5 kV using a Gemini Fe-SEM Ultra-plus Zeiss field emission scanning electron microscope (Carl Zeiss). The electrodes were attached by conductive carbon tapes without further preparation.

Raman spectra were measured with a DXR Raman microscope (Thermo Fisher Scientific Inc.), using a laser power of 0.02 mW and an excitation wavelength of 532 nm.

3.3.3 Results and discussion

The key for ink deposition is a homogeneous and stable dispersion. Pristine OLC dispersions without treatment or additives form aggregates precipitating completely from the dispersion within minutes. To increase the stability of the dispersion and to reduce the particle size in order to avoid clogging of the nozzle during deposition, it was necessary to disperse the OLC aggregates. As explained in literature, the attracting forces between primary particles are not only explained by π-π stacking between single OLC but also by covalent bonds which are connecting the particles. These bonds between OLC form during the high temperature fabrication where sinter necks between spherical OLC were developed.[21, 24] To break these interparticle connections, the force of an attrition mill was needed, as already shown for a dispersion of detonation nanodiamonds by our group.[23] To prevent reagglomeration of the OLC, additional steps are necessary to stabilize the dispersion. Possibilities are to introduce a surface functionalization step like oxidation[19] or fluorination [25]. Another strategy to increase the dispersibility of OLC is to introduce stabilizing additives like polyacrylic acid.[20] With 0.6 Wt% sodium dodecyl sulfate (SDS) an electrochemically stabile, ecologically and economically uncritical additive was used to stabilize ca. 1 wt% of OLC(Scheme.1).

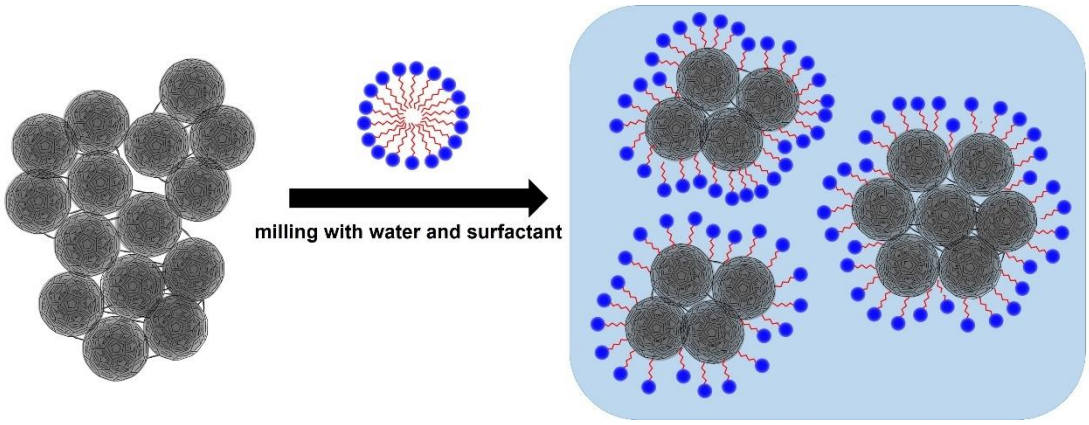

Scheme. 1*: Deagglomeration of onion-like carbon by attrition milling and stabilization of the aqueous dispersion by sodium dodecyl sulfate forming mediating layer at the solid to liquid interface.*

Milling resulted in a black dispersion, stable for over two years, featuring milled OLC with a particle size between 40 and 300 nm and a ζ-potential of -30,3 mV (pH 8.3) (Fig. 1A).

Assuming a diameter of 12 nm of a primary OLC particle [24] and a close packing of equal spheres, a 100 nm secondary particle of the milled dispersion is estimated to consists of around 400 primary OLC particles. The specific surface, determined using the Brunauer-Emmett-Teller method (BET) changed from around 389 $m^2 g^{-1}$ for pristine OLC to 220 $m^2 g^{-1}$ for the milled dispersion (Fig. 1B). A decrease in specific surface after milling of OLC is consistent with literature,[26] and is further promoted by a significant amount of SDS remaining after removal of the liquid by freeze drying. A redispersion of the freeze-dried dispersion, offering possibilities for process engineering was tested, however, did not yield a homogenous dispersion regarding the particle size (Fig. S1). Milling of OLC was also performed without surfactant but lead to an unsatisfying dispersion where the active material OLC precipitated within minutes. Furthermore, a concentration of surfactant 0.6 % was necessary to maintain a high weight fraction (1 %) of OLC in dispersion. Milling of OLC with SDS provided an excellent stability which is also demonstrated by the Tyndall effect observed in a dispersion even after three years of storage (Fig.1c).

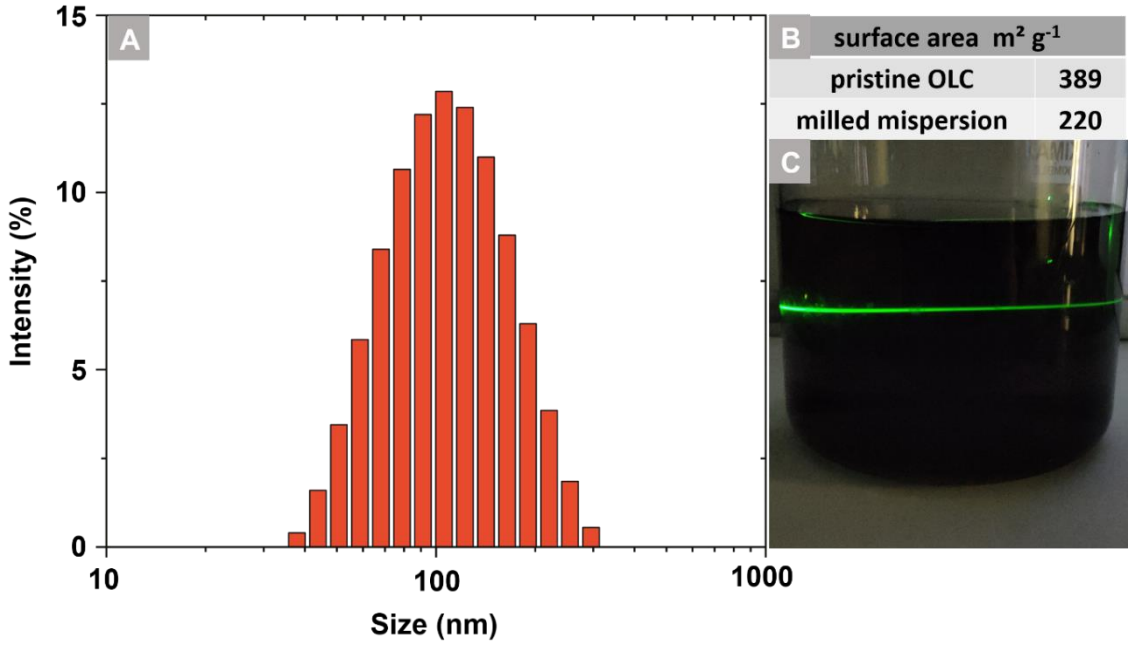

Fig. 1: *Particles size distribution measured by dynamic light scattering of the milled dispersion (A) as well as the impact on specific by milling (B) and its Tyndall effect (C).*

Milling of particles not only reduces the specific surface and size of the agglomerates but can also damage the particle structure, potentially deteriorating the properties of the electrode which has been reported for carbon nanotubes.[27] Especially within the context of additives like surfactants, exfoliation of carbon layers during milling can be promoted.[28]

To research the structural influence of milling, OLC were examined before and after deagglomeration by Raman microscopy as well as HRTEM measurements (Fig. 2).

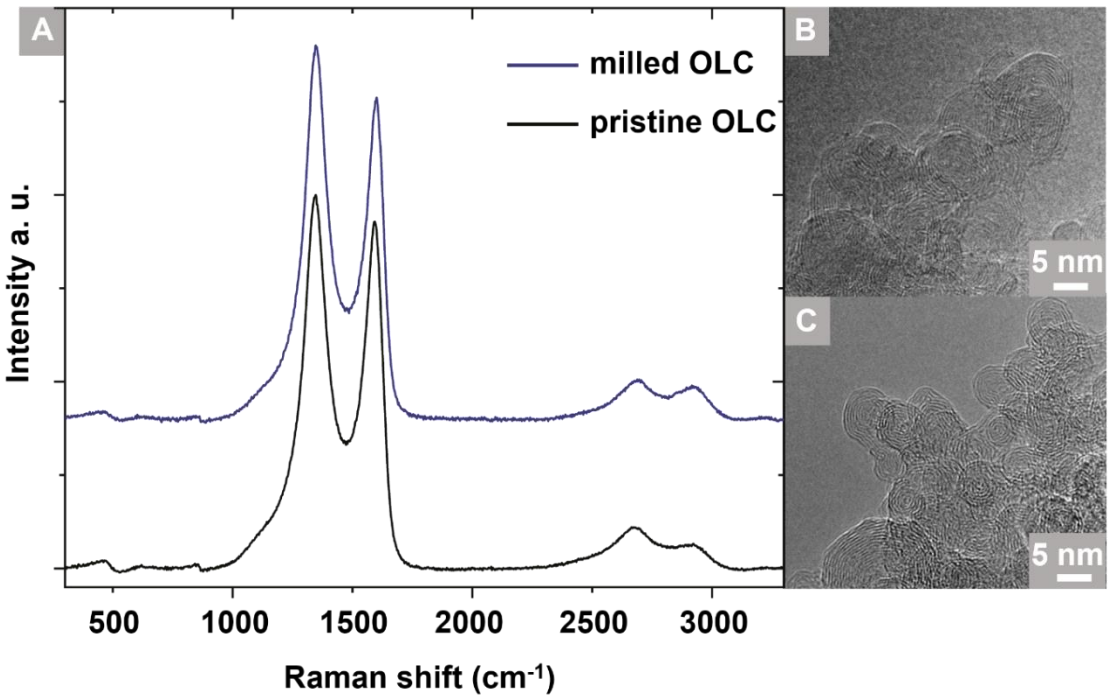

Fig. 2: *Comparison between mOLC and OLC in Raman (A) and HRTEM images of OLC (B) and mOLC (C)*

The D/G ratio of pristine OLC 1.06 (1/0.94) increases to 1.16 for milled OLC (1.4/1.2) after milling. This change is indicating a slight increase in defect density. This supports the results reported by Lee et al.[20] and Reinert et al.[21] where different setups were used to disperse OLC. High resolution transmission electron measurements (HRTEM) underline these observations as they show that the primary structure of OLC (Fig. 2B) is conserved for the milled OLC (Fig. 2C) in the ink. With a high weigh fraction and structural stability of OLC, the dispersion underlines their qualification as functional carbon additive for inks, further rheological details of the ink, like the Ohnesorge Number are provided in the supporting information.

To deposit the OLC based ink, the small size of the OLC primary particles brings two beneficial features. First, small particles are required for inks to prevent nozzle clogging. Literature provides a rule of thumb limiting the maximal particle size to 1/50 of the nozzle diameter. In our case this can be translated to a maximum size of 3 µm for the inkjet printing and 1 µm for spraying. Second, the small primary particles entail a high surface to weight ratio which is a key parameter for capacitive energy storage materials. The packing of spherical

OLC particles results in a mesoporous electrode offering high accessibility and a big reservoir of electrolyte which is beneficial for the reactance of the system especially at high scan rates. Despite the presence of SDS in the electrode, the mesoporous structure remains accessible which can be derived from nitrogen sorption measurements (Fig. S2). The ink could be deposited via piezoelectric spraying and with the addition of DSMO also by inkjet technique. Differences in both techniques which affect the electrode are revealed by SEM measurements (Fig. 3).

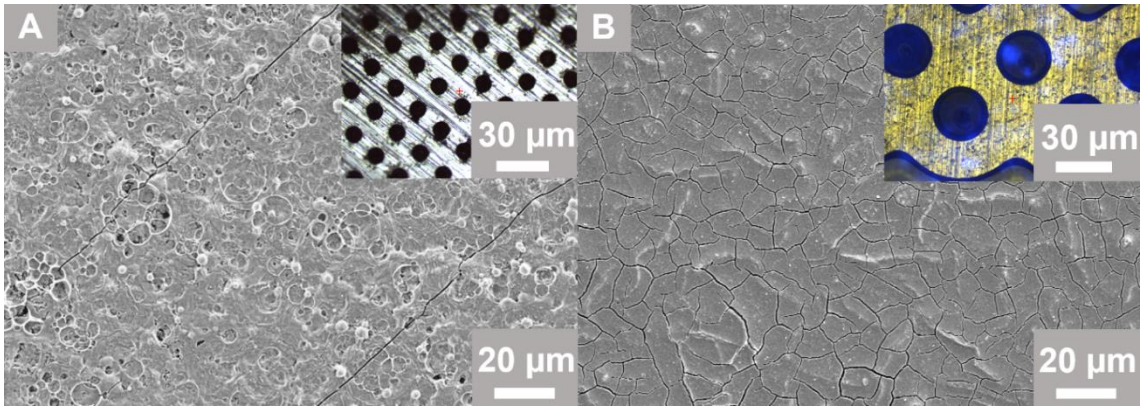

Fig. 3: *Electrode surface shown by SEM measurement for spray- (A) and inkjet printed (B) electrodes. The insert shows reflected light microscope images of the respective nozzle used for deposition.*

It can be seen that the sprayed electrode possesses a rough surface (Fig. 3A) with inhomogeneities in the range of a few micrometers. This structure is a result of the fast coating process to a specific mass of around 0.5 mg cm^{-2} within 25 minutes. The substrate was heated to promote fast solvent evaporation enabling the fast rate of deposition. During the final steps of deposition, the solvent evaporation decelerated as a result of the growing thickness of the coating. This oversaturation with solvent resulted in coffee stain features and inhomogeneities in the form of channels extending deeply into the coating (Fig. S3). The inkjet printed electrode (Fig. 3B) did not show this behavior. The homogeneous surface can be explained by the addition of DMSO as a second phase in the ink to decrease capillary stress during solvent evaporation.[29] The addition of DMSO required a 10 minute break between every printing cycle, allowing the removal of the majority of the solvent, thus prolonging the process significantly. The cracks in the surface visible in the SEM measurement are caused by stress introduced bending of the substrate while it was feed through the printer. Despite the cracks, no delamination of active material was observed, demonstrating the connection between active material and current collector.

After investigating the morphology of the inkjet printed and sprayed electrodes, their electrochemical performance was assessed by measurements in a symmetrical two electrode configuration. This setup allowed the repolarization of the electrode between -2.5 and 2.5 V, featuring a cathodic- as well as an anodic charging and discharging process for every cycle. Regarding distributed demands in applications, a wide range of scan rates was investigated by cyclic voltammetry (Fig. 4).

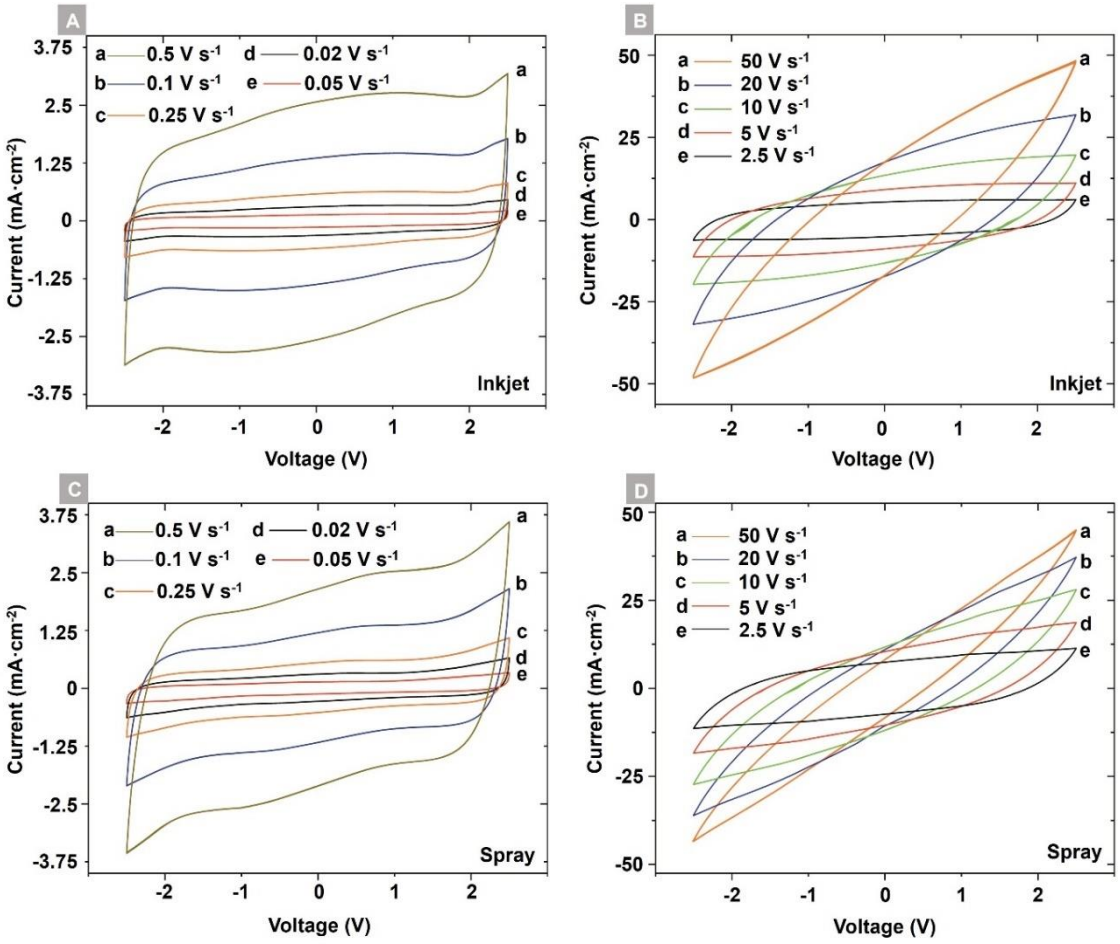

Fig. 4: *Cyclic voltammetry measurements of the electrodes produces by inkjet printing (A and B) and sprayed electrodes (C and D) at different scan rates from 0.02 V s^{-1} up to 50 V s^{-1}.*

Independent from the deposition technique, the electrodes show a quasi-rectangular shape of the voltammograms, which turns into an ellipsoid at high scan rates and increased current densities. The shape of the CV curves demonstrates that the energy is stored in form of electric double layer capacitance for both deposition techniques. Also, the current response at the potential limits is more pronounced for the sprayed electrodes suggesting ongoing charge storage processes. These processes could be caused by tortuosity or additional electrical states

of the active material available at elevated potentials. This could be further explained by a more disordered and less electrically connected structure of the sprayed electrode as observed by SEM measurements.

To evaluate the performance of the differently assembled electrodes, the specific capacitance of the two electrode types was compared (Fig. 5A). It is noteworthy that a mass loading of around 0.5 mg cm^{-2}was deposited in both techniques.

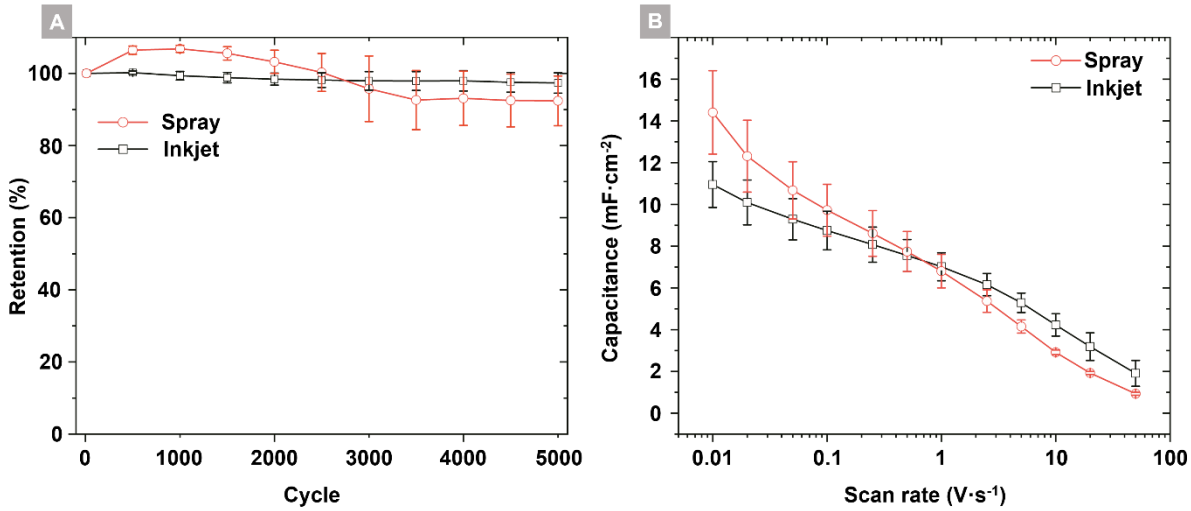

Fig. 5: *Comparison between the electrodes deposited by inkjet) and spray printing technique regarding their capacitance at different scan rates (A) and their long-term stability(B)*

The sprayed and the printed electrodes offer similar specific capacitances of 11 mF cm^{-2} for inkjet printed coatings and 14 mF cm^{-2} for spray coating at a scan rate of 0.01 V s^{-1}. The specific capacitance decreases with increasing scan rate illustrating kinetic limitations providing values of around 1 mF cm^{-2} at 50 V s^{-1} in both systems. Alongside with an increasing frequency of change in current polarity the time for the counterions of the electrolyte to fully occupy the surface of the active material decreases which reduces the specific capacitance.

Slight differences in capacitance between the two electrode types at lower scan rates suggest a higher useable surface for the electrolyte inside the pores of the sprayed electrode compared to the printed electrode. This difference in capacitance can not be explained by a thicker coating of one deposition technique since the gravimetric capacitance are also varies (24 F g^{-1} for printed and 27 F g^{-1} for sprayed electrodes at 0.01 V s^{-1}, Fig. S4). The reduced availability and accessibility of the printed electrode surface could be explained by the closure of cracks after pressing the electrodes (Fig. S5). In contrast, the sprayed electrode was affected less by pressing (Fig. S6) and could maintain a higher area available for the electrolyte to develop an electric double layer necessary for charge storage. This trend vanishes/inverts at scan rates

above 1 V s^{-1} where the effect of electrical connectivity could be favorable in a dense structure offered by the inkjet printed electrodes. A detailed comparison of the electrochemical performance with similar systems from literature is reported in Table S1 in the supporting information.

To assess the long-term stability of the electrodes, the cells were cycled 5000 times with a scan rate of 2.5 V s^{-1}(Fig. 5B). The inkjet printed electrodes reached a retention of 97% of their initial capacitance after the test. For spray coated electrodes, fluctuations between 107% after 1000 cycles and 92% after 5000 cycles were recorded which could originate from rearrangement processes of inhomogeneities in the coating during cycling. Even though the capacitance retention of the printed electrode was more consistent during the stability test, both systems offered a comparable overall electrochemical performance, qualifying the ink in combination with the spray and inkjet printing techniques for future usage in the field of device fabrication.

3.3.4 Conclusions

In summary, we have developed an easily scalable approach for the production of high performance supercapacitor electrodes using the deposition of functional inks based on OLC. With water as solvent and onion-like carbon as active material, the presented ink is based on sustainable components. An outstanding ink stability and high active material concentration of 1% was achieved by using SDS (sodium dodecyl sulfate) as surfactant in combination with physical deagglomeration by ball milling. The ink was deposited via spray and inkjet techniques, demonstrating versatility and compatibility in terms of industrial methodology. The obtained electrodes showed capacitances of 24 mF $cm^{-2}$for electrodes and 11 mF $cm^{-2}$for inkjet printed electrodes. The performance of the electrodes was demonstrated in a wide potential window of 2.5 V and at different scan rates ranging from 0.01 to 50 V s^{-1}. The storage capabilities were further supplemented with a high stability of the electrodes providing 97% (inkjet printing) and 92% (spray coating) of their initial capacitance after 5000 cycles.

The developed ink in combination with the low-cost and scalable deposition techniques of inkjet printing and spraying provides an easy to integrate solution to efficiently produce high-performance electrodes for future energy storage applications.

Tab. S1: *Comparison of ink and electrode with literature values.*

Carbon material	Weith in ink	Additive (amount)	Coating Method	Solvent	Capacitance (scan rate)	Retention	Ref.
Onion-like carbon	0.5[1]	SDS(0.3wt %)	Spray/inkjekt	Water	14 mF cm^{-2} (10 mV s^{-1})	97% (5000)	This work
Graphene	1	PEDOT:PSS(0.2 wt%)	Spray coating	NMP	0.4-1.8 mF cm^{-2} (1V s^{-1})	100% (50000)	[30]
Graphene	3	Ethylene cellulose 1.5wt%	Inkjet	14:3:3 cyclohexanone/terpineol/di(ethylene glycol) methyl ether	0.3mF (10 mV s^{-1})	97% (1000)	[31]
Carbon nano fiber	16.1	PEDOT 11.7 wt%	Spray	Ethylenglycol/Glycerol	5.2mF(1 Ag^{-1})	92% (200)	[32]
aromatic azide functionalized multiwalled carbon nanotubes	0.3	/	Inkjet	water	118 mF cm^{-2} (5 mV s^{-1})	90% (5000)	[33]
Activated carbon	8	PVDF(5 wt%) Triton	inkjet	Ethylene glycol	2.1 mF cm^{-2} (1 mV s^{-1})	/	[34]
Graphene	0.15-0.2	/	Inkjet	water	0.27mF cm^{-2} (5 µF cm^{-2})	75% (5000)	[35]
Arc discharge nanotubes	1,02	1wt% SDS	inkjet	water	26 mF	/	[36]

[1]The ink was diluted prior to deposition

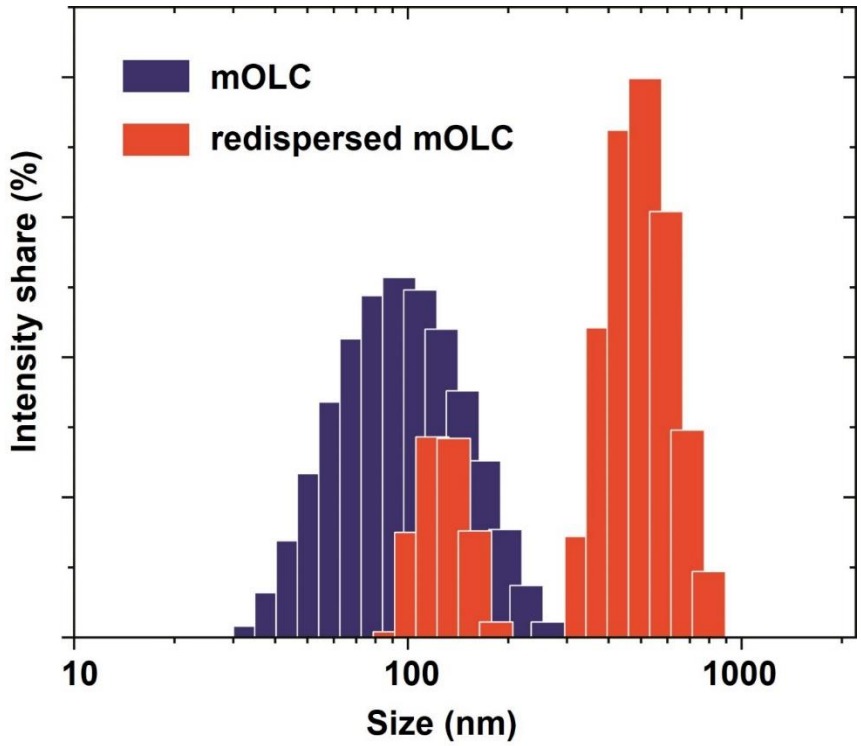

Fig. S1: *Comparison in particle size of the freeze-dried dispersion after redispersion and the dispersion directly after milling.*

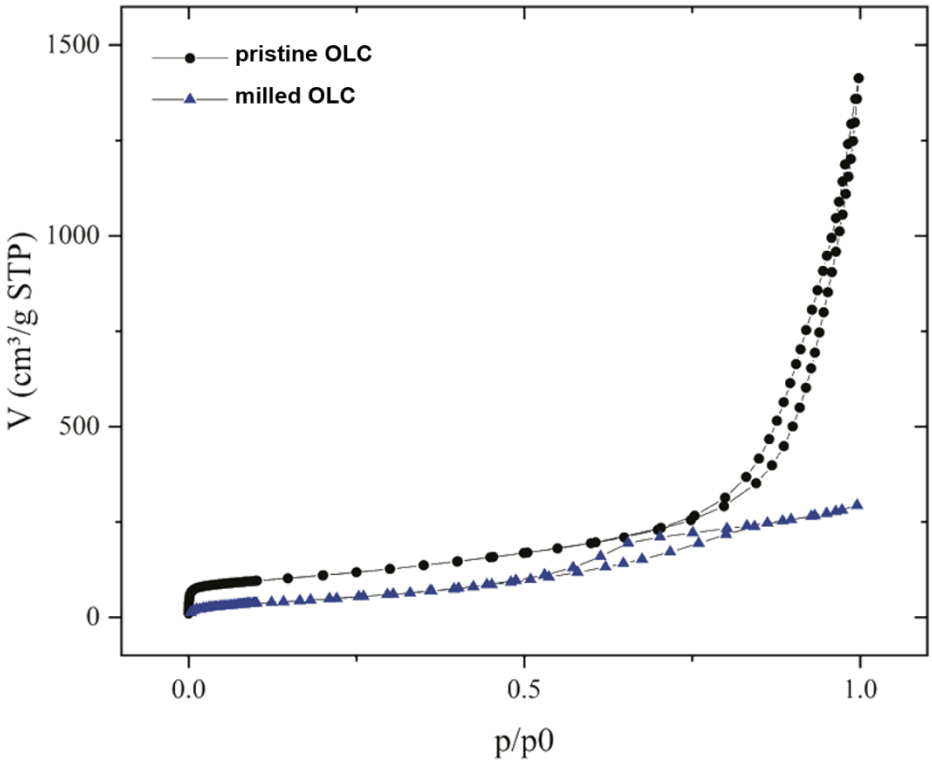

Fig. S2: *Nitrogen sorption measurements for as produced OLC and after ball milling (mOLC).*

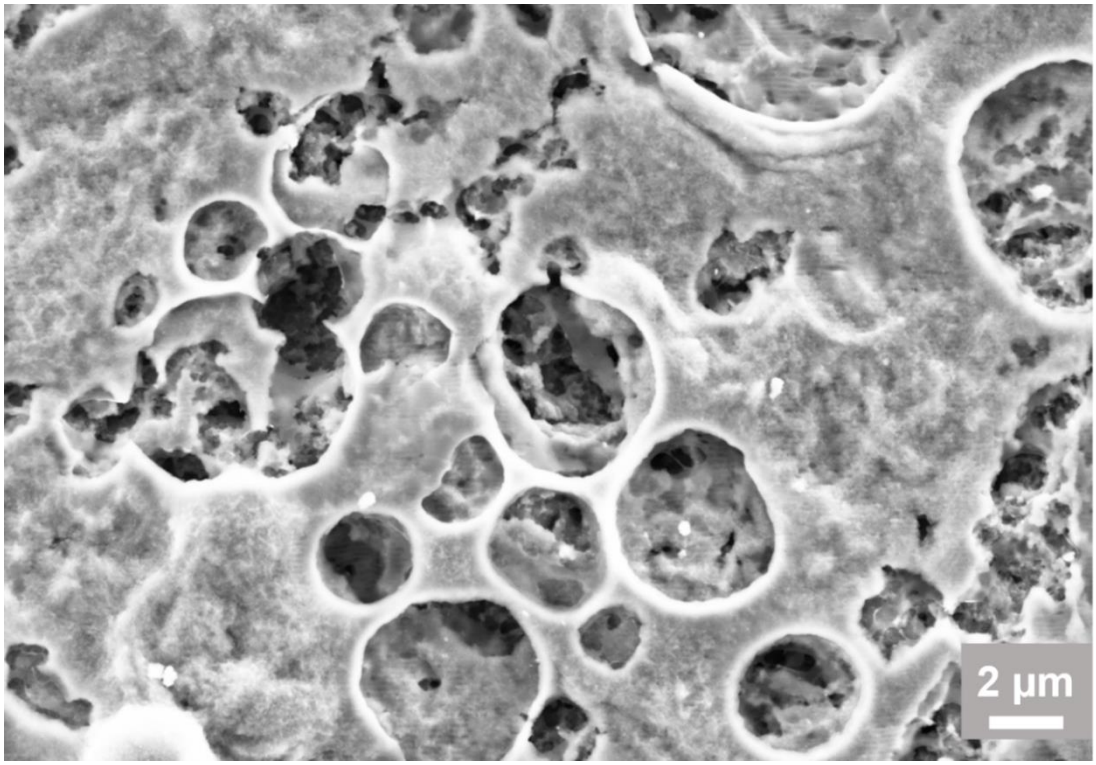

Fig. S3: *SEM of channels of the sprayed electrode.*

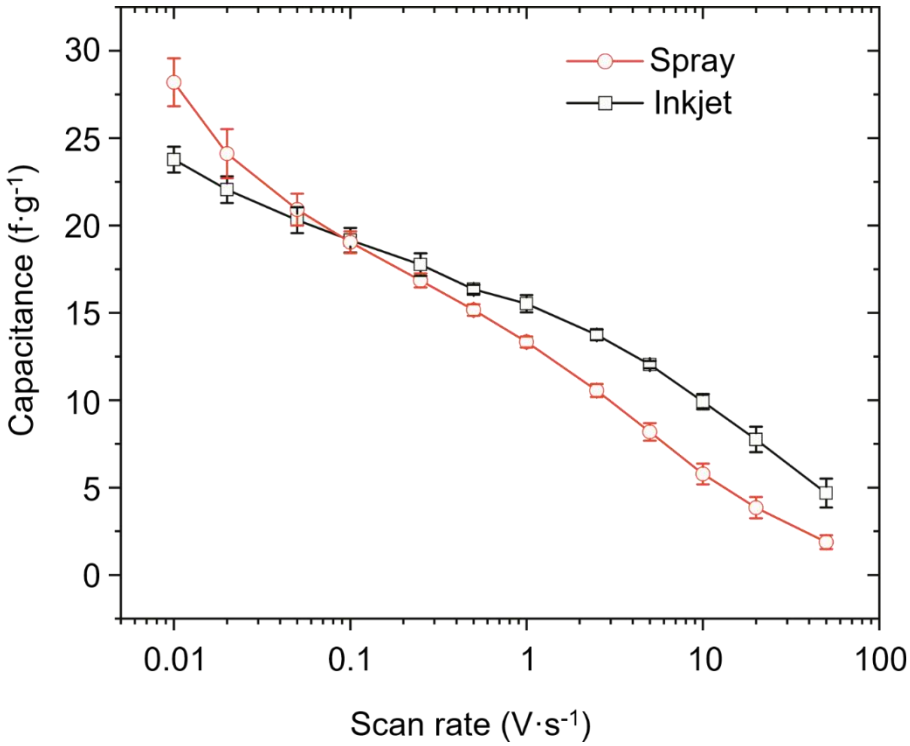

Fig. S4: *Comparison between the electrodes deposited by inkjet (pmOLC) and spray (smOLC) printing technique regarding their gravimetric capacitance.*

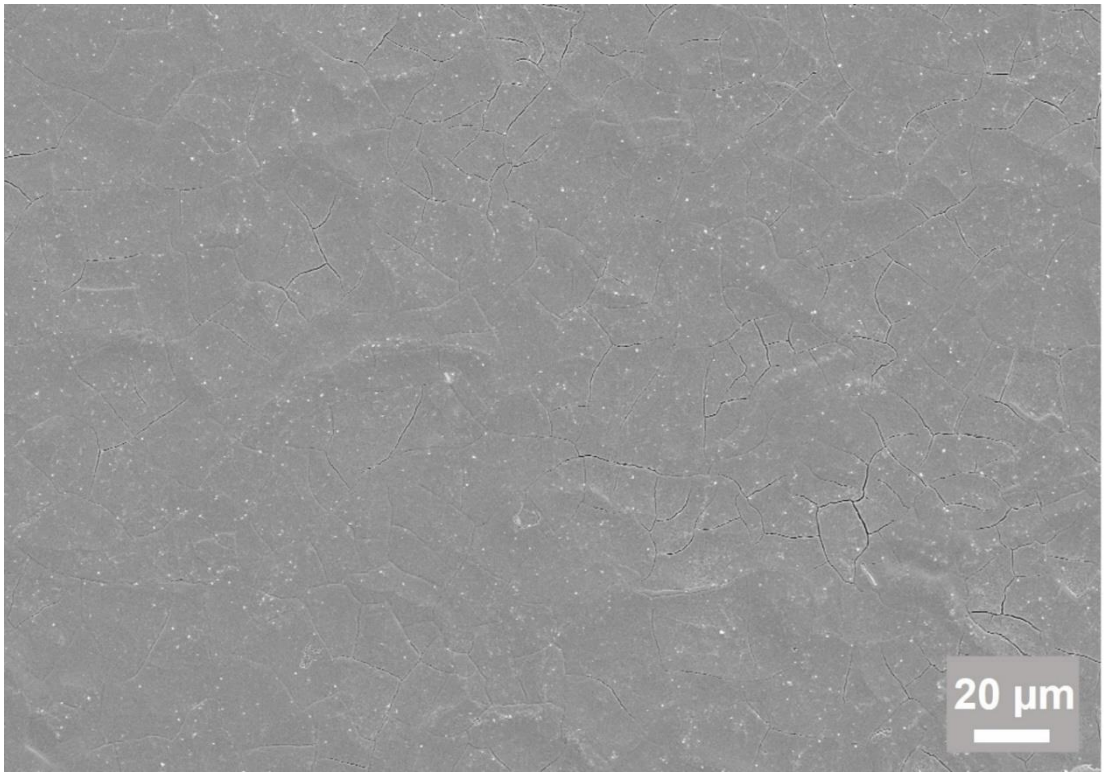

Fig. S5: *SEM of electrode surface of the printed electrode after pressing*

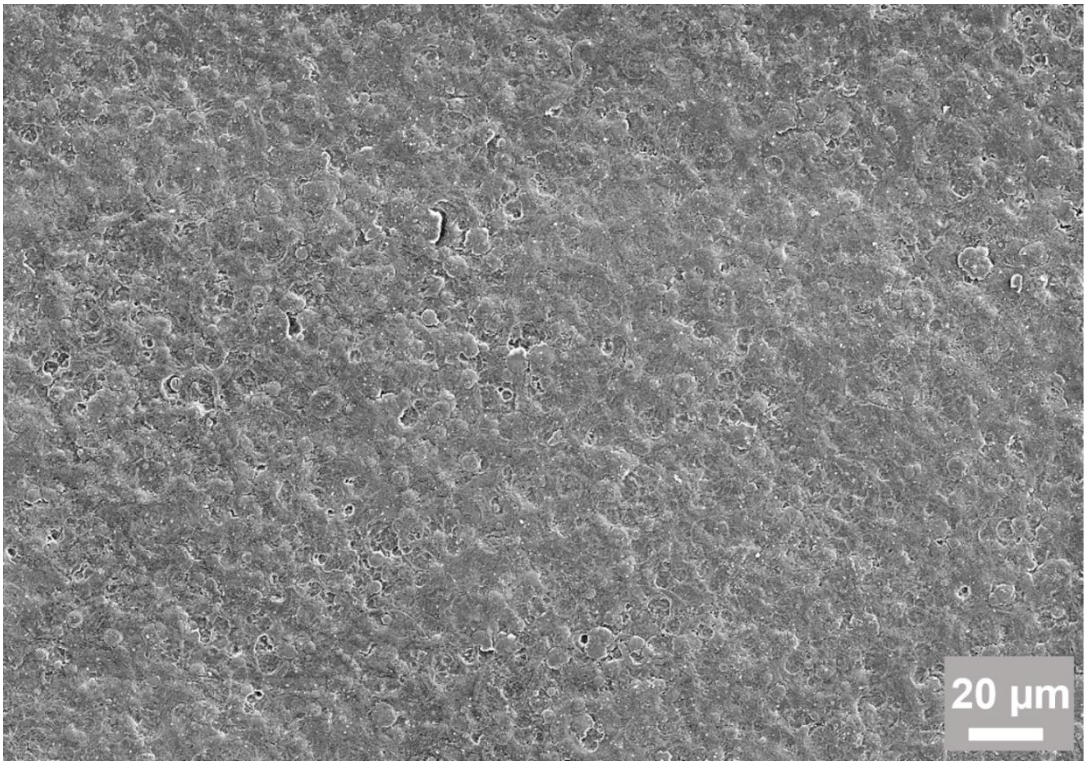

Fig. S6: *SEM of electrode surface of smOLC after pressing*

Ohnesorge number

An empirical parameter often reported in context of inks is the inverse Ohnesorge number Z [37, 38] Using the density ρ, dynamic viscosity η surface tension γ and the nozzle diameter α according to Eq. S1 Z indicates the droplet jetting behavior of the ink.

$$Z = \frac{\sqrt{\gamma \rho \alpha}}{\eta} \tag{S1}$$

Due to the different nozzle diameter a Z value of 75 was determined for inkjet printing while the spray process has a Z value of 41. Compared to the desired range of Z values (1-10) these high values predict the formation of satellite drops during printing.[39] To increase Z, thickening additives can be used to increase the viscosity of the ink. For our setup using a commercial inkjet printer, we experienced problems when increasing the viscosity of the ink using carboxymethyl cellulose as it only lead to nozzle clogging. Therefore, we avoided the usage of thickening additives and even observed an improvement in inkjet printability when reducing the active material concentration from 0.5 to 0.3%. Regardless of the high Z value, printability of the ink was given and the formation of satellite drops was accepted as a compromise to print electrodes with our equipment.

3.3.5 References

[1] T. T. Mai, P. H. Nguyen, Q. T. Tran, A. Cagnano, G. De Carne, Y. Amirat, A. T. Le, E. De Tuglie, An overview of grid-edge control with the digital transformation, Electrical Engineering 103(4) (2021) 1989-2007. https://doi.org/10.1007/s00202-020-01209-x

[2] A. Olabi, C. Onumaegbu, T. Wilberforce, M. Ramadan, M. A. Abdelkareem, A. H. Al–Alami, Critical review of energy storage systems, Energy 214 (2021) 118987. https://doi.org/10.1016/j.energy.2020.118987

[3] K. Janeczek, Composite materials for printed electronics in Internet of Things applications, Bulletin of Materials Science 43(1) (2020) 1-10. https://doi.org/10.1007/s12034-020-02101-x

[4] S. K. Garlapati, M. Divya, B. Breitung, R. Kruk, H. Hahn, S. Dasgupta, Printed Electronics Based on Inorganic Semiconductors: From Processes and Materials to Devices, Adv Mater 30(40) (2018) e1707600. https://doi.org/10.1002/adma.201707600

[5] G. Hu, J. Kang, L. W. T. Ng, X. Zhu, R. C. T. Howe, C. G. Jones, M. C. Hersam, T. Hasan, Functional inks and printing of two-dimensional materials, Chem Soc Rev 47(9) (2018) 3265-3300. https://doi.org/10.1039/c8cs00084k

[6] Q. L. Wang, G. N. Zhang, H. Y. Zhang, Y. Q. Duan, Z. P. Yin, H. A. Huang, High-Resolution, Flexible, and Full-Color Perovskite Image Photodetector via Electrohydrodynamic Printing of Ionic-Liquid-Based Ink, Advanced Functional Materials 31(28) (2021) 2100857. https://doi.org/10.1002/adfm.202100857

[7] R. F. Hossain, M. Min, L. C. Ma, S. R. Sakri, A. B. Kaul, Carrier photodynamics in 2D perovskites with solution-processed silver and graphene contacts for bendable optoelectronics, Npj 2d Materials and Applications 5(1) (2021) 1-12. https://doi.org/10.1038/s41699-021-00214-3

[8] C. Sriprachuabwong, C. Karuwan, A. Wisitsorrat, D. Phokharatkul, T. Lomas, P. Sritongkham, A. Tuantranont, Inkjet-printed graphene-PEDOT: PSS modified screen printed carbon electrode for biochemical sensing, Journal of Materials Chemistry 22(12) (2012) 5478-5485. https://doi.org/10.1039/C2JM14005E

[9] P. He, J. R. Brent, H. Ding, J. Yang, D. J. Lewis, P. O'Brien, B. Derby, Fully printed high performance humidity sensors based on two-dimensional materials, Nanoscale 10(12) (2018) 5599-5606. https://doi.org/10.1039/C7NR08115D

[10] F. Schackmar, H. Eggers, M. Frericks, B. S. Richards, U. Lemmer, G. Hernandez-Sosa, U. W. Paetzold, Perovskite Solar Cells with All-Inkjet-Printed Absorber and Charge Transport Layers, Advanced Materials Technologies 6(2) (2021) 2000271. https://doi.org/10.1002/admt.202000271

[11] S. K. Mondal, A. Biswas, J. R. Pradhan, S. Dasgupta, Inkjet-Printed MoS2 Transistors with Predominantly Intraflake Transport, Small Methods 5(12) (2021) e2100634. https://doi.org/10.1002/smtd.202100634

[12] Y. Bräuniger, S. Lochmann, J. Grothe, M. Hantusch, S. Kaskel, Piezoelectric Inkjet Printing of Nanoporous Carbons for Micro-supercapacitor Devices, ACS Applied Energy Materials 4(2) (2021) 1560-1567. https://doi.org/10.1021/acsaem.0c02745

[13] S. Tagliaferri, G. Nagaraju, A. Panagiotopoulos, M. Och, G. Cheng, F. Iacoviello, C. Mattevi, Aqueous Inks of Pristine Graphene for 3D Printed Microsupercapacitors with High Capacitance, ACS Nano 15(9) (2021) 15342-15353. https://doi.org/10.1021/acsnano.1c06535

[14] B. Yao, H. Peng, H. Zhang, J. Kang, C. Zhu, G. Delgado, D. Byrne, S. Faulkner, M. Freyman, X. Lu, M. A. Worsley, J. Q. Lu, Y. Li, Printing Porous Carbon Aerogels for Low Temperature Supercapacitors, Nano Lett 21(9) (2021) 3731-3737. https://doi.org/10.1021/acs.nanolett.0c04780

[15] M. Salanne, B. Rotenberg, K. Naoi, K. Kaneko, P. L. Taberna, C. P. Grey, B. Dunn, P. Simon, Efficient storage mechanisms for building better supercapacitors, Nature Energy 1(6) (2016) 1-10. https://doi.org/10.1038/Nenergy.2016.70

[16] X. Wu, R. Liu, J. Zhao, Z. Fan, Advanced carbon materials with different spatial dimensions for supercapacitors, Nano Materials Science 3(3) (2021) 241-267. https://doi.org/10.1016/j.nanoms.2021.01.002

[17] M. Zhao, H. H. Song, X. H. Chen, W. T. Lian, Large-scale synthesis of onion-like carbon nanoparticles by carbonization of phenolic resin, Acta Materialia 55(18) (2007) 6144-6150. https://doi.org/10.1016/j.actamat.2007.07.013

[18] O. Mykhailiv, H. Zubyk, M. E. Plonska-Brzezinska, Carbon nano-onions: Unique carbon nanostructures with fascinating properties and their potential applications, Inorganica Chimica Acta 468 (2017) 49-66. https://doi.org/10.1016/j.ica.2017.07.021

[19] K. L. Van Aken, K. Maleski, T. S. Mathis, J. P. Breslin, Y. Gogotsi, Processing of Onion-like Carbon for Electrochemical Capacitors, ECS Journal of Solid State Science and Technology 6(6) (2017) M3103-M3108. https://doi.org/10.1149/2.0181706jss

[20] J. Y. Lee, K. H. Cho, D. P. Lim, Y. B. Lee, D. S. Lim, Effect of attrition milling on dispersion of onion like carbon in aqueous medium, Appl Phys a-Mater 88(4) (2007) 693-697. https://doi.org/10.1007/s00339-007-4029-2

[21] L. Reinert, M. Zeiger, S. Suarez, V. Presser, F. Mucklich, Dispersion analysis of carbon nanotubes, carbon onions, and nanodiamonds for their application as reinforcement phase in nickel metal matrix composites, Rsc Advances 5(115) (2015) 95149-95159. https://doi.org/10.1039/c5ra14310a

[22] C. Portet, G. Yushin, Y. Gogotsi, Electrochemical performance of carbon onions, nanodiamonds, carbon black and multiwalled nanotubes in electrical double layer capacitors, Carbon 45(13) (2007) 2511-2518. https://doi.org/10.1016/j.carbon.2007.08.024

[23] A. Krueger, M. Ozawa, G. Jarre, Y. Liang, J. Stegk, L. Lu, Deagglomeration and functionalisation of detonation diamond, Phys Status Solidi A 204(9) (2007) 2881-2887. https://doi.org/10.1002/pssa.200776330

[24] M. Zeiger, N. Jackel, M. Asian, D. Weingarth, V. Presser, Understanding structure and porosity of nanodiamond-derived carbon onions, Carbon 84 (2015) 584-598. https://doi.org/10.1016/j.carbon.2014.12.050

[25] Y. Liu, R. L. Vander Wal, V. N. Khabashesku, Functionalization of carbon nano-onions by direct fluorination, Chemistry of Materials 19(4) (2007) 778-786. https://doi.org/10.1021/cm062177j

[26] K. L. Van Aken, J. K. McDonough, S. Li, G. Feng, S. M. Chathoth, E. Mamontov, P. F. Fulvio, P. T. Cummings, S. Dai, Y. Gogotsi, Effect of cation on diffusion coefficient of ionic liquids at onion-like carbon electrodes, Journal of Physics: Condensed Matter 26(28) (2014) 284104. https://doi.org/10.1088/0953-8984/26/28/284104

[27] G. P. Wang, M. Li, Y. Qian, L. F. Jia, Y. Q. Tao, J. Qi, X. Y. Lu, Effect of Carbon Nanotube Dispersion on Electrochemical Behavior of the CNTs/LiCoO2 Composite Cathode,

International Journal of Electrochemical Science 16(7) (2021). https://doi.org/10.20964/2021.07.45

[28] C. Knieke, A. Berger, M. Voigt, R. N. K. Taylor, J. Rohrl, W. Peukert, Scalable production of graphene sheets by mechanical delamination, Carbon 48(11) (2010) 3196-3204. https://doi.org/10.1016/j.carbon.2010.05.003

[29] M. Schneider, J. Maurath, S. B. Fischer, M. Weiss, N. Willenbacher, E. Koos, Suppressing Crack Formation in Particulate Systems by Utilizing Capillary Forces, ACS Appl Mater Interfaces 9(12) (2017) 11095-11105. https://doi.org/10.1021/acsami.6b13624

[30] Z. S. Wu, Z. Liu, K. Parvez, X. Feng, K. Mullen, Ultrathin Printable Graphene Supercapacitors with AC Line-Filtering Performance, Adv Mater 27(24) (2015) 3669-75. https://doi.org/10.1002/adma.201501208

[31] W. J. Hyun, E. B. Secor, C. H. Kim, M. C. Hersam, L. F. Francis, C. D. Frisbie, Scalable, Self-Aligned Printing of Flexible Graphene Micro-Supercapacitors, Advanced Energy Materials 7(17) (2017) 1700285. https://doi.org/10.1002/aenm.201700285

[32] M. G. Say, R. Brooke, J. Edberg, A. Grimoldi, D. Belaineh, I. Engquist, M. Berggren, Spray-coated paper supercapacitors, Npj Flexible Electronics 4(1) (2020) 1-7. https://doi.org/10.1038/s41528-020-0079-8

[33] S. K. Ujjain, P. Ahuja, R. Bhatia, P. Attri, Printable multi-walled carbon nanotubes thin film for high performance all solid state flexible supercapacitors, Materials Research Bulletin 83 (2016) 167-171. https://doi.org/10.1016/j.materresbull.2016.06.006

[34] D. Pech, M. Brunet, P. L. Taberna, P. Simon, N. Fabre, F. Mesnilgrente, V. Conedera, H. Durou, Elaboration of a microstructured inkjet-printed carbon electrochemical capacitor, Journal of Power Sources 195(4) (2010) 1266-1269. https://doi.org/10.1016/j.jpowsour.2009.08.085

[35] J. M. Munuera, J. I. Paredes, M. Enterria, S. Villar-Rodil, A. G. Kelly, Y. Nalawade, J. N. Coleman, T. Rojo, N. Ortiz-Vitoriano, A. Martinez-Alonso, J. M. D. Tascon, High Performance Na-O2 Batteries and Printed Microsupercapacitors Based on Water-Processable, Biomolecule-Assisted Anodic Graphene, ACS Appl Mater Interfaces 12(1) (2020) 494-506. https://doi.org/10.1021/acsami.9b15509

[36] P. C. Chen, H. T. Chen, J. Qiu, C. W. Zhou, Inkjet Printing of Single-Walled Carbon Nanotube/RuO2 Nanowire Supercapacitors on Cloth Fabrics and Flexible Substrates, Nano Res: Nano Res 3(8) (2010) 594-603. https://doi.org/10.1007/s12274-010-0020-x

[37] W. V. Ohnesorge, Die bildung von tropfen an düsen und die auflösung flüssiger strahlen, ZAMM-Journal of Applied Mathematics and Mechanics/Zeitschrift für Angewandte Mathematik und Mechanik 16(6) (1936) 355-358. https://doi.org/10.1002/zamm.19360160611

[38] L. Nayak, S. Mohanty, S. K. Nayak, A. Ramadoss, A review on inkjet printing of nanoparticle inks for flexible electronics, Journal of Materials Chemistry C 7(29) (2019) 8771-8795. https://doi.org/10.1039/c9tc01630a

[39] C. O'Mahony, E. U. Haq, C. Sillien, S. A. M. Tofail, Rheological Issues in Carbon-Based Inks for Additive Manufacturing, Micromachines (Basel) 10(2) (2019) 99. https://doi.org/10.3390/mi10020099

3.4 Sodium-ion batteries with onion-like carbon

Research of this chapter was part of the project Na+Nanobattterie funded by Bayerisches Staatsministerium für Umwelt und Verbraucherschutz.

The fourth chapter of the thesis is attributed towards the integration of onion-like carbon (OLC) into the electrode of sodium ion batteries (SIB). As the structure of OLC was not expected to provide structures to host sodium ions, the goal in this chapter was to use a material that can not store sodium ions, for sodium ion battery electrodes. Therefore, different approaches were conducted to introduce structures to store sodium ions. This helped to understand OLC and its possible function in SIB technology.

SIB Technology

Many learnings from the lithium ion batteries (LIB) technology, which is already commercialized, can be transferred and used for SIB. With alkali ions being the backbone for both technologies similarities in chemical behavior are featured. Therefore, a lot of the cell components like the active material or solvents for electrolyte used in lithium ion batteries LIB can also be applied in SIB. For further work on SIB, the differences of both technologies, must be acknowledged and emphasized.[1] The main reason to use sodium ion in batteries is the abundance of sodium which represents 2.83% in the crust of the earth, compared to a share of 0.0063% for lithium.[2] It is still part of discussion, if SIB can be seen as disruptive technology, as the technology is currently lacking power density.[3] However, a superior performance over LIB is not expected nor mandatory for commercial success of SIB. SIB are rather considered a well-balanced technology regarding the trilemma of ecological combability, power density and economical edge.[3] The key challenge for SIB targeted in this chapter arises from a different insertion mechanism of sodium ions in carbon-based anode material compared to LIB. Therefore, the active material has to provide specific structural properties,[4] researched in the following with special focus of troubleshooting alongside half-cell composition and construction. Besides the use of OLC as active material in the anode the role of OLC in SIB is also discussed.

3.4.1 Construction and composition of the half-cells

To research the capabilities of specific anode active materials, half-cells were built using a stainless-steel cell (ECC-Ref, El-Cell) as electrochemical battery test cell in a two- and a three-electrode configuration. The setting for a two-electrode configuration consisted out of a

working electrode (WE) featuring the active material and a counter electrode (CE) which was also used as reference electrode (RE), both electrodes were electrically isolated by a glass fiber separator (El-Cell) (Fig. 16). In a later stage, a three-electrode configuration was used where an additional piece of sodium was used as RE.

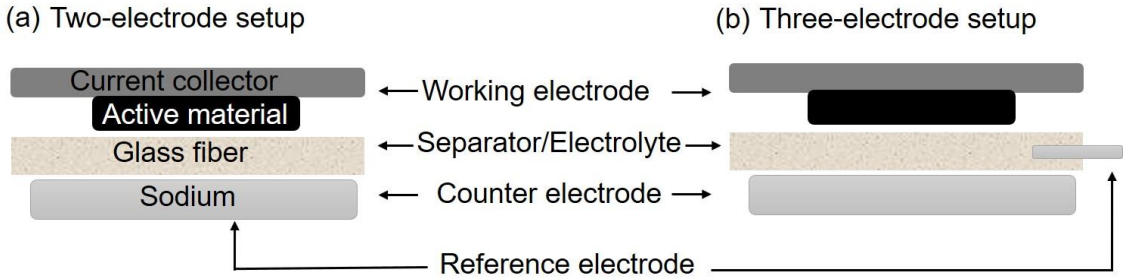

Fig. 16: *Schematic overview of the half-cell setup for (a) a two-electrode and (b)a three-electrode configuration.*

Beside lower costs for sodium, the usage of an aluminum foil as current collector instead of a more expensive copper foil is a another advantage of sodium ion batteries over lithium-ion-batteries (LIB).[5] This different metal can be used because sodium ions in contrast to lithium ions do not form an alloy with aluminum at the operating potential. For lithium ions, the alloying with aluminum process damages the current collector and therefore reduces the performance of the cell.[6] The CE for the SIB was custom-made by rolled metallic sodium ingots, as unlike for the Li-technology, there was no commercial sodium foil available (Fig. 17).

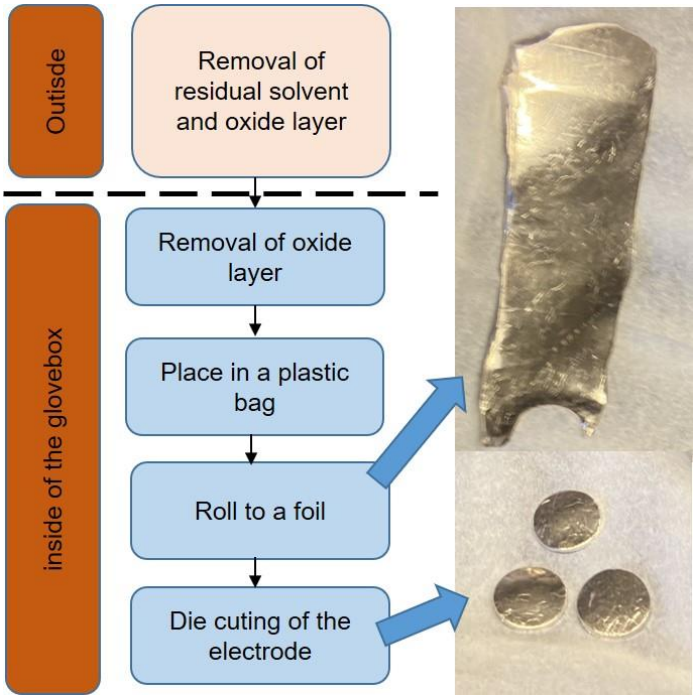

Fig. 17: *Schematic representation of the production of the sodium counter electrode.*

For preliminary work, the sodium ingots were molten in silicon oil at a temperature of around 100°C. The impurities released after melting, discoloring the solvent, were removed by replacing the silicon oil with petroleum ether. The usage of petroleum ether is also desirable over silicon oil due to its lower boiling point. This property is especially favorable as the removal of solvent, necessary before transferring sodium into the glovebox, is facilitated by rapid evaporation. Before introducing sodium cubes to the glovebox, the oxide layer was removed by removing around 0.3 mm of every surface using a knife. In the box, this cutting step was repeated. After this cleaning step, the sodium cube was transferred into a polyethylene pouch (freezer bag). This pouch was then placed into a custom-made stainless-steel mold where it was rolled out using a glass cylinder. The polyethylene pouch avoided contamination and ensured an easy handling of the sodium foil, which otherwise tends to stick to stainless steel. The resulting sodium foil was die cut with a punching iron to yield the CE with the desired diameter. For the cell stack, the separator was soaked with electrolyte (see below) and placed between RE and CE. The cell was sealed, transferred out of the glovebox and left to rest for 6 h before starting the electrochemical characterization. The resting time was necessary in order to allow the electrolyte to wet the porous electrode.

OLC as active material for SIB Anode

Different compositions of the WE, electrolytes and setups were tested. Considerations to use aqueous electrolytes with salts like sodium carbonate were quickly discarded in favor of organic electrolytes. This decision was made for several reasons, as the aqueous electrolyte caused corrosion problems with the aluminum current collector. Furthermore, the potential stability of this electrolyte was not sufficient for sodium intercalation, which was expected to require a potential of around 0.01 V vs sodium (ca. -2.7 V vs SHE).[7, 8] Therefore, a 1:1 mixture of ethylene carbonate and propylene carbonate with $NaPF_4$ (1M) as conductive salt was used subsequently, which is commonly used for SIB.[9] The WE consisted of OLC/CMC (acros organics)/conductive additive (C-nergy65, Imerys) in a ratio of 10:1:1. Here OLC was used as active material which was received by annealing of detonation diamond at 1500°C in vacuum as described elsewhere.[10] This setup was tested using galvanostatic cycling with a current density of 20 mA/g in a potential window between 2.5 and 0.5 V vs. Na/Na^+ (Fig. 3a) with subsequent *post mortem* analysis of the electrode surface by SEM (Fig. 3b). The protocol for the measurement was designed so that the constant charging of the electrode would stop either at the desired voltage of 0.5 V vs. Na/Na^+ or after 10 h of charging (Fig. 3a, spot 1). After reaching a potential of 0.5 V vs. Na/Na^+, a protocol segment was appointed regulating the current in order to maintain the potential 0.5 V vs. Na/Na+ (Fig. 3a, spot 2). The task of this constant voltage step was to reach a local equilibrium by accounting for diffusion and rearrangement of sodium ions in the active material. This step was followed by a 15 min break where the open current voltage was monitored (Fig. 3a, spot 3). A change in voltage during this break would indicate the instability of the current state of charge, probably caused by side reactions. This undesired change in voltage would then trigger an additional charging step in the protocol followed again by a 15 min break. If the voltage now remained stable, side reactions are finished granting a sufficiently stable state of charge before prior to the discharging step of the protocol.

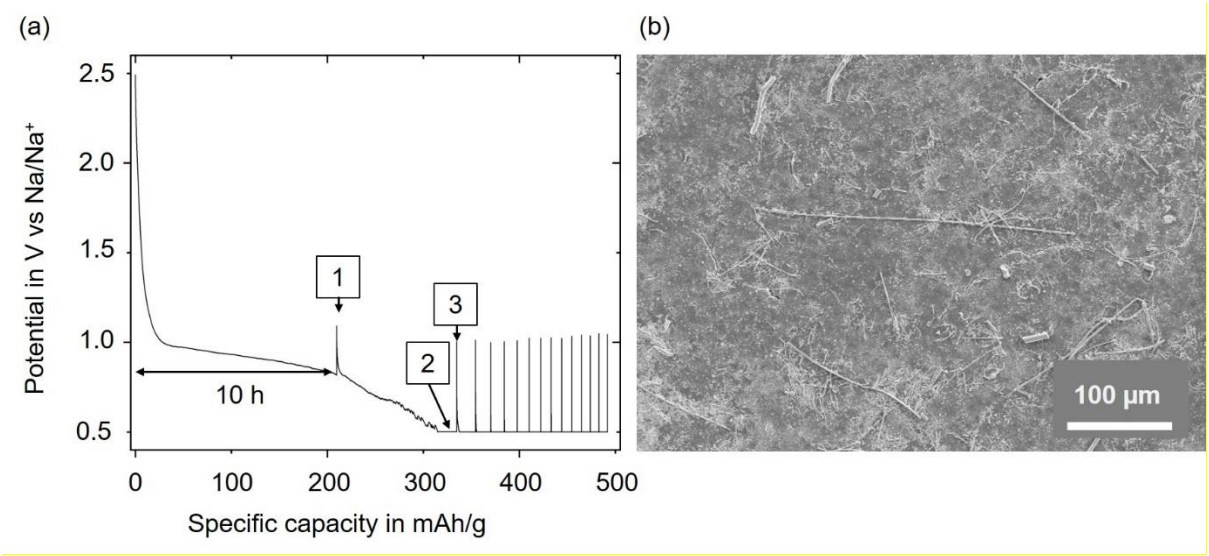

Fig. 3: *Investigation of OLC as anodic active material, with the (a) half-cell measurement of a SIBs using galvanostatic cycling and (b) SEM post mortem analysis of the active layer of the SIB half-cell.*

In the experiments the stable state of charge was never reached, as the voltage did change during the 15 min break (Fig. 3a, spot 3). The measurement was stopped eventually as a safety feature in the protocol was triggered as a certain unexpected charge of ca. 490 mAh/g was reached. The amount of charge was unexpected as it exceeded the estimated theoretical limit of hard carbon (ca. 280 mAh/g)[11] and especially since intercalation, where the main charge storage capacity is attributed, is not expected to happen in the examined potential region.[12] The unstable and irreversible character of the measurement suggested undesirable side reactions rather than reversible energy storage. The absence of a stable local equilibrium proposes ongoing reactions, which either could be an irreversible insertion of sodium ions in the active material or an ongoing SEI formation.[13] If the SEI formation on the surface would result in a stripping of active material, a fresh layer of material to be coated would be available. To identify this looping process a *post mortem* analysis of the electrode surface was conducted using SEM (Fig. 3b). Beside remains of the glass fiber separator, no morphology changes or structural damage was visible. Therefore, ongoing SEI formation at the anode was unlikely the reason for the observed irreversible uptake of charge. Another possible explanation, responsible for irreversible reactions, is trapping of sodium ions in structures of the active material. This phenomenon was also reported for other carbon based active materials.[14, 15] It is noteworthy that sodium ion insertion, as precondition for sodium ion trapping, is expected to occur only at a potential of around 0.35 V vs Na/Na^+.[15] As the conducted measurements only reached a potential of 0.5 V vs Na/Na^+, sodium ion trapping can not serve as explanation

for the observed irreversibility. Another hint was found due to unexpected discoloring of the CE/REF (Fig. 4b and c). The color of the electrode switched from silver to green after passing the measurement program, indicating reactions with the electrolyte at the CE/REF. To investigate and also to solve this problem, the custom mixed electrolyte was replaced with a commercial electrolyte. This premixed electrolyte featured 1M sodium bis(trifluoromethanesulfonyl)imide (solvionic) dissolved in dimethyl carbonate and ethylene carbonate. Additionally, the conductive additive was identified as a source of systematic error, due to its ability to store significant amount of Na-ion itself.[16] Therefore, the conductive additive was removed to avoid any interference with the correct capacity assignment of the active material. The setup itself was further changed from a two- to a three-electrode configuration to unlink the reference potential from irreversible reactions at the CE.

The latter change enabled a discrete observation of the reactions occurring at the CE or WE as well as an independent and therefore stable potential of the REF. The measurement window was changed to 2.5V-0.01 V vs Na/Na^+ to observe sodium ion trapping. To highlight those processes and their corresponding potential, the method of cyclic voltammetry (scan rate 0.2 mV/s) was chosen (Fig. 4a). For further understanding of the processes happening in the galvanostatic cycling experiment (Fig. 4a) the CE of the system using 1M sodium bis(trifluoromethanesulfonyl)imide dissolved in dimethyl carbonate and ethylene (Fig. 4b) was compared with the CE and RE, using 1M sodium hexafluorophosphate in propylene and ethylene carbonate (Fig. c).

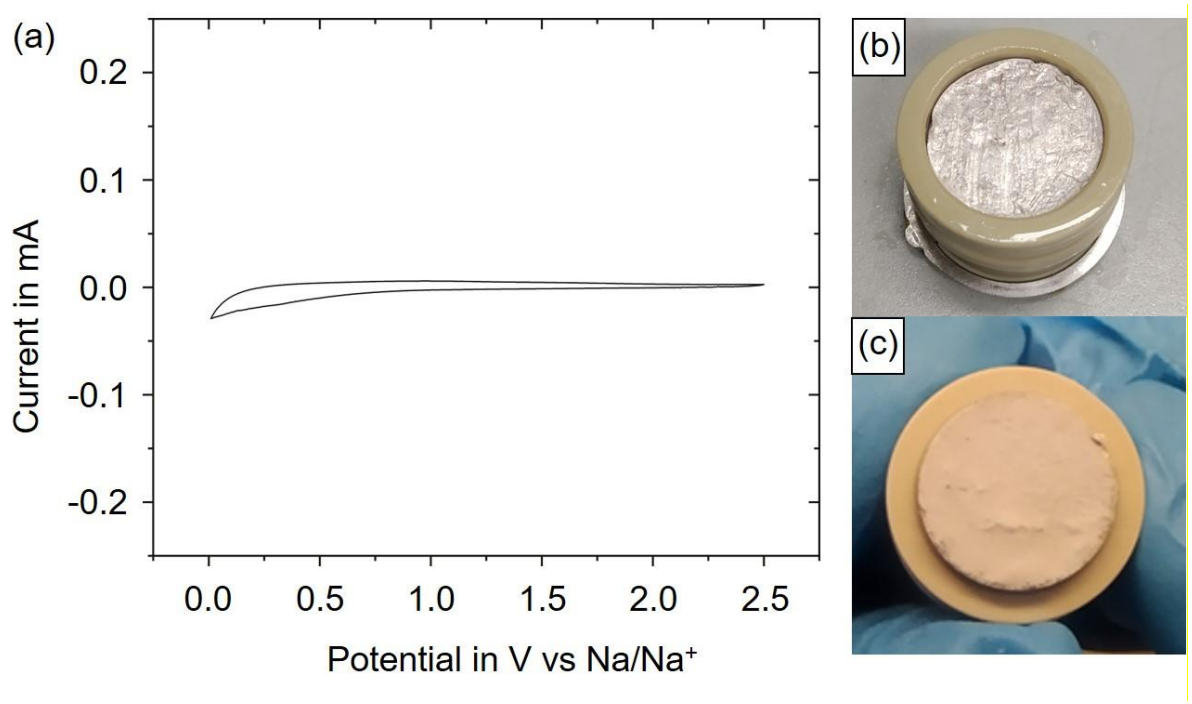

Fig. 4: *Characterization of the sodium ion storage behavior of OLC using (a) cyclic voltammetry. Post mortem analysis of the counter electrode with different electrolytes (b) 1M sodium bis(trifluoromethanesulfonyl)imide dissolved in dimethyl carbonate and ethylene carbonate (c) using 1M sodium hexafluorophosphaste in propylene and ethylene carbonate.*

The cyclic voltammetry measurement of the electrode is showing no peaks and therefore no characteristic side reactions during cycling (Fig. 4a). This indicates that the cause of the irreversibility was not caused by the OLC active material. As the commercial conductive agent was used successfully in other SIBs[16] and the same source of metallic sodium was used for all cells, the problems must have originated from the electrolyte. The error was presumably caused by residual water in the electrolyte. This was supported by the fact that after the changing the electrolyte, the CE did not change the color after cycling (Fig. 4b and c). However, no peaks in the CV also means that no significant sodium ion storage in the active material occurred during cycling. This observation indicated that pristine OLC is not eligible for sodium ion storage. This result was also recently confirmed by Presser et al. whose group measured capacity values in region of 4-8 mAh/g[16] for OLC. To set this into contrast, some conductive agents offer more than tenfold the capacity of OLC.[16] With this knowledge, the importance of the removal of conductive agents for capacity assessment at low values is immanent. As discussed earlier, Presser et al. attributes the inaccessibility of OLC for sodium ions as the reason for their low specific capacity.[16] Even if accessibility for sodium ions would be achieved, the low interlayer distance of the carbon planes remains as barrier for sodium ion insertion into the material. To enable sodium ion intercalation the desired interlayer

distance is around 0.4 nm; below this distance, intercalation compounds of sodium and carbon are unstable from an energetic point of view.[17] OLC features an interlayer distance of only around 0.35 nm.[18] A redesign of OLC has to tackle both, the accessibility for sodium ions as well as the interlayer distance within the carbon spheres.[16, 18]

3.4.2 Redesigning onion-like carbon as active material for sodium ion batteries

Accessibility as well as an increase in interlayer distance was targeted in order to change the character of the OLC primary particles. The motivation for this change was to enable sodium ion insertion, which presumably increases the specific capacity of OLC, making them an eligible active material. In carbon nano structuring an increase in interlayer distance is a common approach, especially applied to produce graphene by exfoliation.[19] With the Hummers method[20] as well as a microwave assisted approach[21] two technologies were utilized to restructure OLC. The basic idea for using the Hummer method was that holes, etched into the layers of the OLC by the nitric acid, are utilized to functionalize inner shells of the OLC eventually pushing those layers apart (Fig. 5).

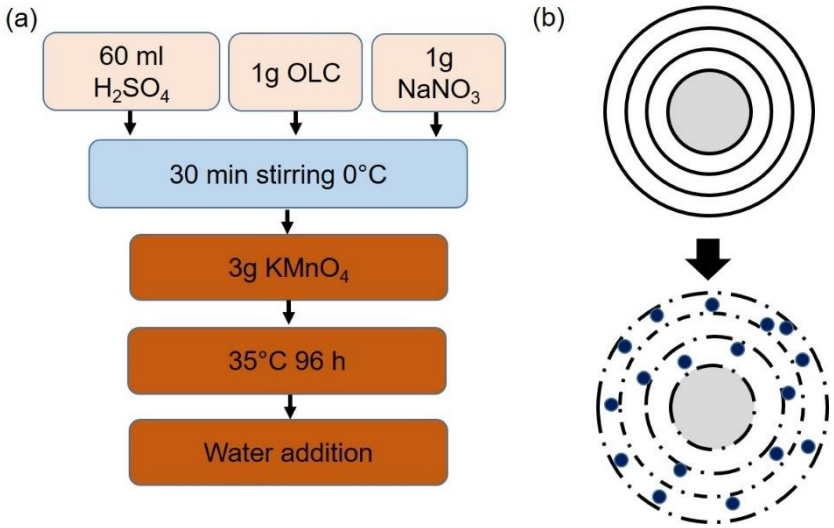

Fig. 5: *Hummer approach to increase the interlayer distance of OLC with the (a) flowchart of the method and (b) schematic idea of the experiment*

Therefore, 1 g of OLC was mixed with 1 g $NaNO_3$ and 60 ml H_2SO_4 stirred at 0 °C prior to the addition of 3 g $KMnO_4$. This mixture was stirred for 96 h at 35°C before adding water. This should introduce functional groups at the carbon planes in various layers to drive them apart (Fig. 5b). The microwave assisted approach targeted to introduce an energy shock and a volume

expansion inside of the OLC. This shock originated from the transformation of solid ammonium bicarbonate, located in the inner layers of OLC towards gaseous ammonia and carbon dioxide. This volume increase was supposed to partially burst the layers which would enable to expand the interlayer distance.

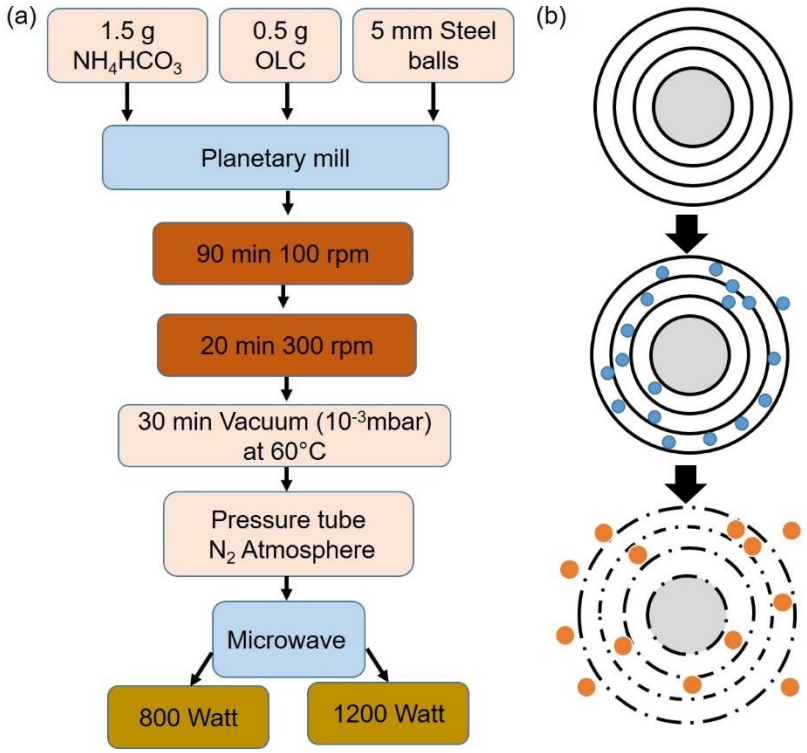

Fig. 6: *Microwave assisted approach to increase the interlayer distance of OLC with the (a) flowchart of the method and (b) schematic idea of the experiment.*

Ammonium bicarbonate (1.5 g) was mixed with OLC (0.5 g) by ball milling (90 min at 100 rpm and 20 min at 300 rpm, Fig. 6a). This should introduce ammonium bicarbonate into the layered structure of the OLC (Fig. 6b). Afterwards, the samples were heated at 60 °C in vacuum for 30 min and filled in a pressure tube. Energy was introduced by microwaving the pressure tube with a power of 800 and 1200 W, respectively. Within seconds of irradiation violent reactions featuring lightning triggered the safety valve of the safety pressure valve and the treatment had to be interrupted. To review the structural changes caused by both methods, the resulting materials were examined by x-ray diffraction and compared with pristine OLC which were annealed at 1500 °C in vacuum.

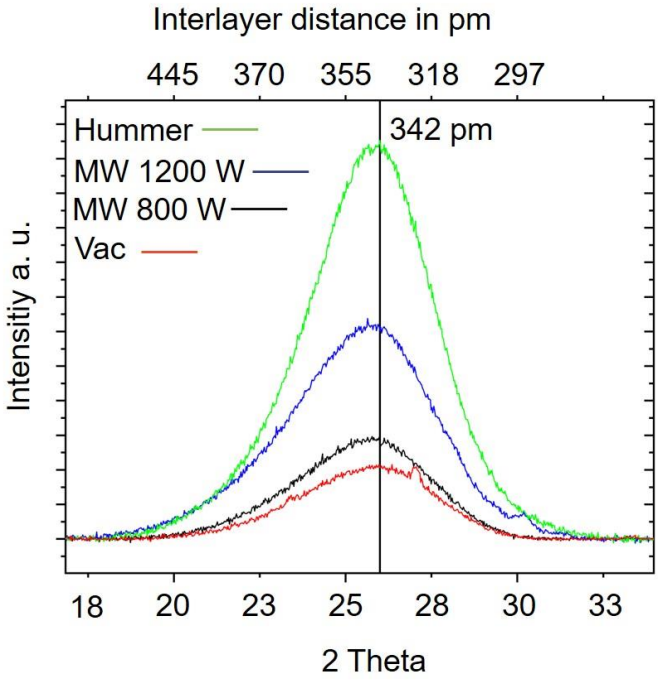

Fig. 7: *X-ray diffraction pattern of the treated OLC samples with regard to the graphitic layer distance reflex (002).*

It can be seen that none of those methods was able to expand the interlayer distance to values of 400 pm which were desired for sodium ion storage. This result can be derived from the peak position in x-ray diffraction (Fig. 7) and is presumably caused by the inaccessibility of the shells of OLC (Fig. 8a and b).

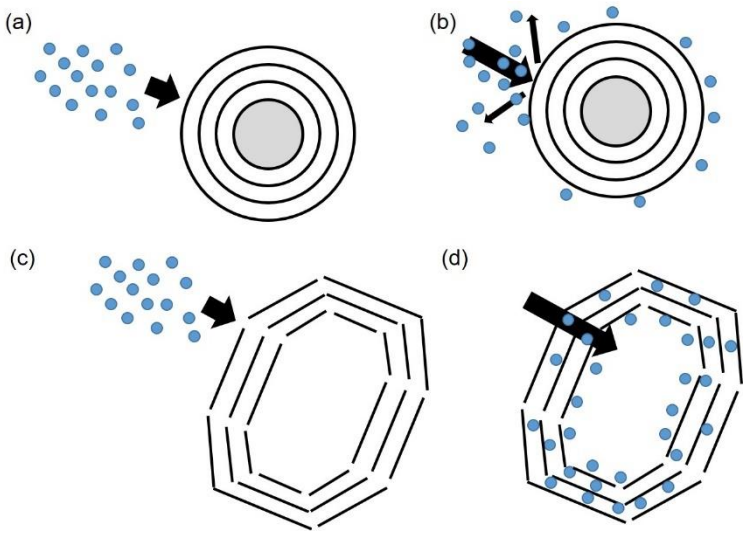

Fig. 8: *Schematic representation of onion-like carbon and graphitized onion-like carbon as well as the introduction of ions (a and c) and the presumed resulting compound (b and d).*

Without the accessibility, the reactants can not reach the intended location to apply pressure and drive the layers apart (Fig. 8b). Without accessing inner layers, there was no effect for the ammonia bicarbonate treatment. Also, the Hummers methods only could lead to surface functionalization of OLC, desired for other applications.[22]

However, accessibility was reported for types of onion-like carbon synthesized under different conditions.[23, 24] To understand why the experiments did not work on OLC but for other related materials, it is noteworthy that these other carbon onions are consisting of connected graphitic segments. Therefore, it is important to distinguish between onion-like carbon (GOC, Fig. 8a) and graphitic onion-like carbon (GOLC, Fig. 8c). GOLC in contrast to OLC is formed from connected graphitic areas rather than of concentrically stacked spherical shells. At the joints of these graphitic areas, GOLC features disorder which is radially propagated towards its center. This disorder offers micropores, which enable intraparticle accessibility[25], not available for OLC derived from detonation diamond, annealed in vacuum[18] at temperatures up to 1800 °C[26] (Fig. 8d). This disorder of GOLC can also be the first point of action when etching is happening and presumably allows access into the layered segments for ions or reactants, which could cause an increase in interlayer distance.[24] For OLC which does not feature this radial disorder, it is still part of research if any activation steps introduces such kind of microporosity or would rather remove the complete layer before etching the next inner layer.[27] Initiated by these considerations, the role of pristine OLC in SIB has to be reassessed.

OLC as conductive agent in hard carbon electrodes

The inaccessibility of OLC can also be a beneficial feature rather than an obstacle, when used in SIB. Especially for conductive additives, interference of the electrolyte with the additive can be minimized as ion trapping would be prevented. Also, the electric conductivity and the interconnected character of OLC agglomerates are beneficial properties for its usage as conductive additives. In contrast to the group of Presser which already tested OLC as conductive additive in SIB with antimony as active material,[16] in this work hard carbon is used as anodic active material. The source of hard carbon for the presented SIB were banana peels, whose pyrolysis product features an interlayer distance suitable for reversible Na-Ion storage.[28] For the preparation of the active material, banana peels were pyrolyzed at 1100 °C for 1 h in vacuum (10^{-3}mbar) in a tubular furnace.

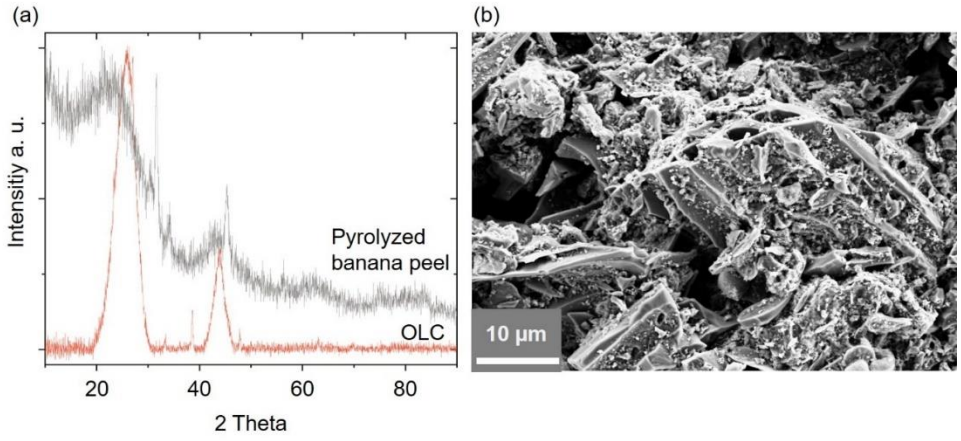

Fig. 9: *Pyrolyzed banana peel (a) X-ray diffraction pattern compared with onion-like carbon (b) SEM measurement*

As expected, the pyrolyzed biomaterial featured a higher degree of disorder compared to OLC. Also the peak related to the interlayer distance is shifted towards 21 °, which indicates a higher interlayer distance more promising to intercalate sodium ions (Fig. 9a). For the electrode which consisted out of biomaterial: OLC : CMC (10:1:1) the biomaterial was ground with a coffee mill to particle sizes in the range of several micrometers (Fig. 9b). For the electrochemical characterization, a three-electrode configuration was used, with metallic sodium as RE and CE, a glass fiber separator and 1M sodium bis(trifluoromethanesulfonyl)imide dissolved in dimethyl carbonate and ethylene as electrolyte (Fig. 10).

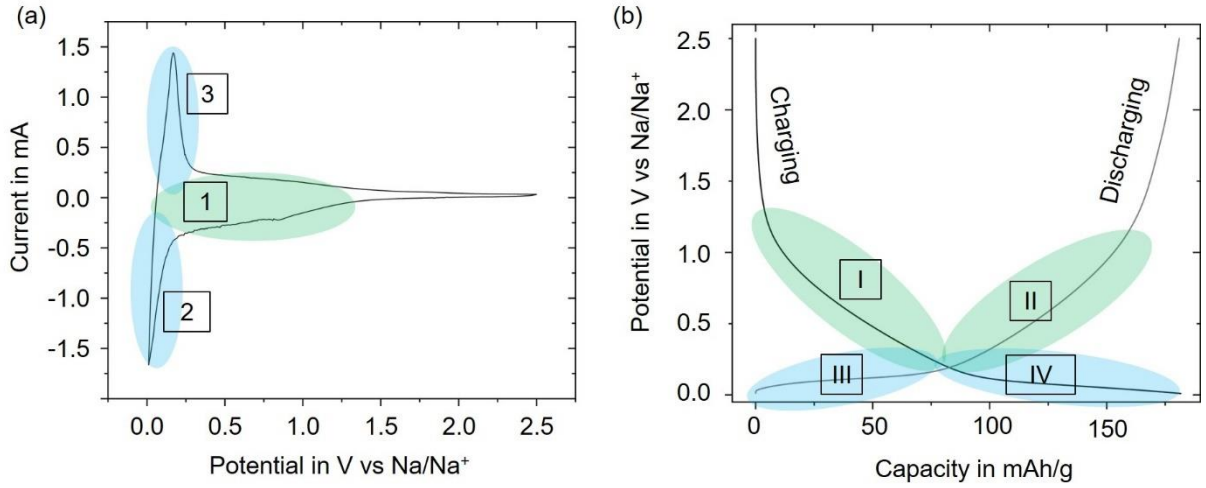

Fig. 10: *Electrochemical characterization of the biomaterial electrode with (a) cyclic voltammetry using a scan rate of 0.2 mV/s featuring different zones (arabic numerals) of sodium ion: (zone 1) storage at the surface (zone 2) storage by intercalation as well as (zone 3) deintercalation. Electrochemical characterization of the biomaterial electrode with (b) galvanostatic cycling using a current density of 0.1 A/g (2 C, 10th cycle) in a potential window between 2.5 and 0.01 V vs. Na/Na$^+$. Different zones (roman numerals) of sodium storage are*

visible for charging and discharging of the electrode. Zone I and II represent surface related ion storage whereas III and IV accounts for intercalation and deintercalation of sodium ions.

Characteristic zones for sodium ion storage can be observed in the CV (Fig. 10a, Arabic numerals) as well as for the GC (Fig. 10b roman numerals).[7, 8, 12, 29] Specifically, the cyclic voltammogram shows signs of sodium ion storage at surface defects (Fig. 10a Zone 1) but also sharp peaks, indicating sodium ion intercalation (Fig. 10 a Zone 2) and deintercalation (Fig. 10a Zone 3). This reversible energy storage can also be observed in galvanostatic charging and discharging measurements, featuring the following zones: (Fig. 10b):

1. I: Charging: Na-ion adsorption in surface related sites
2. II: Discharging: Na-ion desorption in surface related sites
3. III Discharging: Na-ion deintercalation
4. IV Charging: Na-ion intercalation

These electrochemical measurements show a reversible energy storage expected for sodium electrodes. The capacity is around 180 mAh/g and a retention of almost 100% (for the 10^{th} cycle) is comparable with SIB also using banana peel as active material (290 mAh/g at 200 mA/g).[28] This underlines that the choice of active material is crucial for SIB but also demonstrates the viability of a hard carbon anode with OLC used as conductive agent. At this stage, the presented SIB and its electrodes are considered as successful proof-of-concept device. The next steps towards a commercial application require the comparison of different conductive agents, benchmark testing and optimization. The device and the previously mentioned requirements additionally offer a promising starting point for future research on OLC in SIB.

Research on the SIB in this chapter highlighted various difficulties hindering the storage of sodium ions in a carbon active material. At the same time various strategies to solve these challenges were presented and discussed. Also, problems with the half cell production were highlighted and evaluated. Rather trivial but vital factors like the right choice of electrolyte, the half-cell configuration and the counter electrode production were evaluated. The resulting setup has featured three electrodes, an organic electrolyte and a sustainable carbon active material. With microwave treatment and Hummer's method, two methods were unsuccessfully performed to improve the structure of OLC aiming to enable sodium ion insertion. This result was attributed to the inaccessibility of the inner shells of OLC. Inspired by similar results found in literature, the OLC were rather used as conductive agent in SIB electrode using banana peel

as active material with a capacity of 180 mAh/g. This role utilizes and embraces the inability of OLC to store sodium ions rather as feature than as problem as OLC do not compete with the active material nor trap sodium ion.

3.4.3 References

[1] Q. Liu, R. G. Xu, D. B. Mu, G. Q. Tan, H. C. Gao, N. Li, R. J. Chen, F. Wu, Progress in electrolyte and interface of hard carbon and graphite anode for sodium-ion battery, Carbon Energy 4(3) (2022) 458-479. https://doi.org/10.1002/cey2.120

[2] F. Xie, Z. Xu, Z. Guo, M.-M. Titirici, Hard carbons for sodium-ion batteries and beyond, Progress in Energy 2(4) (2020) 042002. https://doi.org/10.1088/2516-1083/aba5f5

[3] L. Zhao, T. Zhang, W. Li, T. Li, L. Zhang, X. Zhang, Z. Wang, Engineering of sodium-ion batteries: Opportunities and challenges, Engineering (2022). https://doi.org/10.1016/j.eng.2021.08.032

[4] T. Zhang, C. Li, F. Wang, A. Noori, M. F. Mousavi, X. Xia, Y. Zhang, Recent Advances in Carbon Anodes for Sodium-Ion Batteries, Chem Rec (2022) e202200083. https://doi.org/10.1002/tcr.202200083

[5] E. Quartarone, T. Eisenmann, M. Kuenzel, C. Tealdi, A. G. Marrani, S. Brutti, D. Callegari, S. Passerini, Towards Advanced Sodium-Ion Batteries: Green, Low-Cost and High-Capacity Anode Compartment Encompassing Phosphorus/Carbon Nanocomposite as the Active Material and Aluminum as the Current Collector, Journal of the Electrochemical Society 167(8) (2020) 080509. https://doi.org/10.1149/1945-7111/ab856e

[6] S. T. Myung, Y. Hitoshi, Y. K. Sun, Electrochemical behavior and passivation of current collectors in lithium-ion batteries, Journal of Materials Chemistry 21(27) (2011) 9891-9911. https://doi.org/10.1039/c0jm04353b

[7] S. Alvin, H. S. Cahyadi, J. Hwang, W. Chang, S. K. Kwak, J. Kim, Revealing the Intercalation Mechanisms of Lithium, Sodium, and Potassium in Hard Carbon, Advanced Energy Materials 10(20) (2020) 2000283. https://doi.org/10.1002/aenm.202000283

[8] C. Bommier, T. W. Surta, M. Dolgos, X. Ji, New Mechanistic Insights on Na-Ion Storage in Nongraphitizable Carbon, Nano Lett 15(9) (2015) 5888-92. https://doi.org/10.1021/acs.nanolett.5b01969

[9] A. Ponrouch, D. Monti, A. Boschin, B. Steen, P. Johansson, M. R. Palacin, Non-aqueous electrolytes for sodium-ion batteries, Journal of Materials Chemistry A 3(1) (2015) 22-42. https://doi.org/10.1039/c4ta04428b

[10] M. Zeiger, N. Jackel, D. Weingarth, V. Presser, Vacuum or flowing argon: What is the best synthesis atmosphere for nanodiamond-derived carbon onions for supercapacitor electrodes?, Carbon 94 (2015) 507-517. https://doi.org/10.1016/j.carbon.2015.07.028

[11] B. W. Xiao, T. Rojo, X. L. Li, Hard Carbon as Sodium-Ion Battery Anodes: Progress and Challenges, Chemsuschem 12(1) (2019) 133-144. https://doi.org/10.1002/cssc.201801879

[12] P. C. Tsai, S. C. Chung, S. K. Lin, A. Yamada, Ab initio study of sodium intercalation into disordered carbon, Journal of Materials Chemistry A 3(18) (2015) 9763-9768. https://doi.org/10.1039/c5ta01443c

[13] L. A. Romero-Cano, H. Garcia-Rosero, F. Carrasco-Marin, A. F. Perez-Cadenas, L. V. Gonzalez-Gutierrez, A. I. Zarate-Guzman, G. Ramos-Sanchez, Surface functionalization to abate the irreversible capacity of hard carbons derived from grapefruit peels for sodium-ion batteries, Electrochimica Acta 326 (2019) 134973. https://doi.org/10.1016/j.electacta.2019.134973

[14] E. M. Lotfabad, P. Kalisvaart, A. Kohandehghan, D. Karpuzov, D. Mitlin, Origin of non-SEI related coulombic efficiency loss in carbons tested against Na and Li, Journal of Materials Chemistry A 2(46) (2014) 19685-19695. https://doi.org/10.1039/c4ta04995k

[15] Z. L. Jian, C. Bomrnier, L. L. Luo, Z. F. Li, W. T. Wang, C. M. Wang, P. A. Greaney, X. L. Ji, Insights on the Mechanism of Na-Ion Storage in Soft Carbon Anode, Chemistry of Materials 29(5) (2017) 2314-2320. https://doi.org/10.1021/acs.chemmater.6b05474

[16] K. Pfeifer, S. Arnold, O. Budak, X. L. Luo, V. Presser, H. Ehrenberg, S. Dsoke, Choosing the right carbon additive is of vital importance for high-performance Sb-based Na-ion batteries, Journal of Materials Chemistry A 8(12) (2020) 6092-6104. https://doi.org/10.1039/d0ta00254b

[17] Y. Li, Y. Lu, P. Adelhelm, M. M. Titirici, Y. S. Hu, Intercalation chemistry of graphite: alkali metal ions and beyond, Chem Soc Rev 48(17) (2019) 4655-4687. https://doi.org/10.1039/c9cs00162j

[18] M. Zeiger, N. Jackel, V. N. Mochalin, V. Presser, Review: carbon onions for electrochemical energy storage, Journal of Materials Chemistry A 4(9) (2016) 3172-3196. https://doi.org/10.1039/c5ta08295a

[19] A. Ibarra-Hernandez, A. Vega-Rios, V. Osuna, Synthesis of Graphite Oxide with Different Surface Oxygen Contents Assisted Microwave Radiation, Nanomaterials (Basel) 8(2) (2018) 106. https://doi.org/10.3390/nano8020106

[20] W. S. Hummers Jr, R. E. Offeman, Preparation of graphitic oxide, Journal of the american chemical society 80(6) (1958) 1339-1339. https://doi.org/10.1021/ja01539a017

[21] J. X. Lin, Y. J. Huang, S. Wang, G. H. Chen, Microwave-Assisted Rapid Exfoliation of Graphite into Graphene by Using Ammonium Bicarbonate as the Intercalation Agent, Industrial & Engineering Chemistry Research 56(33) (2017) 9341-9346. https://doi.org/10.1021/acs.iecr.7b01302

[22] J. Bartelmess, S. Giordani, Carbon nano-onions (multi-layer fullerenes): chemistry and applications, Beilstein J Nanotechnol 5(1) (2014) 1980-98. https://doi.org/10.3762/bjnano.5.207

[23] A. Dimas Chandra Permana, A. Omar, I. Guillermo Gonzalez-Martinez, S. Oswald, L. Giebeler, K. Nielsch, D. Mikhailova, MOF-Derived Onion-Like Carbon with Superior Surface Area and Porosity for High Performance Lithium-Ion Capacitors, Batteries & Supercaps (2022) e202100353. https://doi.org/10.1002/batt.202100353

[24] S. Zhang, J. Niu, H. Song, L. Zhu, J. Zhou, X. Chen, J. Liu, S. Hong, R. Song, Can closed shell graphitic materials be exfoliated? Defect induced porphyra-like graphene from the cooperation of activation and oxidation, Journal of Materials Chemistry A 1(45) (2013) 14103-14107. https://doi.org/10.1039/c3ta13383d

[25] M. Klose, K. Pinkert, M. Zier, M. Uhlemann, F. Wolke, T. Jaumann, P. Jehnichen, D. Wadewitz, S. Oswald, J. Eckert, L. Giebeler, Hollow carbon nano-onions with hierarchical porosity derived from commercial metal organic framework, Carbon 79 (2014) 302-309. https://doi.org/10.1016/j.carbon.2014.07.071

[26] M. Klose, R. Reinhold, K. Pinkert, M. Uhlemann, F. Wolke, J. Balach, T. Jaumann, U. Stoeck, J. Eckert, L. Giebeler, Hierarchically nanostructured hollow carbon nanospheres for ultra-fast and long-life energy storage, Carbon 106 (2016) 306-313. https://doi.org/10.1016/j.carbon.2016.05.046

[27] M. Zeiger, N. Jackel, M. Asian, D. Weingarth, V. Presser, Understanding structure and porosity of nanodiamond-derived carbon onions, Carbon 84 (2015) 584-598. https://doi.org/10.1016/j.carbon.2014.12.050

[28] E. M. Lotfabad, J. Ding, K. Cui, A. Kohandehghan, W. P. Kalisvaart, M. Hazelton, D. Mitlin, High-density sodium and lithium ion battery anodes from banana peels, ACS Nano 8(7) (2014) 7115-29. https://doi.org/10.1021/nn502045y

[29] J. M. Stratford, P. K. Allan, O. Pecher, P. A. Chater, C. P. Grey, Mechanistic insights into sodium storage in hard carbon anodes using local structure probes, Chem Commun (Camb) 52(84) (2016) 12430-12433. https://doi.org/10.1039/c6cc06990h

4 Summary and outlook

In this thesis, the usage of onion-like carbon (OLC) for energy storage applications was researched regarding sustainability, performance and processability. This work targets to increase the scientific understanding regarding the role of OLC in electrodes and to facilitate a large-scale production, which is the foundation for commercial application. Research was devoted to increase the knowledge in the particular field, to yield synergistic approaches and a shared value regarding sustainability and performance.

The study of the first chapter was dedicated to increase the sustainability of OLC electrodes for supercapacitors. Up to date, the usage of fluorinated polymers as binder is a point of concern. A desirable replacement is carboxymethyl cellulose because of the plant based and therefore sustainable background. Although this binder was successfully applied in electrodes using different active materials, it caused problems when combined with OLC as the structure of the OLC agglomerates features big macropores. These voids absorbed a huge amount of binder, which was problematic for the intended usage as supercapacitor electrodes. Firstly, binder in voids is not available for cohesion with other particles and secondly, this inactive binder adds dead weight to the electrode. Additionally excess binder clogs the pores of the electrodes. Therefore, the goal for the first chapter could be formulated:

Reduce the specific volume agglomerate while maintaining the specific surface of onion-like carbon.

Hereby, OLC was agglomerated prior to electrode production. Even though the volume was decreased, agglomeration did not clog the porosity of the material. The initial specific surface of 527 m^2/g could be maintained by simply forming bigger and denser agglomerates, which only reduced the size of big voids. Preagglomeration enabled the use of green cellulose based binder. The resulting green electrodes provided a capacitance of 56 F/g, which was 22% higher compared to electrodes relying on a conventional fluorinated binder. These electrodes provide a shared value regarding sustainability and performance.

For the system presented in the second chapter, a superior performance of the electrodes was targeted. To increase the capacitance, a functionalization with pseudocapacitive functional groups was chosen. This strategy is commonly applied when using a carbon template due to its conductivity and mechanical stability. For the material selection, it was critical to work with the strong point of OLC, which is a fast power handling. Although PEDOT showed a moderate

specific capacitance, the remarkable stability of the oxidized state, the power handling and commercial availability was convincing. Besides its boost in capacitance, this conductive polymer also should replace the binder in order to gain a sturdy electrode without the drawback of dead weight usually added by using an electrochemically inactive binder. The challenges for this system were to maintain a homogeneous coating of OLC, while PEDOT and OLC are insoluble in common solvents and to maintain a stable connection between PEDOT and OLC when used in the electrode. Therefore, the challange was:

Develop a system, which is soluble (during production) but also insoluble (as electrode).

The solution was to functionalize OLC with sulfonic groups, followed by the in situ polymerization of EDOT at the OLC particles. By phenylation to POLC and sulfonation to SPOLC, those functionalized OLC particles were readily dispersible in a water/ethanol mixture. During the polymerization of EDOT, the sulfonic groups electrostatically attracted PEDOT molecules to the surface of the OLC particles. The formed PEDOT@SPOLC composite precipitated, as electrostatic repulsion of the sulfonic groups was compensated by PEDOT. Electrochemical measurements showed a specific capacitance of around 77 F/g featuring a 27% increase over the first system. Also, a composite without functionalization, only featuring PEDOT and pristine OLC, was tested but lacked mechanical stability compared to the PEDOT@SPOLC system. This observation could be explained by HRTEM measurements, where a homogeneous coating of PEDOT could be verified for PEDOT@SPOLC while PEDOT@OLC only features high PEDOT aggregation in voids of OLC agglomerate.

For the third chapter, the manufacturing methods were in focus involving the usage of ink-jet printing technology. Thereby, a fast and resource efficient preparation method for electrodes was targeted. For inkjet printing, a stable dispersion of the active material was required. This approach entails the same problem of indispersibility of pristine OLC as discussed in the previous chapter. Therefore, the goal was:

Produce a stable ink with an unstable OLC particle dispersion.

The solution for this challenge was to use a surfactant, which facilitated the dispersion of OLC. The addition of a surfactant alone was not sufficient to achieve a stable dispersion due to the size of the OLC agglomerates. With the attrition mill, a standard technique was used to break up the OLC agglomerates. With smaller agglomerates in size of round 100 nm and the addition of surfactant during milling, a dispersion was obtained, which was stable over years. To

maintain sustainability, water was used as a solvent and for the surfactant, the widely commercially used sodium dodecyl sulfate (SDS) was used. The dispersion was adapted for inkjet printing supercapacitor electrodes. The small particle size resulting from milling was also important to prevent clogging of the nozzles of the inkjet printer. Several printing cycles were performed to deposit 0.5 mg/cm² of OLC active material onto an aluminum current collector. The specific capacitance of the printed supercapacitor electrodes (ca. 27 F/g) was smaller compared to the previous electrodes, which is related to surfactant remaining in the pores of the electrodes.

The last chapter of the thesis is dealing with the usage of OLC in sodium ion batteries. The main objective involved several attempts to increase the interlayer distance of OLC to enable sodium-ion storage. Graphene exfoliation inspired techniques like the Hummers method and explosive microwave experiments did not feature legible changes in active material. These results were mainly attributed due to the inaccessibility of the interlayer space of OLC. Therefore, the goal was:

To use material for sodium ion batteries which can not store sodium ions.

This contradiction was solved by using OLC as conductive agent rather than active material. To maintain the idea of sustainability, a biomaterial derived active material was chosen, which was found in banana peel. In this work, electrodes featuring pristine OLC as conductive agent, a cellulose-based binder and banana peels as active material were manufactured and electrochemically characterized. The successful combination of those materials was proven by the ability to reversible store energy, featuring a capacity of around 180 mAh/g.

All these applications reflect the diverse properties and innovative potential of OLC fulfilling multiple roles in energy storage. The main challenge was to solve or work around the problem of insolubility for OLC particles, where the transition between dispersion and dry state was always the key step and innovative driver for all applications. Regarding sodium storage, the key challenge was and still is to achieve a radial porosity in OLC, potentially unlocking additional opportunities to extend the role of OLC in the field of energy storage.

German Summary

Im Rahmen dieser Arbeit wurde die Verwendung von Onion-like Carbon (OLC) als Aktivmaterial zur Energiespeicherung untersucht. Die Arbeit zielte darauf ab, das

wissenschaftliche Verständnis der Rolle von OLC im Kontext der elektrochemischen Energiespeicherung zu verbessern. Hierfür wurde an den Prozessschritten und Verfahren gearbeitet, um OLC-basierte Elektroden erfolgreich in Superkondensatoren und Pseudokondensatoren zu verwenden. Auch der Einsatz von OLC als Aktivmaterial für Natriumionenbatterien wurde erforscht, wobei sich das Material in dieser Anwendung als Aktivmaterial ungeeignet erwies. Die Bearbeitungen dieser Fragestellungen war darauf ausgerichtet, das Wissen in diesem Bereich zu erweitern, synergetische Ansätze für Problemlösungen zu finden und einen Mehrwert in Bezug auf Nachhaltigkeit, Performance und Prozessierbarkeit zu schaffen.

Das erste Kapitel widmet sich der Verbesserung der Nachhaltigkeit von OLC-basierten Elektroden für Superkondensatoren. Für die Elektrodenherstellung stellt die Verwendung von fluorierten Polymeren als Binder ein Problem dar. Ein sinnvoller Ersatz war Carboxymethylellulose, da dieser Binder auf Pflanzen basiert und somit nachhaltig ist. Obwohl dieser Binder in Elektroden mit verschiedenen Aktivmaterialien erfolgreich eingesetzt wurde, war die Kombination mit OLC problematisch. Dafür verantwortlich war die Struktur der OLC-Agglomerate, genauer gesagt, deren Makroporen. Diese Hohlräume absorbierten eine große Menge an Binder, der erstens nicht für den Zusammenhalt mit anderen Partikeln zur Verfügung stand und zweitens der Elektrode aufgrund ihrer elektrochemischen Inaktivität überschüssiges Eigengewicht verlieh. Außerdem blockierte diese zusätzliche Menge Binder die Poren. Daher wurde folgendes Ziel für das erste Kapitel formuliert:

Erhöhung der spezifischen Porosität durch Verringerung des Volumens.

Die Innovation bestand darin, OLC noch vor der Elektrodenherstellung zu agglomerieren. Obwohl das Volumen verringert wurde, führte die Agglomeration nicht zu einer Verstopfung der Poren des Materials. Die ursprüngliche spezifische Oberfläche von 527 m^2/g konnte beibehalten werden, indem größere und dichtere Agglomerate gebildet wurden. Dies verringerte somit lediglich das Volumen der großen Hohlräume. Diese Methode ermöglichte die Verwendung von grünem Cellulosebinder und die Herstellung von Dünnfilmelektroden mit Rakeltechnik in einem wässrigen Verfahren. Die resultierenden grünen Elektroden lieferten eine Kapazität von 56 F/g, was einer Erhöhung um 22 % entspricht im Vergleich zu Elektroden, die mit fluorierten Bindemitteln hergestellt wurden. Diese Ergebnisse belegten den Wert dieser Entdeckung in Bezug auf Nachhaltigkeit und Leistung.

Für das im zweiten Kapitel vorgestellte System wurde eine höhere Leistung des Kondensators angestrebt. Um die Kapazität zu erhöhen, wurde eine Funktionalisierung mit pseudokapazitiven funktionellen Gruppen gewählt. Für die Materialauswahl war es entscheidend, mit den Stärken von OLC zu arbeiten, nämlich der Zugänglichkeit für den Elektrolyten und der damit verbundenen schnellen Ausbildung der Doppelschicht. Obwohl PEDOT eine mäßige spezifische Kapazität aufweist, überzeugte die bemerkenswerte Stabilität des oxidierten Zustands, die Leistungsaufnahme als auch die kommerzielle Verfügbarkeit. Neben der Kapazitätssteigerung sollte dieses leitfähige Polymer auch das Bindemittel ersetzen. Die Herausforderung bei diesem System bestand darin, eine homogene Beschichtung der unlöslichen Edukte OLC und PEDOT zu erhalten, die zu einer stabilen und unlöslichen Elektrode führen. Daher war das Ziel:

Entwicklung eines Systems, das bei der Verarbeitung zunächst löslich, als Elektrode jedoch unlöslich ist.

Dieses Ziel konnte durch die Funktionalisierung von OLC mit Sulfonsäuregruppen und die in situ Polymerisation von EDOT an den OLC-Teilchen realisiert werden. Durch Phenylierung zu POLC und Sulfonierung zu SPOLC waren die so erhaltenen funktionalisierten OLC-Partikel (SPOLC) leicht in einem Wasser-Ethanol-Gemisch dispergierbar. Während der Polymerisation von EDOT wurden die PEDOT-Moleküle elektrostatisch an die Sulfonsäuregruppen der OLC Partikeloberfläche gebunden. Das gebildete PEDOT@SPOLC-Komposit fiel aus der Lösung aus, da die elektrostatische Abstoßung der Sulfonsäuregruppen nun durch PEDOT kompensiert wurde. Elektrochemische Messungen der aus diesem Aktivmaterial hergestellten Elektroden ergaben eine spezifische Kapazität von etwa 77 F/g, was einer Steigerung von 27 % gegenüber dem System aus Kapitel 1 entspricht. Es wurde auch ein Komposit ohne Funktionalisierung getestet, das nur PEDOT und funktionalisiertes OLC enthielt, welchem es jedoch an mechanischer Stabilität mangelte. Dies konnte durch HRTEM-Untersuchungen erklärt werden, bei denen eine homogene Beschichtung von PEDOT für PEDOT@SPOLC nachgewiesen werden konnte, während PEDOT@OLC nur eine hohe PEDOT-Aggregation in den Hohlräumen des OLC-Agglomerats aufwies.

Im dritten Kapitel stand die Herstellungsmethode für Superkondensatoren im Mittelpunkt, die den Einsatz der Tintenstrahldrucktechnologie beinhaltete. Dabei wurde eine schnelle und ressourceneffiziente Herstellungsmethode für die Elektrode angestrebt. Für den Tintenstrahldruck war eine stabile Dispersion des aktiven Materials erforderlich. Mit der nicht

vorhandenen Dispergierbarkeit von unbehandelten OLC brachte dieser Ansatz eine ähnliche Problematik mit sich, wie im vorherigen Kapitel beschrieben. Daher war das Ziel:

Herstellung einer stabilen Tinte mit einer OLC-Partikel-Dispersion.

Hierbei wurde ein Tensid verwendet, um die Dispergierbarkeit von OLC zu erleichtern. Aufgrund der Größe der OLC-Agglomerate reichte die Zugabe von Tensid allein jedoch nicht aus, um eine stabile Dispersion mit OLC herzustellen. Mit der Vermahlung in einer Kugelmühle wurde daher eine Standardtechnik zum Aufbrechen der OLC-Agglomerate verwendet. Mit kleineren Agglomeraten in der Größe von rund 100 nm und der Zugabe von Tensid beim Mahlen wurde eine Dispersion erreicht, die über Jahre hinweg stabil war. Zur Aufrechterhaltung der Nachhaltigkeit wurde Wasser als Lösungsmittel und als Tensid das handelsübliche Natriumdodecylsulfat (SDS) verwendet. Die Dispersion wurde außerdem für den Tintenstrahldruck von Superkondensatorelektroden angepasst. Die geringe Partikelgröße, die sich aus dem Mahlen ergibt, verhinderte auch ein Verstopfen der Düse des Tintenstrahldruckers. Es wurden mehrere Druckzyklen durchgeführt, um 0.5 mg/cm² des aktiven OLC-Materials auf einen Aluminium-Stromkollektor aufzubringen. Dadurch konnten stabile und funktionsfähige Superkondensatorelektroden mit einer Kapazität von bis zu 27 F/g herstellt werden.

Das letzte Kapitel der Arbeit befasste sich mit der Verwendung von OLC in Natriumionenbatterien. Hierbei wurden mehrere Versuche unternommen den Zwischenschichtabstand auf bis zu 400 pm zu erhöhen, um die Aufnahme von Natriumionen zu ermöglichen. Sowohl durch Graphen-Exfolierung inspirierte Techniken wie die Hummer-Methode als auch explosive Mikrowellenexperimente brachten keine erkennbaren Veränderungen des Aktivmaterials. Dies wurde hauptsächlich auf die Unzugänglichkeit des Zwischenschichtraums von OLC zurückgeführt. Daher war das Ziel:

Verwendung von OLC in Natriumionenbatterien, obwohl OLC keine Natriumionen speichern kann.

Dieses Ziel wurde durch die Verwendung von OLC als leitfähiges Additiv statt als Aktivmaterial erreicht. Um den Gedanken der Nachhaltigkeit Folge zu leisten, wurde hier auf ein aus Biomaterialien gewonnenes, Aktivmaterial gesetzt. Mit pyrolysierten Bananenschalen Aktivmaterial, OLC als leitfähigem Additiv sowie einem Bindemittel auf Cellulosebasis wurden Messzellen gebaut und elektrochemisch charakterisiert. Die erfolgreiche Kombination

dieser Materialien wurde durch die Fähigkeit der reversiblen Energiespeicherung der Zelle nachgewiesen, wobei eine Kapazität von etwa 180 mAh/g erreicht werden konnte.

All diese Anwendungen spiegeln die vielfältigen Eigenschaften und das innovative Potenzial von OLC wider. Eine wesentliche Herausforderung der Projekte war stets, das Problem der Unlöslichkeit von OLC-Partikeln zu umgehen, wobei der Übergang zwischen Dispersion und trockenem Zustand immer der Schlüsselschritt und der Innovationstrieb für alle Anwendungen war. Im Hinblick auf die Natriumspeicherung bestand und besteht die größte Herausforderung darin, Zugänglichkeit ins Innere der OLC zu schaffen, um den Ebenenabstand der „Zwiebelschichten“ zu erweitern. Gelingt dies in zukünftigen Arbeiten, könnten sich zusätzliche Möglichkeiten zur Verwendung von OLC im Bereich der Energiespeicherung eröffnen.

Erklärung

Die vorliegende Arbeit wurde unter der wissenschaftlichen Betreuung von Prof. Dr. Anke Krüger von April 2018 bis September 2022 an der Fakultät für Chemie und Pharmazie der Julius-Maximilians-Universität Würzburg angefertigt.

Hiermit versichere ich, dass ich die vorliegende Arbeit ohne unzulässige Hilfe Dritter und ohne Benutzung anderer als der angegebenen Hilfsmittel angefertigt habe. Die aus fremden Quellen direkt oder indirekt übernommenen Gedanken sind als solche kenntlich gemacht. Die Arbeit wurde bisher weder im Inland noch im Ausland in gleicher oder ähnlicher Form einer anderen Prüfungsbehörde vorgelegt.

Ort, Datum Christian Bauer

Eigenanteil

Sustainable supercapacitor electrodes based on preagglomerated carbon onions and a green binder, Autoren/innen: Christian Bauer, Abdurrahman Bilican, Stephan Braxmeier, Gudrun Reichenauer, Anke Krueger, Zeitschrift: Carbon, Jahr September 2022, Ausgabe 197, Seiten 555-562

https://doi.org/10.1016/j.carbon.2022.06.041

Christian Bauer (CB), Abdurrahman Bilican (AB), Stephan Braxmeier (SB), Gudrun Reichenauer (GR), Anke Krueger (AK)

Autor	**CB**	**AB**	**SB**	**GR**	**AK**	**∑ in Prozent**
Konzeptionierung des Forschungsprojektes	45	0	0	5	50	100
Experimentelle Durchführungen	85	10	5	0	0	100
Auswertung und Diskussion der Messungen	50	5	5	5	35	100
Schreiben des ersten Entwurfs	100	0	0	0	0	100
Erstellen und Veröffentlichung des finalen Manuskripts	50	0	5	5	40	100
Korrektur der Veröffentlichung	50	0	5	5	40	100
Koordination der Veröffentlichung	30	0	0	0	70	100
Summe	58	2	3	4	33	100